The National Nanofabrication Users Network

Research Experience For Undergraduates

Research Accomplishments 1998

NNUN National Nanofabrication Users Network

1998 marked the first year I worked on the NNUN REU Program from Day One. It was fun putting together the initial ad poster (except when our color printer chose that week to absolutely STOP working...). I was excited when we received our first application and then worried that it would be the only one. But I ended up copying and sending to the other sites one hundred applications from which to choose 44 interns. The 1998 NNUN REU Program was in full swing!

The best part was calling the students to let them know they had been chosen for an internship. Twelve accepted right on the spot! The last few awards were given to those who had stuck with us and had kept in touch, letting me know that, yes, they were <u>really</u> interested. And they were the most gratifying to contact when I was finally able to offer them a place in our program.

Forty-three students from 29 US colleges or universities and representing 18 different majors joined our five-site network for ten weeks of hands-on nano-research. For the convocation, we flew everyone to Santa Barbara, California, where we spent three days hearing from each intern about the results of their project, and took in a few of the sights, sounds and tastes of the West Coast. The weather was perfect, the mountains distracting, and the company interesting and friendly. A good year!

I would especially like to thank the four site people I contact most regarding this program: Evelene Duhart at Howard University, Sarah Hernandez at Penn State, Jane Edwards at SNF and Brian Wolf at UCSB. (Brian also wins the "hearty-handshake" award for putting the convocation together.)

The NNUN REU Program would not be possible without the National Science Foundation. We would like to thank Drs. Janet Rutledge and Rajinder Khosla for their continued assistance and confidence.

However, we are also indebted to the generous financial support of each of the five sites, and these companies:

Advanced Micro Devices
Analog Devices
Applied Materials
Ericsson
Hewlett Packard
Hitachi
IBM
Intel
LAM Research
Lucas Novasensor
Motorola
National Semiconductor
Philips Research
Rockwell International Corporation
Siemens AG, Corporate Research Development
Texas Instruments
VLSI Technology, Inc.
Xerox. Inc

Melanie-Claire Mallison
Corporate & Public Relations, CNF
Cornell University

Melanie-Claire formatted and laid-out this publication and would like to thank the interns and the site support staff for their timely reporting and for following most of the rules! She also apologizes for the lateness of this release.

1998 NNUN REU Research Accomplishments

(in Alphabetical Order by Site and Intern's Last Name)

Cornell Nanofabrication Facility ..... 1 - 28

Optimization of Dry Plasma Etching Techniques Using the SLR 770 ICP Etcher 3

Fabrication of Composite Cantilever Beams for Microelectromechanical Systems (MEMS) 5

The Fabrication of Photonic Bandgap Crystals and Optical Fiber Support Grooves in Single Crystal Silicon Wafers 7

Fabrication and Characterization of Silicon Carbide MOS Capacitors 9

Characterization of Supercritical CO_2 Developable Photoresists for Non-Wetting Surfaces 11

SCREAM Applications: Flow Visualization with Microfluidic Channels 13

Making Atomically Flat GaAs Surfaces 17

Protein Patterning using Avidin/Biotin Chemistry 19

Use of Surface Topography in Patterning Neurons 21

Fabrication of High Aspect-Ratio Nanometer Scale Structures using Electron Beam Lithography and Reactive Ion Etching 23

Characterization of Thin Films Deposited Using Highly Collimated Molecular Beams of Variable Kinetic Energy 25

Howard University Materials Science Center of Excellence ..... 29 - 40

Designing an Internal Dialysis Unit 31

Characterization of Polyethylene Wear Particles from Artificial Implants Using Atomic Force Microscopy 36

Blackbody Emission from Resistively Heated Thin Films of Silicon Carbide 38

The Pennsylvania State University Electronic Materials and Processing Research Lab ..... 41 - 52

UV-Ozone Development Steps for Contrast Enhancement in Electron Lithography Using Ultrahigh Resolution Monolayer Resists 43

An Approach to Electron-Beam Induced Non-Epitaxial Crystallization of Amorphous Si Thin Films 45

High-Resolution Dry Etching of Si-Based Dielectrics Using a Chemically Amplified Electron-Beam Resist 49

Etching of SiO_2 High Aspect Ratio Trenches 51

Stanford Nanofabrication Facility ..... ***53 - 84***

Fabrication of Sub-Micron Spin-Dependent Tunneling Junctions Using E-Beam Lithography 55

Inducing Protein Crystallization Using the Electric Field from an Atomic Force Microscope 57

Studying Si/Si1-x-yGexCy Band Offsets using MOS Capacitors 59

Process Development of Chlorobenzene and LOL2000 Liftoff Processes with Stable Overhang Structures 61

Grain Structure in Thin Polycrystalline Silicon Lines 63

Fabrication of Nanostressors for Patterned Self-Assembly of SET Junctions 66

Protein Crystal Growth on Rough Silicon Surfaces 69

Microstamping Mazes onto Glass Substrates for Separating Integral Membrane Proteins .. 72

Characterization of Plasma Etching Using Alternative Gases 75

Control of AFM Anodization for Lithography of Single-Electron Transistors 78

The Enabling of Germanium Processing and Measurement of Film Uniformity for Dark Matter Detectors 80

Resist Charging and Heating in Electron Beam Lithography 82

University of California Santa Barbara ..... ***85 - 96***

Near Field /Atomic Force Microscopy Using GaN Lenses 87

Phage Display Libraries Used for Inorganic Material Recognition 88

Non-Lithographic Nanoscale Fabrication 89

Laser Enhanced Debonding of Nitride Semiconductor Films 90

The Near-Field Scanning Optical Microscope (NSOM) 91

The Effects of Adding Emulsion Droplets to a Polyacrylamide Gel 92

Mechanical and Microstructural Properties of Lightweight Ceramic Ablators 93

Annealing Behavior of Ar+ Plasma-Damaged InAs Quantum Dots & InGaAs Quantum Wells 94

II-VI Semiconductor Nanocrystals Synthesized in Solution Phase 95

Index ***97***

The 1998 NNUN REU Interns by Last Name

Ashish Ahuja	*Columbia University*	*AP*	*SNF*
Joe Altepeter	*Washington University*	*Physics / Comp Sci*	*SNF*
Kyndall Barry	*Bethune-Cookman*	*Physics*	*SNF*
Sigal Bekker	*American University*	*EnvirSci / PreMed*	*CNF*
Sam Bishop	*U of Washington*	*Chem Engr*	*SNF*
Raiza Calderon	*University of South FL*	*Chem Engr / Math*	*HU*
Sarah Carroll	*U of Notre Dame*	*Elec Engr*	*CNF*
Phyllis Chen	*CalTech*	*Chem Engr*	*SNF*
Tanja Cuk	*Princeton University*	*ElecEngr/Engr Physics*	*SNF*
Yuri Dancik	*Princeton University*	*Chem Engr*	*SNF*
Thomas Davidsmeier	*Illinois Wesleyan U*	*Physics*	*CNF*
Glenn Deardorff	*The Pennsylvania State U*	*Chemistry*	*PSU*
Michael Gutman	*Cornell University*	*Elec Engr*	*CNF*
Eric Hayduk	*Univ of Rochester*	*Chem Engr / Chem*	*CNF*
Ali Herrera	*UCSB*	*MechEngr / Physics*	*UCSB*
Helena Holeckova	*SUNY at Buffalo*	*Chem Engr / Chem*	*UCSB*
Blair Irwin	*Princeton University*	*Chem / Bio*	*SNF*
John Jochum	*USAF Academy*	*Elec Engr / Math*	*CNF*
Philip Jones	*Southern University*	*Physics / CompSci*	*CNF*
Diana Landwehr	*Cornell University*	*Mat Sci & Engr / BioMat*	*CNF*
Erick Lavoie	*Cornell University*	*Mech Engr*	*CNF*
Jackson Lee	*Cornell University*	*Elec Engr / Math*	*PSU*
Nin Loh	*Pomona College*	*Physics*	*SNF*
Andrew MacBeth	*Swarthmore College*	*Elec & Comp Sci*	*SNF*
Tavia Marshall	*Fisk University*	*Bio/Spanish*	*HU*
Rafael McDonald	*Princeton University*	*ChemEngr/EnvirStudies*	*UCSB*
Catherine McPherson	*Princeton University*	*MechEngr /Spanish*	*HU*
Marc Meyer	*Cornell University*	*AEP*	*CNF*
LaRon Phillips	*Xavier University*	*Bio / Chem*	*HU*
Lezlie Potter	*U of Notre Dame*	*Elec Engr*	*UCSB*
Jeremy Rowlette	*PSU*	*ElecEngr / Math*	*PSU*
Mahima Santhanam	*Boston University*	*Biomedical Engr*	*PSU*
Chancy Schulte	*Swarthmore College*	*Engr / Physics*	*SNF*
Gavin Scott	*UCSB*	*Physics*	*UCSB*
Keith Slinker	*Southern Nazarene U*	*Physics / Chem / Math*	*CNF*
Jeremiah Smith	*UMD Baltimore Cnty*	*App Physics / Math*	*HU*
Linda Steinberger	*UCSB*	*Physics*	*UCSB*
Ben Sturm	*University of Michigan*	*Engr Physics*	*CNF*
Corina-Elena Tanasa	*Bard College*	*Physics / Math*	*SNF*
Patricia Valenzuela	*SUNY at Albany*	*Physics / Math*	*UCSB*
Benjamin Werner	*UCSB*	*ElecEngr*	*UCSB*
Isaiah W Williams	*CSU, Sacramento*	*Bio / Chem*	*PSU*
Katie Wooton	*Wake Forest University*	*Chem / Bio*	*UCSB*

The National Nanofabrication Users Network (NNUN)
URL: http://www.nnun.org/
is comprised of these five sites:

Cornell Nanofabrication Facility
Dr. Sandip Tiwari, Director
Cornell University, Knight Laboratory
Ithaca, New York 14853-5403
Voice: (607) 255-2329
Fax: (607) 255-8601
URL: http://www.cnf.cornell.edu/

Materials Science Center for Excellence
Dr. Michael Spencer, Director
Howard University School of Engineering
2300 Sixth St, NW
Washington, D.C. 20059
Voice: (202) 806-6618
Fax: (202) 806-5367
URL: http://www.msrce.howard.edu/~nanonet/nnun.htm

Electronic Materials & Processing Research Laboratory
Dr. Robert Davis, Director
MR Institute Bldg
The Pennsylvania State University
University Park, PA 16802
Voice: (814) 865-0870
Fax: (814) 865-6581
URL: http://www.emprl.psu.edu/

Stanford Nanofabrication Facility
Dr. James Plummer, Director
Stanford University
CIS Building
Stanford, CA 94305-4070
Voice: (415) 725-6266
Fax: (415) 725-6278
URL: http://www-snf.stanford.edu/

University of California at Santa Barbara
(UCSB) - Nanofabrication Facility
Dr. Evelyn Hu, Director
Department of Electrical & Computer Engineering
Santa Barbara, CA 93106-9560
Voice: (805) 893-4130
Fax: (805) 893-8170
URL: http://www.ece.ucsb.edu/nnun/

Cornell NanoFabrication Facility

1998 REU Participants

REU Participant	Home Institution	Prinicipal Investigator
Front Row:		
Sigal Bekker	American University	Hercules Neves
Erick Lavoie	Cornell University	Norman Tien
Keith Slinker	Southern Nazarene University	Dustin Carr
Diana Landwehr	Cornell University	Harold Craighead
Sarah Carroll	University of Notre Dame	Norman Tien
John Jochum	USAF Academy	Hercules Neves
Philip Jones	Southern University	Jack Blakely
Back Row:		
Michael Gutman	Cornell University	Kevin Kornegay
Eric Hayduk	University of Rochester	Christopher Ober
Ben Sturm	University of Michigan	James Enstrom
Marc Mayer	Cornell University	Michael Isaacson
Thomas Davidsmeier	Illinois Wesleyan University	Yuri Suzuki
Melanie-Claire Mallison	CNF Corporate and Public Relations	

REU Project Title:

Optimization of Dry Plasma Etching Techniques Using the SLR 770 ICP Etcher

REU Intern, Major, Home Institution:

Sigal Bekker, Environmental Science, American University

REU Principal Investigator, Dept, Institution:

Hercules Neves, Electrical Engr, Cornell University

REU Principal Investigator Email Address:

Herc@ee.cornell.edu

Abstract:

As dimensions of integrated circuits are being minimized, efforts are being made to reduce roughness of device sidewalls. Dry plasma etching of silicon is the main step in achieving uniformity and smoothness of features. The predominant method for dry plasma etching has chlorine as its main component. This technique allows for fine features (<1 μm) to be etched leaving smoother sidewalls behind. Although it has been providing two decades of efficient device processing, chlorine etching indeed has some side effects. Aside from slightly tapered sidewalls, its potential for trenching, and poor selectivity to oxide mask, the C_{l2} technique has a low etch rate. This provides a serious obstacle and demand for new techniques has been on the rise. The Bosch method of dry plasma etching revolutionized micromachining architecture about 1.5 years ago. Indeed this new technique offers a fast etch rate, high selectivity and very vertical sidewalls. Both oxide and photoresist masks can be used. Many parameters can be manipulated during Bosch etches in order to fine-tune the final product. So many parameters, in fact, that the task of constructing a recipe for a specific etch is not trivial. The Bosch process brings along some flaws as well. Mask undercutting and ripples on the sidewalls are observed. Fine features or shallow etches are almost impossible to fabricate. This new technology is yet to be fully explored. The focus of this research is in finding a midpoint, a balance between chlorine and Bosch etching, that will maximize the advantages and minimize the disadvantages. If achieved, this can have a great impact on the optics and electromechanical microfabrication industry.

What is Dry Plasma Etching?

Dry plasma etching involves the use of two RF sources: Inductively Coupled Plasma (ICP) and RF high-density plasma created independent of sample bias. In a computer-controlled environment with proprietary software, two methods are utilized for the purpose of high-aspect ratio etches. Until recent years, the predominant method for fine-featured etches has been the chlorine technique. Lately, the Bosch technique has gained popularity due to a high demand for faster rates of etching. Both techniques prove advantageous in some aspects and disadvantageous in others. The project of finding an efficient combination of both was assigned and undertaken in the summer of 1998.

The Chlorine Technique:

With a decade of experience under its belt, the chlorine method has proven quite efficient in producing finely featured structures with smooth sidewalls. This could have been ideal, if not for the low etch rate. The chlorine method yields about a 12-micron depth in one hour. Aside from that, this method leaves trenching and tapering of sidewalls behind and proves to have poor selectivity between oxide mask and silicon. Demand for a new process that will accelerate the etch rate and eliminate any damage to the sidewalls is on the rise.

The Bosch Technique:

Young and unexplored, the Bosch method has been gaining momentum in the micromachining market. Bosch brings with it a long-awaited fast etch rate (100 microns/hour), high selectivity, and very vertical etches. Both oxide and photoresist mask may be used with it. Although this new technology has revolutionized dry plasma etching, it carries with it some flaws as well. The Bosch method is unable to etch finely featured structures. A mask undercut occurs after each etch and, worse of all, observations of rippling on sidewalls have been reported. A need arose to find a way of retaining the fast etch rate while minimizing harm to sidewalls.

Project Goal:

In this project, we attempted to experiment with etching on the SLR 770 using both techniques. We were on the search for ideal recipes that will provide for accelerated etch rate and an acceptable texture of sidewalls. The actual proposal offered to etch very deep trenches in the Bosch chamber of the SLR 770 and then allow the wafer to be smoothened in the chlorine chamber of the SLR 770. The project design included manipulation of four parameters: time, gas flow concentration, pressure, and RF power.

Experiment #1: Manipulating Time Intervals.

Before proceeding to locate ideal concentrations of C_{l2} and BC_{l3}, it was necessary to declare a time interval in which an etch would be accomplished with minimal damage. After a few trial experiments, it was decided to etch for 40 minutes in the Bosch chamber and 13 minutes in the chlorine chamber. That way about 80 microns depth would be achieved after Bosch plus a few more microns etched after chlorine. In total, depth would reach about 85 microns. Chlorine has a tendency to be quite hostile to silicon so any "smoothening" done in this chamber that is over 13 minutes, proves to cause damage to sidewalls, such as severe cracking and peeling.

Experiment #2: Manipulating Gas Flow Concentrations.

Once a time standard has been set, it was decided to keep the parameters in the Bosch chamber constant throughout the rest of the experiments and manipulate the chlorine parameters. A pre-designed program named "ClAli" was used. The initial gas flow concentrations were set at C_{l2}=2.0 sccm and BC_{l3}=14 sccm. At first, it was attempted to decrease C_{l2} concentration and increase BC_{l3}. This provided negative results evidenced by more definite horizontal rippling of sidewalls. When the opposite was done (ie. Increasing C_{l2} and decreasing BC_{l3}), more positive results were achieved. The new concentration ratio is larger with C_{l2}=10.0 sccm and BC_{l3}=10.0 sccm. H_2 and O_2 were kept constant at 7.0 sccm and 0.0 sccm, respectively. The smoothening effect was starting to be indicated smoother sidewalls with some vertical rippling.

Experiment #3: Manipulating Pressure.

Manipulation of pressure led to negative results. Original pressure was set at 20 millitorr and rendered very rough texture of sidewalls. When lowered to 15 millitorr the results were worse. More experimentation is necessary to determine effects of pressure on smoothness of sidewalls. It seems that higher pressure yields better texture.

Experiment #4: Manipulating RF Power.

The manipulation of RF power sources yielded the best results. RF_2 power source is responsible for the density of the plasma (ie. Concentration of free radicals). RF_1 power source is responsible for the force with which these radicals hit the surface to be etched. Original set power levels were: RF_1=75 Watts and RF_2=800 Watts. When decreasing the force with which radicals hit the surface (new RF_1=65 Watts) and increasing the plasma density (new RF_2=815 Watts) the results were worthy. Smoother sidewalls are detected with little to no rippling. More experiments with this parameter are necessary to fine-tune and achieve perfectly vertical walls.

Conclusion:

* Using the "Bosch-Chlorine Combo" may yield to a fast etch rate with a good texture of sidewalls.
* Smoothing silicon wafers that were etched in the Bosch chamber in the chlorine chamber should be done in a 12-15 minute interval.
* Increasing C_{l2} concentration and decreasing BC_{l3} concentration does promote some smoothing effects.
* Lowering the pressure set point in the chlorine chamber does not contribute to smoothing.
* Increasing RF_2 power (density of plasma) and decreasing RF_1 (force with which particles hit the surface) leads to efficient smoothing effects.

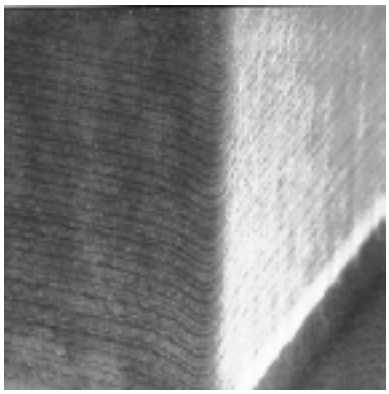

Figure 1

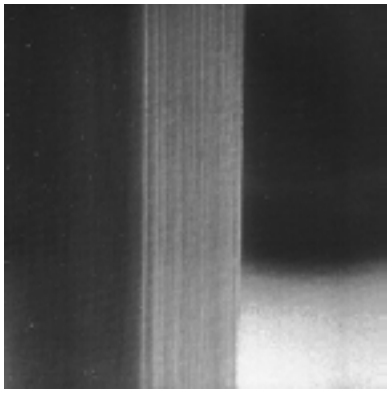

Figure 2

REU Project Title:

Fabrication of Composite Cantilever Beams for Microelectromechanical Systems (MEMS)

REU Interns, Major, Home Institution:

Sarah Carroll, Electrical Engr, University of Notre Dame
Erick Lavoie, Mechanical Engineering, Cornell University

REU Principal Investigator, Dept, Institution:

Norman Tien, Electrical Engineering, Cornell University

REU Principal Investigator Email Address:

ntien@anise.ee.cornell.edu

Abstract:

Composite structures have applications in MEMS to control ringing in rigid structures. The focus of this paper is the development of a process to create and test composite cantilever beams for microelectromechanical systems (MEMS). These beams were fabricated using polyimide as an interstitial layer between aluminum to act as a dampening material. Furthermore, cantilever beams were chosen to facilitate the measurement of the material properties of the composite. To fabricate these structures we exploited integrated-circuit fabrication techniques on a silicon wafer substrate. As a result, the fabrication techniques discussed in this paper can be easily implemented in existing microelectromechanical applications. During the course of this research we had to be particularly attentive to the compatibility of the subprocesses involved in using certain combinations of materials, in addition to maintaining an awareness of material compatibility.

Introduction:

Integrated-circuit compatible fabrication techniques for micromechanical structures are desirable to expedite both the mass fabrication of these structures and the integration of these structures into more complex MEMS devices. Composite structures fabricated in this fashion can be particularly challenging and compromises often must be drawn between processes used to introduce the constituent materials of the composite. Indeed, the authors of this paper became acutely aware of this as we endeavored to develop a process to fabricate the composite cantilever beams mentioned above.

Experimental Procedure:

This process involved applying five layers of material on a 3" silicon wafer, patterning the beams, and releasing the beams by removing the sacrificial layers. (The type of silicon wafer is not significant in this process.) An HMDS vapor prime was applied to each wafer using Yield Engineering Systems Vapor Prime and Image Reversal Vacuum Oven. The first layer, Shipley S1818 photoresist, acted as a sacrificial layer. The second and fourth were structural layers of aluminum evaporated onto the sample with a CHA Thermal Evaporator. Probimide 285 polyimide was spun in between to act as the dampening material in the cantilever beams. Finally, another layer of photoresist was spun on top to act as a mask layer for all three structural layers of the beam. To pattern the beams, two masks were used in conjunction with a GCA-6300 5X g-Line Stepper. After spinning and baking the first layer of photoresist on the wafer, the photoresist was patterned such that the aluminum would anchor directly to the wafer. The other mask, designed to be aligned with the first, was used to pattern the top layer of photoresist with beams of varying length.

All three structural layers were one half a micron thick. The bottom layer of resist was two microns thick, and the top layer of resist was three microns thick. These dimensions were sufficient to allow the beams

to be etched using Plasmatherm reactive ion etchers before completely losing the mask layer. More specifically, the SSL-720 was used to remove the unmasked aluminum via a three minute chlorine etch. Then, the PT-72 was used to etch the unwanted polyimide with a three minute oxygen etch. Finally, another three minute chlorine etch completed the beams. The final step of this process is to remove all of the resist and release the beams. It is important to note that the specimen should be washed with deionized water and dried after performing the chlorine etch, as small amounts of HCl may form and attack the aluminum.

As this process was developed, the bake schedules specified by the resist and polyimide manufacturers were found to be incompatible with the process. Thus, some variations were tried as discussed in the next section.

Results and Conclusions:

Problems with the bake schedules were first observed when the polyimide layer was baked according to the manufacturer recommendations. The manufacturer of Probimide 285 suggests a bake at 90°C for a half-hour directly followed by a 180°C bake for another half-hour. The first bake caused marked popcorning of the aluminum. The second bake exacerbated this undesirable side effect. It was suspected that this is due to solvents escaping from the resist and becoming trapped under the aluminum layer. In an attempt to circumvent this problem, the authors of this paper tried varying the bake time and temperature of the photoresist. It was found that higher bake temperatures caused the resist to be very difficult to remove, an undesirable effect. An optimal bake time has not yet been determined as of this paper.

The etching procedures used in this process did not appear to be a problem. Of note are the selectivities of the materials used in an etch, as these values govern the thickness of the mask layer. Polyimide etched 1:1 with resist, and aluminum etched twice as fast as the resist. A three-micron thick layer of resist protected the beam through all three levels of etching. Therefore, if the problems with the sacrificial layer can be resolved, this process could be useful to fabricated composite structures for MEMS.

REU Project Title:

The Fabrication of Photonic Bandgap Crystals and Optical Fiber Support Grooves in Single Crystal Silicon Wafers

REU Intern, Major, Home Institution:

Thomas Davidsmeier, Physics, Illinois Wesleyan University

REU Principal Investigator, Dept, Institution:

Yuri Suzuki, Materials Sci & Engr, Cornell University

REU Principal Investigator Email Address:

suzuki@msc.cornell.edu

Abstract:

A possible process for the fabrication of photonic bandgap crystals and optical fiber support grooves in single crystal silicon wafers was explored. The process utilized both hot potassium hydroxide and chlorine based reactive ion etching to achieve the large scale support grooves and the high aspect ratio structures of the photonic crystal. The combination of these two etches necessitated the deposition and patterning of multiple masking layers. The process was explored up to the patterning of the final masking layer, however, no samples were completed with both photonic crystals and support grooves.

Introduction:

Photonic crystals are structures that exhibit conduction bandgaps for photons in much the same way that semiconductors exhibit bandgaps for electron conduction. While the phenomena of photonic bandgaps can be derived from Maxwell's Equations, the bandgaps for actual photonic crystals must be calculated numerically [1]. Also, the photonic crystal possessing a particular bandgap can be calculated from that bandgap. Photonic crystals preform as excellent filters and wave guides, and fabricating structures effective in the range of frequencies used in fiber optic networks has long been a goal in this field.

But beyond the obvious industrial applications, photonic crystals present interesting possibilities in the age old study of light. For thousands of years, scientists have puzzled over the nature of light. Photonic crystals offer the chance to shape and control light in ways never thought possible, like a beam of light turning 90° with no loss in intensity.

The photonic crystal this project attempted to produce would have had a bandgap around 1.5μm. It was a hexagonal array of approximately 1200 nm wide columnar holes, 4 mm deep, and spaced 700 nm apart. The optical fiber support grooves were v-shaped channels approximately 150 μm wide etched so that the optical fiber core would be at the same height as the photonic crystal.

Experimental Procedure:

The first step in patterning the Silicon wafers was to deposit a thin masking film of plasma enhanced chemical vapor deposited (PECVD) Silicon dioxide. This mask layer was then patterned with e-beam lithography and reactive ion etching (RIE), to leave the photonic crystal pattern in the SiO_2. Next, optical lithography was used to remove the sections of SiO_2 that were not acting as masks for the photonic crystal. Another masking layer this time of SiN_4, was deposited over the entire sample, SiO_2 mask and all. This layer was patterned using optical lithography to achieve the optical fiber support grooves mask. The SiN_4 was removed using RIE. The support grooves were to be etched using hot KOH, however, this liquid etch lead to the lift off of the SiN_4 mask layer, and the etching of the whole sample.

Results and Conclusions:

While no photonic crystal and optical fiber support grooves were produced on the same sample, much of the processing necessary to achieve that goal was explored and perfected. No final conclusion can be drawn yet with regards to the practicality of this particular method of fabrication. Further exploration of the possibilities of utilizing well known silicon processing techniques for optical applications would certainly be well justified. With the opportunities present in the field, adaptation of these well know techniques would be very beneficial and well worth the time and effort.

References:

[1] "Photonic Crystals: Molding the Flow of Light," Joannopoulos, Meade, and Winn.

REU Project Title:

Fabrication and Characterization of Silicon Carbide MOS Capacitors

REU Intern, Major, Home Institution:

Michael Gutman, Electrical Engineering, Cornell University

REU Principal Investigator, Dept, Institution:

Kevin Kornegay, Electrical Engr, Cornell University

REU Principal Investigator Email Address:

kornegay@ee.cornell.edu

Abstract:

The interest in using Silicon Carbide (SiC) as a semiconducting material has increased in recent years due to its potential use for microelectronic applications that involve high power, high temperature, and high frequency. Because of this, experimentation on Metal Oxide Semiconductor (MOS) devices which utilize SiC as the semiconductor is essential to develop further understanding of Silicon Carbide's potential. One of the devices used in this study is the MOS capacitor. Numerous SiC capacitors are fabricated and characterized to determine their current-voltage characteristics. The fabrication procedure involved numerous stages including oxidation, metal deposition, and photolithography. In doing the fabrication, we were able to standardize a method for future MOS SiC device fabrication as well. The fabrication process along with the analysis results will be described in this report.

Introduction:

To establish a standard procedure for the fabrication of SiC devices, a test fabrication run was performed using a Silicon substrate. This test run effectively enabled all the unanticipated problems and mistakes to be handled without the need to waste any unnecessary costly SiC material. Problems encountered during the test run were limited to the photolithography steps. The photomask was initially made incorrectly, so a new one had to be generated. Pinpointing the optimal exposure time for the contact aligner was troublesome and took quite a few iterations on the Si wafer to determine. The following procedure was then carried out on a one-quarter piece of a p-type 6H SiC wafer.

SiC MOS Fabrication Procedure:

Cleaning the substrate is first. The standard MOS clean procedure is used. The substrate is soaked for ten minutes each in an acid bath consisting of HCl + H_2O_2 +H_2O and then a base bath of NH_4OH + H_2O_2 + H_2O.

Growing a layer of SiO_2 on the SiC substrate is next done by doing wet thermal oxidation. 2 runs were done, one for 3.5 hours at 1100°C resulting in 125Å grown; and another for 4 hours at 1150°C resulting in a total of 255Å grown. It is assumed that approximately 20Å of oxide were removed by doing a subsequent clean step prior to the second oxidation run. A 30 minute Argon anneal follows each oxidation run.

Evaporating a layer of metal over the oxide layer to form the MOS capacitor gate was done using the thermal evaporator. A single Aluminum pellet was used which has a maximum deposition of ~3000Å. The actual thickness of the deposited metal is controlled by the user. A thickness of ~2000Å is normal. On this run, 1850Å of Aluminum was deposited.

The photolithography is the final stage. Prior to beginning the patterning, a CAD layout of the mask was made. The mask's basic pattern is a ring 20mm in thickness with an inner radius of 200mm. This ring pattern creates an isolated circular area with a radius of 200mm which is used as the gate of the MOS

capacitor. Using the CAD layout, a 4" mask was made using the pattern generator. The wafer was then hardbaked for 10 minutes on a hotplate at 115°C in order to remove moisture and promote good resist adhesion. HDMS was next spun onto the wafer to prime the surface. Positive photoresist AZ1813 was next spun onto the wafer. Both the resist and HDMS applications were done for 40 seconds at 5000 RPM. The wafer was then softbaked for 10 minutes on a hotplate at 90°C to improve adhesion and remove solvent from the resist. The contact aligner was then used to expose the mask's pattern onto the resist. Approximately 10-15 patterns were exposed on the wafer at various exposure times ranging from 3.0 to 4.6 seconds. This multiple patterning was done to ensure the existence of at least a couple of "good" patterns. To develop the patterns, the wafer was dipped in a 1:1 mixture of Microposit Developer concentrate and Deionized water for 1 minute. Etching was done in Aluminum etch "A" for 7 minutes. The resist was then stripped away using acetone. Isopropyl Alcohol and Methanol were then successively spun onto the wafer to clean it. The fabrication was then completed.

The wafer was examined with a microscope and a number of "good" patterns were observed. The current-voltage characteristics of the fabricated device were done on a probe station.

Analysis:

The current-voltage analysis of one of the SiC MOS capacitors is shown in figure 1. Note the presence of the accumulation region on the left side where the capacitance =dQ/dV is highest. The depletion region occurs on the right side as the gate voltage increases. The capacitance levels off as the voltage goes increasingly more positive. This is all consistent with the characteristic curve of the p-type MOS capacitor. Capacitance measurements were made at the temperatures of 27, 100, 200, and 300°C. A reverse measurement was made at 300°C beginning from 10V and finishing at –10V to see the characteristic hysteresis effect.

Summary:

The fabrication procedure is now standardized. The current-voltage analysis showed good results. Further work on SiC MOS devices will take place at Cornell.

References:

[1] "A Study of P-Type Activation in Silicon Carbide", Sujoyita Dastidar, Purdue University, 1998.

Current-Voltage Characteristics

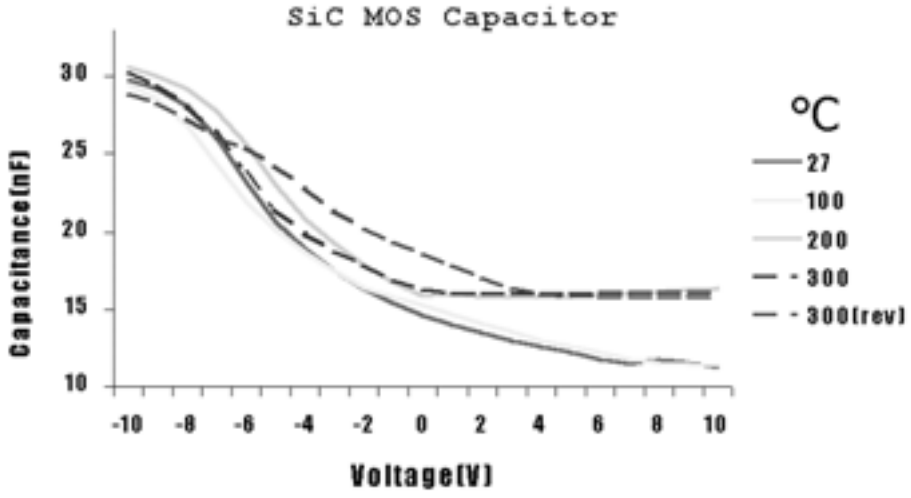

REU Project Title:

Characterization of Supercritical CO_2 Developable Photoresists for Non-wetting Surfaces

REU Intern, Major, Home Institution:

Eric Hayduk, Chemical Engr, University of Rochester

REU Principal Investigator, Dept., Institution:

Christopher Ober, Materials Sci & Engr, Cornell Univ

REU Principal Investigator Email Address:

cober@msc.cornell.edu

Abstract:

As the microelectronics industry grows, it constantly demands improvements in photo-lithographic techniques that lead to smaller integrated circuits and other electronic components. To that end, fluorinated block copolymer photoresists have been developed for exposure at 193 nm. These resists promise both high resolution and selective solubility in supercritical carbon dioxide (SC CO_2). SC CO_2 offers a cost effective, environmentally friendly alternative to conventional aqueous solvent systems.

Several photoresist systems that utilize SC CO_2 as a developer were characterized. Parameters including the exposure dosage, minimum resolvable feature size, CF_4 plasma etch rate and optimum temperature, pressure solubility conditions were determined. Results indicate that exposure doses are less than 10 mJ/cm^2 for selected photoresists and features down to 0.3 mm are resolved. Their etch rates varied from 800 to 1300 Å/min and solubility conditions ranged from 2800 psi, 45°C to 7000 psi, 85°C.

Finally, as a novel application of fluorinated block copolymers, high contact angle (155°), non-wetting surfaces which mimic the topography of Lotus leaves were manufactured. Ultimately, the goal is to synthesize surfaces with contact angles greater than 160° for use as innovative coatings. In this case, the surfaces become self-cleaning and easily wash away surface particulate matter.

Introduction:

As the microelectronics industry grows, it constantly demands improvements in photolithographic techniques that lead to smaller integrated circuit devices. Smaller circuits result in both increased productivity for manufacturers and the increased availability of microprocessors in consumer products. To achieve miniaturization of integrated circuits, scientists and engineers are continually researching new photoresist systems that are meant for exposure at shorter wavelengths. The decrease in wavelength allows the maximum achievable resolution to increase resulting in both an increased number of chip components within a given area and smaller circuits.

We are currently developing the next generation photoresists for exposure at 193 nm and beyond. These photoresist systems consist of fluorinated block copolymers that have been chemically amplified with photoacid generators (PAG). Upon exposure to UV radiation, acid is generated which causes the exposed region to become insoluble to SC CO_2.

SC CO_2 also has many advantages that make it an ideal photoresist solvent. It offers high selectivity, tunable solubility, high diffusivity which leads to faster sample development and low viscosity which eliminates resist pattern collapse. Finally, supercritical fluids are environmentally friendly. The production of liquid waste found in conventional development systems is eliminated and all of the CO_2 produced may be recycled.

In addition to photoresist systems, the fluorinated block copolymers can also be used in other innovative applications. One such interesting application involves the mimicry of Lotus Leaf surfaces. Biologists have noted that Lotus Leaves exhibit non-wetting, self-cleaning surfaces. That is, water easily beads on these surfaces and rolls off even at near zero degree angles of inclination. As water rolls off the surface, particulate matter is easily washed away as well leaving the surface exceptionally clean. The nonwetting, self-cleaning nature of Lotus leaves is due not only to hydrophobic waxes found in the leaves' epicuticule but also to the specific leaf topography. Our goal is to approximate this topography and produce non-wetting, self-cleaning surfaces. Please see the references listed for further information.

Methodology:

Several copolymer/PAG systems were characterized during this study. Fifteen weight percent polymer solutions were prepared and then the appropriate PAG was then added. Next, the solution was filtered and spun cast. After annealing, small sections were then placed in a supercritical fluid extractor. The extractor consists of a high-pressure pump and a oven that raises the temperature and pressure of carbon dioxide above the critical point. By allowing samples to remain immersed in SC CO_2 at a particular temperature and pressure for a period of 15 to 30 minutes, a condition was determined for which the polymer completely cleared off of the wafer.

To determine the correct exposure dosage, small areas of a

wafer coated with a copolymer/PAG system were exposed to 193 nm radiation. The samples were then developed using the solubility condition found previously. At this stage, each area was inspected to determine whether the negative tone photoresist adhered well to the wafer or cleared due to overexposure. The minimum resolvable feature size was then determined by exposing test patterns of various sizes at a certain dosage. Unfortunately, the optimized exposure dosages determined above could not be used for exposure but samples will be exposed at a later stage. SEM inspection determined the smallest well defined feature. Finally, CH_4 plasma etch rates were determined by placing small samples in a PlasmaTherm 72 and covering one half of the sample with a glass microscope slide. The samples were then etched at settings of 0.17 W/cm^2, 30 sccm CF_4, and 5 Pa. The change in film thickness was measured using a Sloan Dektak II Profilometer.

Nonwetting surfaces were created by etching a variety of patterns that mimic Lotus leaf topography into a silicon substrate. The following patterns were examined: 10 μm squares with both 2 μm and 10 μm spacing, 10 μm hexagons, and a 10 μm checkerboard pattern. Silicon wafers were spun cast with Shipley 1813 photoresist and then patterns were transferred to the wafer using an HTG contact aligner. Following a YES oven ammonia diffusion image reversal process and development, the patterns were then etched into the silicon substrate using a PlasmaTherm 770 ICP. Following etching, samples were coated with one of the copolymer photoresists described above and then dissolved in SC CO_2 leaving a monolayer coating. A 10 μm square patterns with 10 mm spaces is shown below.

Once surfaces were manufactured, the water contact angle was measured to quantify the nonwetting quality of the surface using a backlit microscope system. Essentially the larger the angle, the more nonwetting the surface is. The contact angle is measured between the surface and a tangent to the droplet at the surface, droplet, air interface.

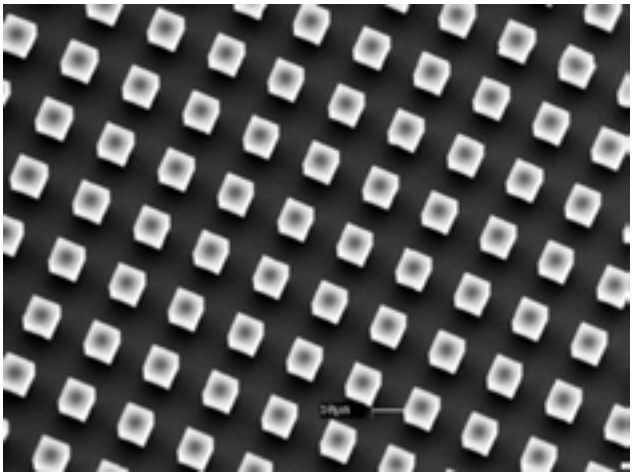

Figure 1: 10 μm squares with 10 μm spacing.

Results and Conclusions:

The solubility conditions found for all fluorinated copolymers range between 45°C, 2,800 psig, 15 min and 85°C, 6,900 psig, 30 min. As expected, either higher temperature, larger pressure or a longer dissolution time was required to clear polymers with lower fluorinated block volume fractions. The sensitivity for all polymers tested was less than 10 mJ/cm^2. This result is comparable to current photoresists. The maximum resolution is determined to be approximately 0.3 mm for most polymers. This is quite good compared to the current maximum resolution of 0.25 μm achieved in industry. Resolution should increase to at or beyond the industry level once samples are exposed at the optimum dosage. The average CF_4 etch rates were all between 800 to1300 Å/min and are comparable to PMMA, a standard E-beam photoresist. As a result of this study, several candidates were identified for further optimization.

Finally, high contact angle surfaces were synthesized. Contact angles varied from 134° to 155°. The 155° angle was observed on a surface covered with 10 mm squares (see photo below). This makes sense since this pattern is most similar to Lotus leaf topography. These surfaces will eventually be used as a part of innovative coating processes designed to produce commercially available self-cleaning surfaces.

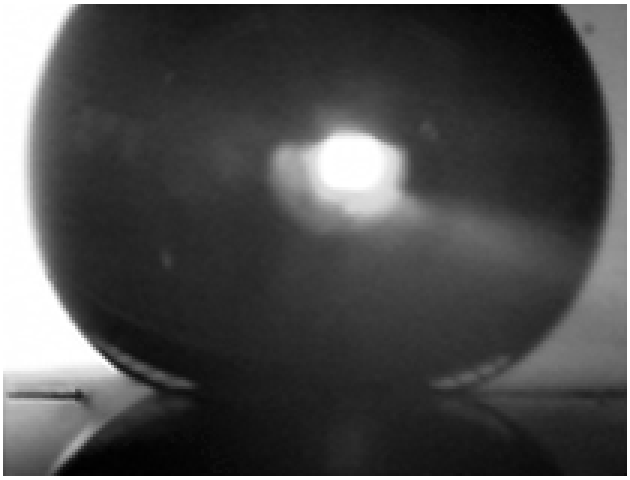

Figure 2: Water droplet on a patterned surface (155° angle).

References:

[1] "Block Copolymers as Supercritical CO_2 Developable Photoresists", N. Sundararajan, S. Valiyaveettil, K. Ogino, X. Zhou, J. Wang, S. Yang and C. K. Ober, Proc. ACS Div. Polym. Mat. Sci. & Eng. v79, p. 130 (1998).

[2] "Purity of the Sacred Lotus, or Escape from Contamination in Biological Surfaces", W. Barthlott, C. Neinhuis, Planta, 202: 1-8 (1997).

REU Project Title:

SCREAM Applications: Flow Visualization with Microfluidic Channels

REU Intern, Major, Home Institution:

Cadet First Class John Jochum, Electrical Engineering, United States Air Force Academy

REU Principal Investigator, Dept, Institution:

Hercules Neves, Electrical Engr, Cornell University

REU Principal Investigator Email Address:

Herc@ee.cornell.edu

Abstract:

Microfluidic channels have emerged as an exciting field with a diverse spectrum of applications. At Cornell University, using an adaptation of the SCREAM [1] microfabrication process, microfluidic channels have been incorporated on the same chip with extremely robust, high-aspect-ratio MEMS. This report discusses work done using this established approach to both create fluidic-channel MEMS and visualize fluid flow. On-chip pumps were designed but not tested, using micromachined actuators coupled with passive flow geometries. Fluid flow visualization through the channels was successfully accomplished using fluorescent microspheres and optical microscopes.

Introduction:

Microelectromechanical systems (MEMS) is an emerging field with a wide range of applications. Professor Noel MacDonald's Research Group at Cornell University has a patented bulk micromachining process known as Single Crystal Reactive Etching And Metallization (SCREAM) which creates released beams with high-aspect-ratios greater than 50 to 1 (height to width) and minimum feature sizes smaller than 0.7 microns [1]. With the strength inherent to the single crystal silicon, SCREAM spring structures can withstand substantial stresses under large ranges of movement and many cycles.

One MEMS application called microfluidic channels presents a particularly interesting array of uses, including ink-jet printers, micro-dosing systems, micro-chemical analysis systems, a wide array of micro-sensors, and even "labs-on-a-chip" [2]. Using a variation of the SCREAM process, as shown by a cross section of a fabricated device in figure 1, the MacDonald Group has developed a reliable method to fabricate microchannels in both suspended beams and channels embedded into the single crystal silicon substrate [3]. Moreover, this process benefits from the same advantages of other SCREAM MEMS, including integration with VLSI electronics, high-aspect-ratio actuation with large displacements, and integration with optical components [3]. The complete process to fabricate the channels is straightforward, and requires only 3 masks. The embedded channels created with an isotropic reactive ion etch (RIE) are typically 10 microns in diameter. The released channels which are restricted by the silicon dioxide walls, have a minimum channel width of about 2 microns and a variable channel height of approximately 2 to 20 microns.

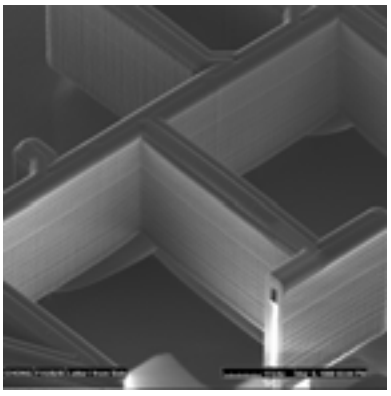

Figure 1. *Focused ion beam (FIB) image of cross-sectioned beam released from the single crystal silicon substrate [3].*

The advantages of microfluidics over macroscopic systems are many, and these benefits make microfluidics especially applicable in the chemical and medical fields. These advantages include making microfluidic systems more portable, decreasing waste of expensive or limited reagents, and increasing precision and measurement on microscopic scales [3]. Given these benefits, an obvious design requirement and goal is to integrate all system components onto a single chip using an inexpensive and high-throughput fabrication process. One such component needed for complete system integration is the on-chip pump. Designing such a pump at this scale is particularly challenging, given the two-dimensional nature of the process and the material thicknesses at this size. This makes fabrication of conventional valves with moving parts and sealed joints very difficult. Given this limitation, the current pump design focuses on electrostatic actuation coupled with an arrow or nozzle-like passive flow check.

Finally, in order to implement an entire system on a chip, a reliable method for characterizing flow and mixing within microfluidic channels is vital. One solution to such a requirement is optical microscopy, using fluorescent microspheres and elaborate optical filters. Microspheres fluoresce at a specific color when excited by higher wavelength light. Using the optical filters, it is possible to filter out all wavelengths except those emitted by the microspheres. Given that the oxide layer which covers the single silicon crystal base of the channels is transparent, with the minuscule spheres suspended in a pumped fluid, flow visualization of the moving spheres is realized.

Theory:

Pump design on such a small scale using a two dimensional process presented two fundamental problems. The first problem was creating a pump with such high-aspect-ratio channels, when the side-walls of these channels are very rigid. To overcome this problem, an intuitive approach using passive flow geometries was adopted. Such geometries have been shown to work on larger-scale microfluidic pumps, using surface micromachining [4]. The idea was to apply a high ramping voltage to the actuator shown in figure 2, thus driving the arrow like structures rapidly to the right, and then allow the pump to gradually return to equilibrium. This would produce fluid momentum and laminar flow through the nozzles of the pump on motion to the right, while relaxing the pump back to the left would create diffuser-like fluid motion and turbulent flow. Thus the design lacked conventional compressor actuation typically associated with pumps.

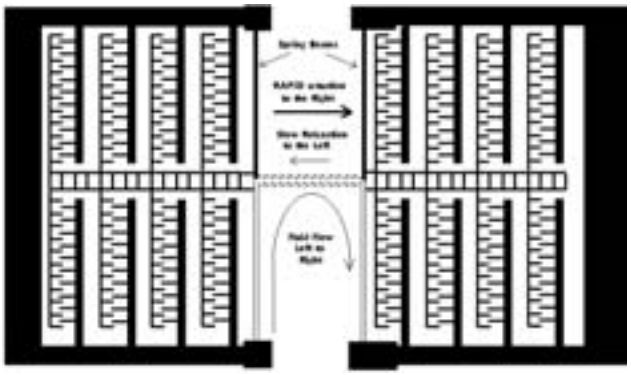

Figure 2. *Diagram of comb-drive actuator pump design coupled with passive nozzle/diffuser geometries, showing the direction of fluid flow from the left to the right.*

The second limitation dealt with the ability to pump fluids on such a small scale. Flow is typically characterized by the Reynold's number (1). For Reynold's numbers less than 1 (1), liquid motion enters what is called Stoke's flow, in which the fluid exhibits purely viscous or inertialess motion [5]. Without creating actuation at velocities high enough to produce fluid momentum, the pump design could not make use of the passive flow geometries mentioned above. Rather, in such a purely-viscous flow region, even water would produce molasses-like flow [6]. The pump's rapid motion to the right would be negated by the slow return to the left, resulting in no net flow. In order to produce a Reynold's number greater than 1, given channel diameter of 2 microns, and assuming a maximum beam displacement of about 3 microns, the actuators would have to be excited at over 150 MHz. Although such actuation is not unheard of, SCREAM structures produced at Cornell are typically actuated at tens of kiloHertz.

In order to visualize flow, microspheres from Bangs Labs, Inc. were used along with an Olympus® optical microscope. The microspheres, with the excitation-emission spectrum shown in figure 3a, had to match the barrier filter, dichroic mirror, and emission filter of the microscope as shown in figure 3b. The entire setup is shown by figure 4, in which incident light filtered to 360 nm excites the microspheres flowing in the channels, which in turn emit 420 nm light. All light

greater than 400 nm passes through the dichroic mirror in the microscope column and then is finally filtered by the barrier filter to be visually captured.

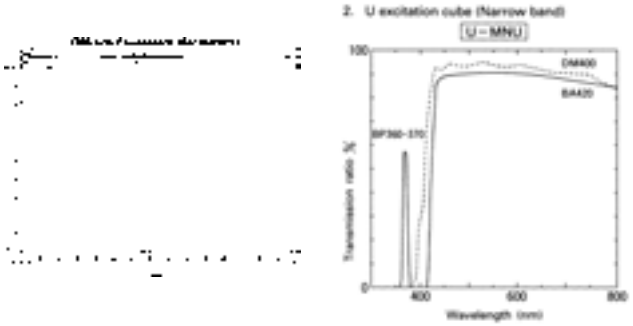

Figure 3a, top. *Excitation (360 nm) and emission (420 nm) bands for the microspheres used to visualize fluid flow [7].*
Figure 3b, bottom*. Optical filter setup for the Olympus® optical microscope cube, including the bandpass exciter filter (360-370 nm), the highpass dichroic mirror (greater than 400 nm), and the highpass barrier filter (greater than 420 nm) [8].*

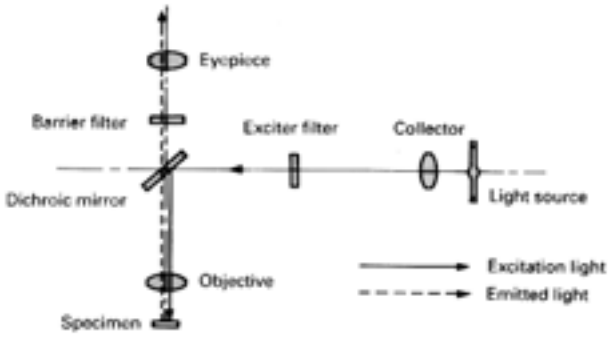

Figure 4. *Simplified set-up for visualizing the microspheres with the optical filters [8].*

Procedures:

Microfluidic channel fabrication was an established process given to me by Ph.D. candidate John Chong, at the MacDonald research group at Cornell. All fabrication was performed at the Cornell Nanofabrication Facility, in the Knight Lab at Phillips Hall. Although there are a couple methods to create the channels, the simplest version requires only three masks [3]. The first mask defines the channels, and the second patterns the released beams and actuators. Finally, after an oxide deposition seals the channels, a third mask selectively removes aluminum sputtered onto the beams, thereby providing the ability to actuate the structures. The completed cross-section is modeled in figure 5, and an actual cross section is shown in figure 1. Figure 6 also shows channels filled with fluid, viewed by an optical microscope.

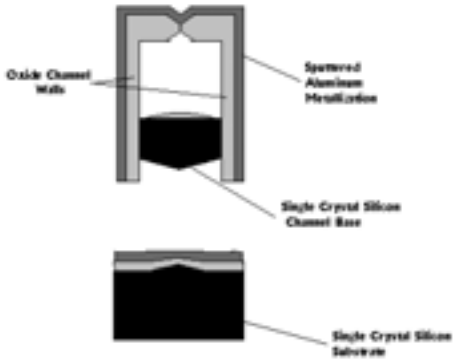

Figure 5. A simple model of the SCREAM microfluidic channel cross section (not drawn to scale).

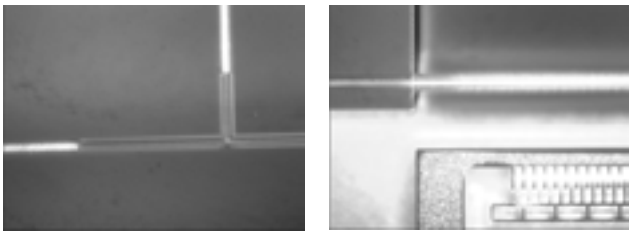

Figure 6a. Captured image of fluid splitting between a t-junction of embedded channels. Figure 6b. An image of a meniscus in a released channel, with fluid directed left to right.

The actual design and experimentation parts of my project involved designing the passive-flow pump, and experimenting with the microspheres. Design was accomplished with a powerful CAD application from Mentor Graphics called ICStation. Experimentation with the microspheres was exciting andvery reliable, as the Bangs Labs spheres and the Olympus microscope performed exactly to specifications. Flow visualization involved capturing the beads with both static pictures and video recordings, while focusing at the maximum possible magnification setting.

Results and Conclusions:

The passive microfluidic pump was designed but not fabricated during my short nine-week stay the CNF, due to an error during mask fabrication which occured with too little time left to complete and test the fabrication.

Microspheres were nonetheless tested on a previous fabrication and showed promising results. Flow was visualized and captured on video, and individual particles were seen. Using external pressure to direct the fluid through the channels, particulates and microspheres were clearly seen flowing around right-angled junctions and moving from embedded

channels into suspended channels. Especially interesting flow characteristics where visualized along the channel walls and at abrupt diameter changes. These characteristics appeared to show irregular flow, which pointed to the possibility that Reynold's numbers of greater than one were generated within the channels.

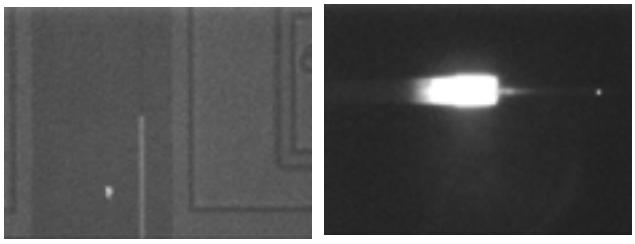

Figure 7a. Captured image of microspheres being introduced into a channel moving up the page. Figure 7b. An accumulation of microspheres at blockage or air bubble as they travel from the embedded channel into a smaller released channel.

Microspheres made it possible to view flow within a filled channel, as opposed to having to follow a liquid-air meniscus through the channels. I hope these microsphere successes open the door to other exciting experimentation such as pumping and mixing with SCREAM-style microfluidics. It was very rewarding to work with microfluidics, as it is still a fledgling technology, and I am excited to watch the field continue to grow in both academia and industry.

References:

[1] N.C. MacDonald, SCREAM MicroElectoMechanical Systems, Microelectronics Engineering, 32, (1996) 49-73.

[2] P. Gravesen, J. Branebjerg, O.S. Jensen, Microfluidics – a Review, J. Micromech. Microeng. 3, (1993) 168-182.

[3] J.M. Chong, Suspended Moving Channels and Channel Actuators for Microfluidic Applications, To be published.

[4] Stemme, A Valve-less Diffuser, Tech. Digest IEEE Transducers 93 (Yokohama, 1993) 110-113.

[5] M.M. Denn, Process Fluid Mechanics (1980), Prentice Hall: Englewood Cliffs, New Jersey, 52-55, 95.

[6] Olbricht, Professor, Chemical Engineering, Cornell University. Personal communication.

[7] Bangs Laboratories, Inc. Product List, for Standard Fluorescent Microspheres.

[8] AX Reflected Light Module manual, Transmission Curves of Filters, Olympus

Acknowledgements:

I'd like to thank the MacDonald Group and Professor Herc Neves for all their help and for making my stay at Cornell run as smooth as possible. I'd especially like to thank John Chong for inviting me to help with his project, and for all the time he spent giving direction and instruction. Finally, I'd like to thank the National Science Foundation, CNF, and Melanie-Claire Mallison for her help in getting me to Cornell despite my summer schedule time constraints.

REU Project Title:

Making Atomically Flat GaAs Surfaces

REU Intern, Major, Home Institution:

Philip Jones, Physics, Southern University

REU Principal Investigator, Dept, Institution:

Jack Blakely, Materials Sci & Engr, Cornell University

REU Principal Investigator Email Address:

blakely@msc.cornell.edu

Abstract:

We report attempts to fabricate arrays of step-free areas on Si(111). The motivation for this research is the fabrication of better microelectronic devices. As device dimensions become smaller, the need for a step-free surface will be critical. These devices will require a much smoother interface between the silicon and silicon dioxide layers. The reason is that individual steps or step bunches may significantly affect the local field, channel mobility, and breakdown characteristics of such devices. Two-dimensional grating patterns of ridges were generated on the surface by e-beam lithography, and plasma etching. The patterned areas were then flashed and annealed in an ultra high vacuum at various temperatures and time intervals. The patterned areas were then characterized by atomic force microscopy. We succeeded in fabricating step-free arrays for patterns with a repeat spacing as long as 25 microns. For the patterns with a large repeat spacing, we did not see completely step-free areas; however, we could decrease the step density for these areas.

Experimental Procedure:

A three inch wafer of silicon was obtained from Dr. Blakely's group in the Materials Science and Engineering Department at Cornell University. It was first degreased to prepare it for processing. The first step was to deposit a thin film of about 72-76nm thick of silicon dioxide onto the silicon substrate by means of chemical vapor deposition. The wafer was then prepared for the e-beam lithography. With the help of David Spencer in the Cornell Nanofabrication Facility, a pattern was designed, that was to be written with the e-beam. It was degreaesd with acetone and isopropanol, a resist was spun onto it, and then the resist was pre-baked. Next came the e-beam lithography, in which the e-beam wrote the pattern into the resist. The pattern was exposed by post baking the e-beam patterned wafer, developing the pattern in the resit, rinsing the wafer in deionized water, and confirming the pattern exposure by optical microscopy.

The sample was now ready for processing, and during processing, the sample was etched using the Applied Materials Etcher. It first etched the silicon dioxide, and then stripped the resist. The Plasma Therm PK 1250 was then used to etch both the silicon and silicon dioxide with a 10:1 etch rate. The sample was then cleaned by degreasing it in methanol with agitation, rinsing it in deionized water, growing a thin oxide in sulfuric acid, rinsing it in deionized water, etching the oxide in a buffered HF solution, rinsing in deionized , and repeating the third step to the sixth step until the surface would not wet when removed from the water. The sample was then annealed in an ultra high vacuum at various temperatures, and for varying periods of time. During the annealing, the atoms along the edge of the steps diffused onto a neighboring terrace, and evaporated. After a period of time, more and more atoms along the edges of steps diffused and evaporated, which created a general movement of the steps into the wall of the pattern, until there were no more steps. The samples were finally characterized using atomic force microscopy.

Summary:

In summary, we successfully fabricated step-free arrays for patterns with a repeat spacing as long as 25 microns. Our best annealing results came at 900°C for 5 hours. For patterns with larger repeat spacing , we did not see completely step-free areas; however, we could significantly decrease the step density for these areas.

References:

[1] "Fabrication of arrays of large step-free regions on Si(001)", S. Tanaka, C.C. Umbach, J.M. Blakely, R.M. Tromp, and M. Mankos Appl. Phys. Lett., vol. 69, p. 1235-1237, 1996

[2] "Step Permeability and the Relaxation of Biperiodic Gratings on Si(001)", S. Tanaka, N.C. Bartlett, C.C. Umbach, R.M. Tromp, and J.M. Blakely, Physical Review Letters, vol. 78, no. 17, p. 3342-3345, 1997

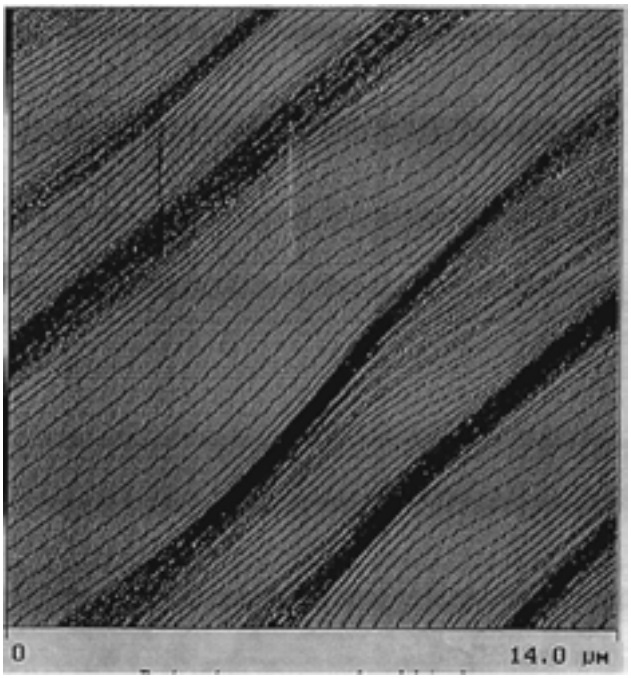

Figure 1. *Steps on Si (111)*

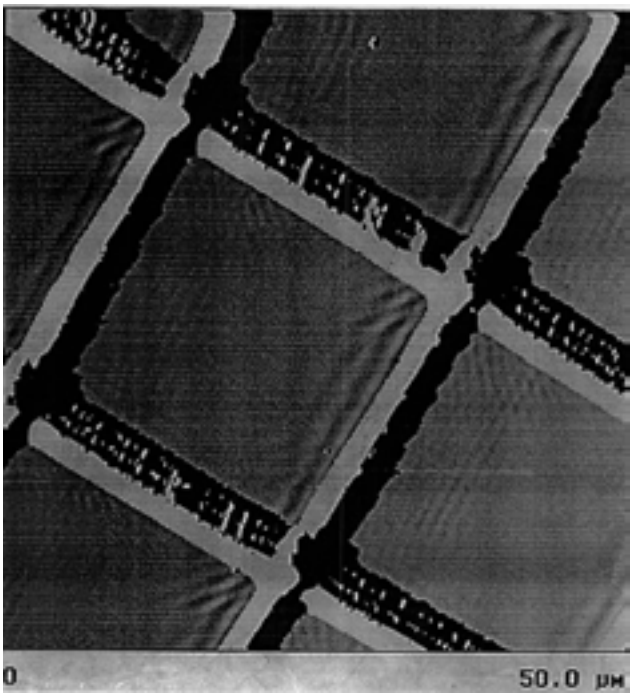

Figure 2. *25 x 25 µm Step-Free Regions*

REU Project Title:

Protein Patterning using Avidin/Biotin Chemistry

REU Intern, Major, Home Institution:

Diana Landwehr, Materials Sci & Engr, Cornell University

REU Principal Investigator, Dept, Institution:

Harold Craighead, Applied Physics, Cornell University

REU Principal Investigator Email Address:

hgc1@cornell.edu

Abstract:

Avidin and biotin, two commonly found molecules in nature, can be used in a variety of molecular labeling and detection techniques. Because of their natural affinity for each other, and photolithographical conjugates, the system is ideal for experimentation in protein patterning applications. The chemistry was applied to successfully pattern a fluorescent pattern on a sample wafer.

Introduction:

Neuronal cells can be grown on electrode arrays for electrical testing. Because of the size and complexity of these arrays, it is crucial each axon and dendrite are led to the correct electrode pad, and that cell bodies grow only in the designated area. Protein monolayers are used to aid and direct neuronal growth. The previous method of protein patterning, which is micro-contact printing, did not allow for the resolution and control of neuronal growth that was needed. When polylysine, the protein of choice, was printed on lines as small as 1mm wide, cell bodies would grow inside the lines. This is undesirable for control of the experiment. The method that will get each axon to the correct array is etching trenches 3 μm wide and 5 μm deep in the substrate. However, because of the size of the structures, photolithography is the most apparent way to get proteins to the bottom of the trenches. Utilizing avidin/biotin chemistry, with their photolitographical conjugates, was the goal of this research project.

Avidin and biotin are two biological molecules that are found in abundance in nature. They were discovered in the 1970's and much is known about the chemistry of their interaction, as they have the greatest non-covalent bond between a protein and a ligand in naturally occurring biological molecules. There are two conjugates of biotin, which are altered when exposed to light. Photocleavable biotin acts as a negative photoresist and photoactivatable biotin acts as a positive photoresist. Most of the applications of these conjugates have been in areas such as molecular probes and detection, and are usually used in solution. Because of the strong affinity of avidin to biotin, it makes an ideal candidate for protein patterning. Essentially any protein can be biotinylated; therefore making the desired pattern with resolution as fine as the stepper it was patterned with.

Experimental Procedure:

Since the final arrays will be on glass wafers, the experiment was done on a silicon wafer with an oxide layer. It was cleaned in the CNF to remove any possible biological contaminants. The wafer was cleaved into 2cm by 2cm size chips on which the processing is done. The cleaned chip was placed in a solution of 3-aminopropyl-triethoxysilane and acetone. This makes a self-assembled monolayer of free amine groups available for bonding on the surface. Because of the sensitivity to light, the next few steps are done in the dark. A layer of photoactivatable biotin was dried on the surface. When light hits the dried photoactivatable biotin, the reactive group is released, and the biotin

binds with the free amines. A TEM mounting grid was used as a mask, and a Zeiss microscope mercury lamp in bright field mode was used to expose the pattern. The wafer was exposed for 10 min, then rinsed vigorously with water to remove the biotin that was not bonded with the amines. The sample was then incubated with bovine serum albumen (BSA) blocker that acted to bind with any amines that did not have biotin on them. The sample was then incubated with Alexa-488 NeutraAvidin fluorescently labeled conjugate.

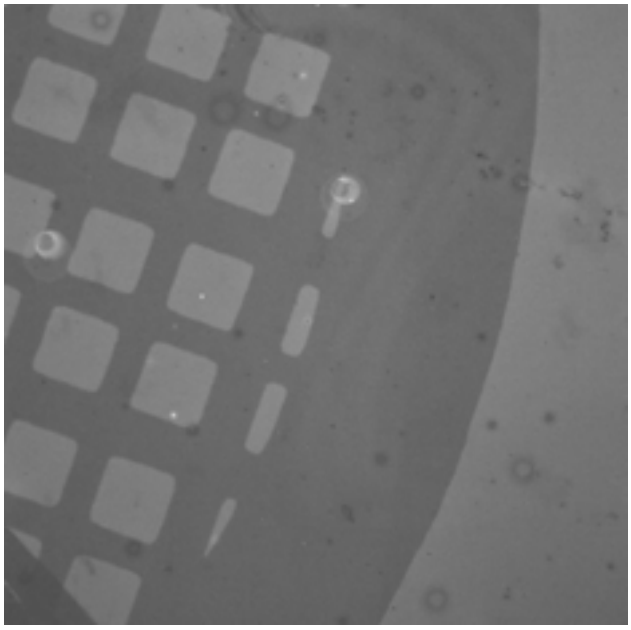

Results and Conclusions:

The sample was inspected using the Zeiss microscope, and the pattern from the TEM grid was easily viewed. A picture of the pattern can be seen in Figure 1. Since the early stages of this project were successful, research on this method of protein patterning will be continued throughout the year. The next steps are to determine optimum exposure time, concentrations, and experiment with patterning inside the trenches.

REU Project Title:

Use of Surface Topography in Patterning Neurons

REU Intern, Major, Home Institution:

Marc Meyer, Applied and Eng. Physics, Cornell University

REU Principal Investigator, Dept, Institution:

Michael Isaacson, Applied & Engr Physics, Cornell University

REU Principal Investigator Email Address:

msi4@cornell.edu

Abstract:

The ability to pattern neurons and neuronal connections has many possible applications, including a neuronal computer. Chemical patterning, specifically microcontact stamping of polylysine has been partially successful in patterning neurons, but has significant limitations. Topographical patterning has been tested in this experiment to determine if, in conjunction with chemical patterning, it could lead to precise control of both neuron cell bodies and processes. Encouraging results were obtained using a grid of trenches and holes and the next step, combining the topographical and chemical patterning, is currently being attempted.

Introduction:

The ability to direct cell growth, more specifically neurons, has many applications in both basic and applied sciences. However, both the placement of neuron cell bodies on the substrate and the paths available for the neural processes as they grow must be controlled accurately before any of these applications can be put into effect.

Chemical patterning of polylysine using microcontact stamping has been used to pattern neurons, but it has a strong limitation because it can not adequately control where the neuron cell bodies adhere to the surface. Neuron cell bodies, which are 10-20 microns in diameter, can grow on polylysine lines that are less than one micron thick, which is neither expected nor desired. One possible way to solve this problem is to make polylysine-coated trenches. The neuron cell bodies would only be able to attach to the substrate where the holes are wide enough for the neurons to fit into them and reach the polylysine at the bottom. Trenches, too small for cell bodies, would then lead the neuron processes in the desired direction.

In order to test if a grid of trenches and holes could both guide neuronal projections and control the position of neuron cell bodies, a series of grids and holes were made in silicon dioxide and polyimide. The first set samples had trenches that were 0.75, 1.5, and 3 microns wide and about 8 microns deep and holes that were 3, 5, and 7.5 microns wide and 8 microns deep.

Experimental Procedure:

The process begins with a 75 mm silicon wafer on which 360 nm of Plasma Enhanced Chemical Vapor Deposition (PECVD) silicon dioxide is deposited. The next step is to spin between 4 and 8 um of polyimide onto the wafer. The desired thickness is spun on by varying the rate and time of spinning. The polyimide must then be baked in an oven and hotplate to evaporate the polyimide solvent. Finally, another 360 nm layer of PECVD oxide is deposited on top of the polyimide.

Photoresist is spun on to the wafer and is exposed in a 10x stepper using a mask with a grid of lines and dots of varying sizes. After the lithography step, the photoresist is used as an etch mask for the oxide layer during a CHF_3 plasma etch performed in a Materials Research Corp. Model 720 Magnetron Ion Etcher (MIE). The patterned oxide then acts as a etch mask for the polyimide layer during an O_2 plasma etch which

is also performed in the MIE. Finally, a thin 100 nm PECVD oxide layer is deposited on the trench sample to provide a uniform surface for the cell culturing.

After the fabrication of the trenches is completed, the samples must then be chemically treated. Samples are either bathed or microcontact stamped with polylysine. The stamped samples were stamped at an oblique angle to the trenches. After the trenches were treated with polylysine, they were sent off for neuron cell culturing by Bill Shain and Jim Turner at the Wadsworth Center, Albany, NY. After culturing, the samples were critical-point-dried and sputtered with a thin layer of gold. The samples were then examined in a scanning electron microscope (SEM). All the microfabrication and electron microscopy are performed at the Cornell Nanofabrication Facility.

Results and Conclusions:

The fabrication of the trenches was successful as seen in Figure #1, a SEM of the cross-section of a trench. An example of the results from the neuron culturing is shown in Figure #2. The figure shows a neuronal process, most likely an axon, being guided by the trench. Once the process is inside the trench, it attempts to get out of the trench. However, as shown by the process bouncing back and forth between the walls of the trench, it can not leave the trench. These results show that once a neuronal process is inside a trench, the trench can control the growth of the process very well. The other important result is that cell bodies were not observed inside the trenches.

These results indicate that topographical patterning has the ability to both guide neuronal processes, and more importantly, to limit where neuron cell bodies can adhere to the surface. A second set of trenches have been made which have the same trench widths, but are only 4 microns deep and the holes are 10, 15, and 20 microns wide. In this second set, the holes are wide enough for cell bodies to fit in the holes and the assumption is that neuron cell bodies will attach to the substrate in these holes. The results from the neuron culturing on these samples have not yet been determined yet.

The results from these topographically patterned samples give encouraging results about controlling both the neuron cell bodies and processes in the future by combining topographical and chemical patterning using polylysine coated trenches and holes.

References:

[1] "Topographical control of cell behavior: II. multiple grooved substrata", P. Clark, et al., Development, 108, pp. 635-644, 1990.

[2] "Growth cone guidance and neuron morphology on micropatterned laminin surfaces", P.Clark, et al., Journal of Cell Science, 105, pp. 203-212, 1993.

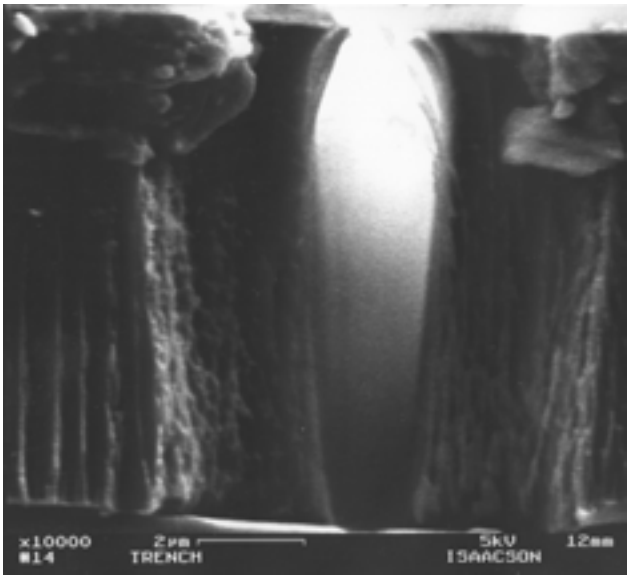

Figure 1

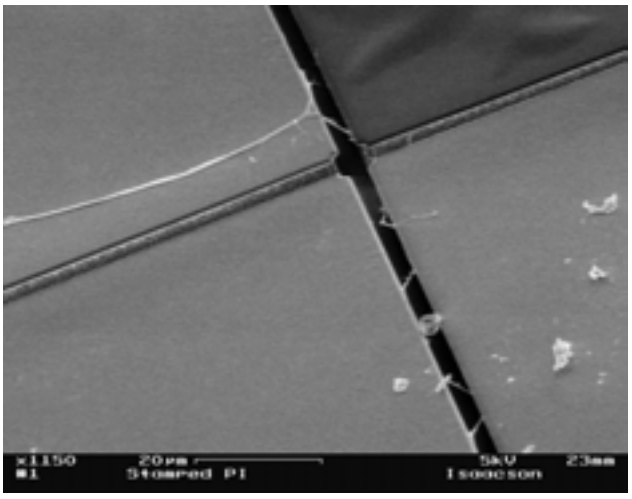

Figure 2

REU Project Title:

Fabrication of High Aspect–Ratio Nanometer Scale Structures using Electron Beam Lithography and Reactive Ion Etching

REU Intern, Major, Home Institution:

Keith Slinker, Physics & Chemistry, Southern Nazarene Univ

REU Principal Investigator, Position, Institution:

Dustin Carr, Cornell Nanofabrication Facility

REU Principal Investigator Email Address:

dwc5@cornell.edu

Abstract:

We have developed and characterized etching processes that overcome the difficulties associated with etching anisotropic high aspect ratio structures at the size scale associated with high-resolution electron-beam lithography. We refined a CF_4/H_2 reactive ion etch (RIE) and a $Cl_2/BCl_3/SF_6$ electron cyclotron resonance (ECR) etch for etching silicon with a metal mask, resulting in minimal sidewall etching. We also developed a process for using NEB_{22} as an etch mask, a negative tone resist that exposed many times faster than PMMA and proved to be an adequate etch mask in our ECR etch.

Introduction:

Two problems associated with nanometer scale structures were approached in this project. Sidewall deformation changes from an unattractive feature to the limiting factor for etching processes; previous capabilities have produced aspect ratios no greater than 1:1 for structures on the order of 100 nm. Secondly, exposure time is relatively slow for e-beam lithography processes, which makes mass production of nano-scale devices unpractical. Our project was aimed at developing silicon etches that prevented sidewall deformation and characterizing a resist that allowed for faster e-beam lithography process time over PMMA.

Experimental Procedure:

We patterned ~50nm features in PMMA on Si using e-beam lithography for use in developing our silicon etches. The patterns consisted of lines and dots that resulted in pillars and walls after etching, structures that are sensitive to sidewall etching effects. We deposited 20nm of chrome after developing the PMMA features, followed by liftoff. The Cr was then used as an etch mask.

A CF_4 RIE etch is mostly a physical etch, but some chemical etching does take place which allows for careful control of the sidewall etching. Undercutting is the limiting factor for this etch, so we added H_2 as a sidewall pacifying agent. We varied the amount of H_2 to determine the ideal proportions and ran the process for various intervals of time to determine the etch rate and selectivity.

The dense plasma associated with a Cl_2/BCl_3 ECR etch allows for a less physical, more chemical etch and more control of the sidewall etching. Sidewall deposition was found to take place in this case, so SF_6 was added to compensate. The ideal gas ratios, etch rate, and selectivity, were again determined.

Previous work led us to believe that NEB_{22} could possibly be used as an e-beam resist. Since it had not been thoroughly developed as an e-beam resist, we had to develop a suitable process including methods for spinning, baking, and exposing the resist. NEB_{22} is a

negative tone resist so the evaporation and liftoff steps are eliminated. This also means that the resist itself serves as the etch mask, so the resist was characterized for a RIE etch and the ECR etch mentioned above to determine its suitability as an etch mask.

Results:

In the case of the CF_4/H_2 RIE etch, the ideal proportion of gases was found to be 29.4 sccm CF_4 and 6.06 sccm H_2. If less H_2 is used, undercutting occurs; whereas, if more is used, the etch rate decreases. The selectivity of Si to Cr proved to be better than 12:1, the etch rate was on the order of 25 nm/min, and aspect ratios were achieved that were greater than 9:1. Figure 1 shows an eight minute etch under these conditions.

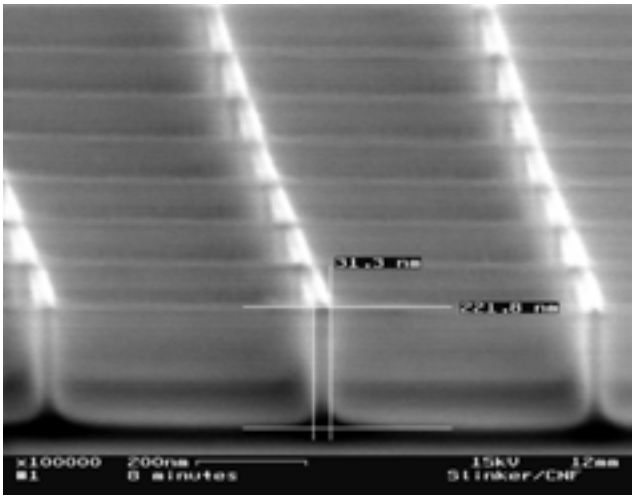

Figure 1. 8 minute CF_4/H_2 RIE etch.

The addition of SF_6 to the Cl_2/BCl_3 ECR etch had a two-fold affect: not only were etches anisotropic, but the etch rate also increased. The gas ratios were found to be highly sensitive to the conditions of the chamber, giving different results before and after the chamber had been cleaned. In general, too much SF_6 resulted in undercutting while too little showed sidewall slanting as a result of deposition. The selectivity of Si to Cr for the etch was found to be about 24:1 and gave an etch rate on the order of 300 nm/min. For this etch, aspect ratios better than 6:1 were achieved, but greater aspect ratios could be accomplished as this was not the goal of this experiment. Figure 2 shows a one minute ECR etch of Si with 7 sccm Cl_2, 3 sccm BCl_3, and 2.5 sccm SF_6.

The NEB_{22} resist showed faster process time, exposing fifty times faster than PMMA in addition to eliminating the need for evaporation and liftoff steps. The selectivity to Si in a bulk CF_4 RIE etch was less than 1:1, showing unacceptable results in this highly physical etch. Etching in the more chemical $Cl_2/BCl_3/SF_6$ ECR etch gave acceptable results, displaying a selectivity to Si better than 3:1.

In conclusion, both etches studied give aspect ratios that exceed most current demands, and the NEB_{22} yields a faster process time than PMMA and serves as an adequate etch mask.

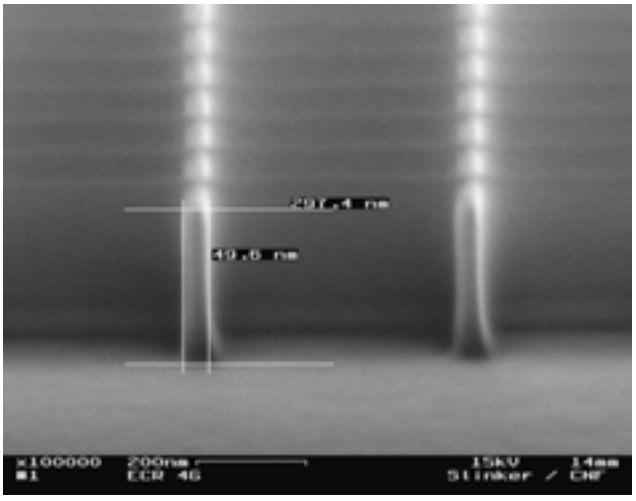

Figure 2. One minute ECR etch.

REU Project Title:

Characterization of Thin Films Deposited Using Highly Collimated Molecular Beams of Variable Kinetic Energy

REU Intern, Major, Home Institution:

Ben Sturm, Engineering Physics, The University of Michigan

REU Principal Investigator, Dept, Institution:

James Engstrom, Chemical Engr, Cornell University

REU Principal Investigator Email Address:

jre@cheme.cornell.edu

Abstract:

Thin films of polycrystalline silicon deposited on thermally oxidized silicon substrates by means of supersonic molecular beams of tunable kinetic energy were characterized to investigate deposition kinetics. Both a differentially pumped collimated supersonic molecular beam and a supersonic "free jet" were used as sources. Two distinct studies were initiated to probe deposition kinetics. One explored the use of a large area deposition source to address throughput issues, while the other observed the non-steady state process of nucleation, as part of a selectivity study. It was found that nucleation kinetics can be effectively quantified with scanning electron microscopy (SEM). Initial results suggest a reduction in nuclei density in the presence of atomic hydrogen.

Introduction:

Thin films play a crucial role in the fabrication of nearly every microelectronic and optoelectronic device. It is thus crucial to investigate novel processes and to better understand existing processes of thin film deposition. In this study, thin films of polycrystalline silicon were deposited by means of supersonic molecular beams of tunable kinetic energy through the use of a custom-designed multiple-stage ultrahigh vacuum (UHV) chamber, which has been described elsewhere [1]. This process is unique in that it allows for the precise control of both the incident beam kinetic energy and molecular flux. Also unique, is the generation of highly collimated reactant beams. Under conditions of steady state film growth, average thin film growth rates were measured as a function of substrate nozzle distance by ex-situ thickness measurements using profilometry. The source used in this particular study was a large area (> 3 x 3 cm^2) "free jet" source where the limiting factor effecting growth rate is molecular beam flux (T_S=700°C). Spatial flux variations compared favorably to recent simulation results [2]. In the non-steady state case, the nucleation process was examined using the collimated source (beam spot area 1.25 x 1.25 cm^2). Nuclei densities were measured during initial stages using SEM.

Experimental Procedure:

All films were deposited on 3 inch thermally oxidized wafers, employing a UHV thin film deposition platform which allows the use of two different sources. All substrates were RCA cleaned and annealed immediately prior to deposition. In the first study a "free jet" source consisting of a beam of Si_2H_6 / H_2 that passes through an array of 30 μm apertures was employed. Due to blanket deposition, a process of measuring thin film thicknesses requiring the use of standard photolithography techniques to create a sharp film interface has been adopted. As a result of this interface, a stylus profilometer can be used to measure thicknesses. Briefly, this process consists of exposing the sample to a mask consisting of a cross-hair pattern. The sample was then developed and hard-baked at 140ºC. For the etching process, two separate etches were used, one being polysilicon etch (150 parts HNO_3 : 1 part HF : 75 parts H_2O) the other being buffered

oxide etch (6:1). Two different etches were used due to the lack of selectivity of the polysilicon etch (8:1) and the sharply peaked thickness profiles.

The other source is a collimated, differentially pumped supersonic molecular beam of neutrals. The beam is a result of gas expansion through a 150 μm nozzle that passes through two pumping stages and a beam defining aperture before striking the sample. An approach to study the nucleation process where the substrate is translated a fraction of the width of the beam several times during growth has been used. This results in areas on the substrate that have been exposed to the beam for varying amounts of time all during one deposition experiment. Because the characteristic size of the nuclei prior to coalescence were very small (8 to 35 nm), good imaging tools were required. Imaging took place on the LEO 2 in the Cornell Nanofabrication Facility at medium acceleration voltages of 5 kV. Surface charging, always a concern in this material system, was minimal. Images were acquired at each step translation, thus providing a series of snap shots of the nucleation process as a function of time.

Results and Conclusions:

Our study of the steady state kinetics of film growth resulted in some important findings. From Fig. 1, it is observed that the measured film growth rate data behaves in agreement with recent simulation results at a fixed nozzle distance. It can also be observed that for large nozzle distances (15 cm), the growth rate across the sample remained nearly constant, while the magnitude of the growth was decreased by a factor of two. Moving on to the case of nucleation, it can be seen from Fig. 2 the manner in which nuclei density varied as a result of the beam exposure time of the sample at the indicated experimental conditions. The peak of Fig. 2 occurs just prior to nuclei coalescence (image B on Fig. 3). In addition to the expected relationship built with nuclei density versus exposure time, it was also found that nucleation kinetics exhibited a strong dependence with incident beam kinetic energy where nuclei density decreased by a factor of 10 when incident kinetic energy was reduced from 2.2 eV to 1.1 eV. Fig. 3 represents a typical set of micrographs of nuclei density versus exposure time. Recent results suggest that nuclei formation is very much inhibited in the presence of a hydrogen atom source. In a recent result, nuclei density decreased by a factor of ~4 when an atomic hydrogen flux was present at fixed reactor conditions. This analysis is the initial stages of a larger study aimed at understanding and optimizing selective silicon film deposition.

Acknowledgments:

Many thanks must be said for all the people and organizations who have helped to make this research project both possible and successful. Included in this are the National Science Foundation, Cornell University, and the Cornell Nanofabrication Facility. A heartfelt thanks goes out to the Engstrom Research Group, and especially S.E. Roadman whose time and dedication provided so much of what was necessary for me to be successful in this research.

References:

1. "Study of thin film deposition processes employing variable kinetic energy, highly collimated neutral molecular beams", S. E. Roadman, N. Maity, J. N. Carter, and J. R. Engstrom, J. of Vac. Sci. and Technol. A., vol16, pg 3423 (1998).
2. "Three dimensional modeling of silicon deposition process scale-up employing supersonic jets", G. Chen, I. D. Boyd, J. R. Engstrom, J. of Vac. Sci. and Technol. A., (in press).

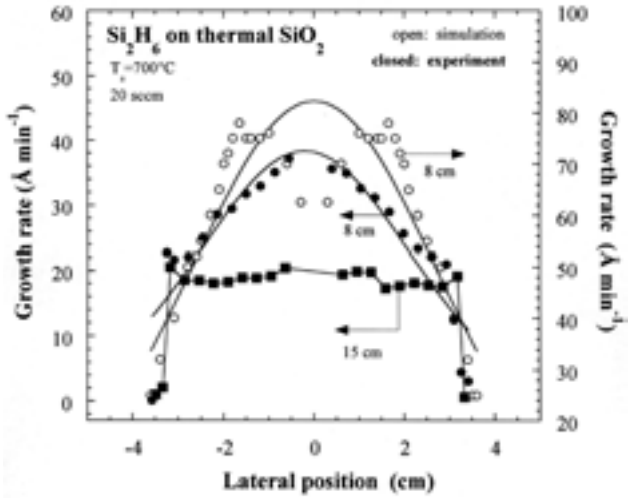

Figure 1. Measured growth rates at nozzle

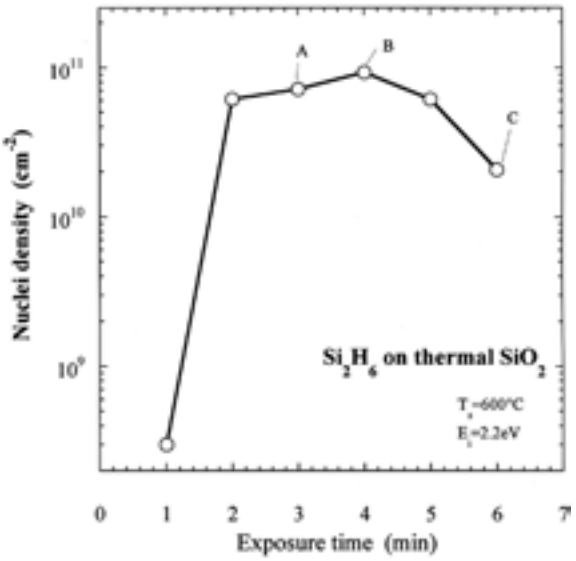

Figure 2. Nuclei density versus exposure distances of 8 and 15 cm with comparison to time. Points A, B, and C correspond to formation, simulation results at a nozzle distance of 8 cm. growth, and coalescence of nuclei (See Fig. 3).

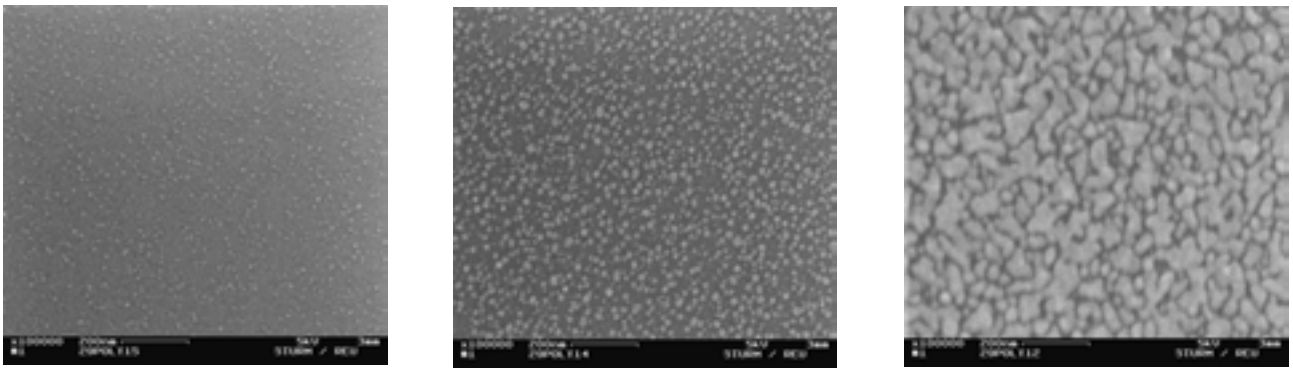

Image A (3 min) *Image B (4 min)* *Image C (6 min)*

Figure 3. Characteristic SEM Micrographs taken at three different stages during the nucleation process

Howard University
Materials Science Center of Excellence

1998 REU Participants

REU Participant	Home Institution	Prinicipal Investigator
From Left to Right:		
Jeremiah Smith	Univ of Maryland, Baltimore County	J. Lindasey & M. Spencer
Tavia Marshall	Fisk University	Kimberly Jones
Catherine McPherson	Princeton University	Xiao Tang
Raiza Calderon	University of South Florida	Kimberly Jones
LaRon Phillips	Xavier University	Kimberly Jones

REU Project Title:

Designing an Internal Dialysis Unit

REU Interns, Major, Home Institution:

Raiza Calderon, Chem Engr/Math, The Univ of South Florida
Tavia Marshall, Biology/Spanish, Fisk University
LaRon Phillips, Biology/Chem, Xavier University

REU Principal Investigator, Dept, Institution:

Kimberly Jones, Howard University

REU Principal Investigator Email Address:

spencer@msrce.howard.edu

INTRODUCTION

Treatment:

Treatment options for those with renal failure are two types: dialysis and kidney transplantation. Doctors can determine when patients need dialysis by measuring the levels of several blood chemicals; the two major blood chemicals that are measured are the creatine and blood urea nitrogen (BUN) levels. As these two levels rise, it indicates to the doctor of the kidney's decreasing ability to rid the body of waste products. Once the doctor has determined the patient's need of dialysis, one of two types may be used: peritoneal and hemodialysis.

Hemodialysis involves the use of a dialysis membrane, which carries out the functions of the kidneys. During hemodialysis, blood passes from the patient through a dialysis membrane that filters the metabolic wastes from the body. Treatment takes place in a hemodialysis unit at a hospital. Patients generally go to the dialysis unit three times a week for treatment which last from $2\ ^1/_2$ to $4\ ^1/_2$ hours. The other dialysis method used is called peritoneal dialysis. Peritoneal dialysis uses the patient's own body tissue inside the abdomen (peritoneum) as a filter. A tube called a dialysis catheter is placed through the abdominal wall into the abdominal cavity where dialysate fluid is flushed, thus filtering the patient's blood by osmosis and diffusion.

This type of dialysis requires the patient to play a more active role in their dialysis treatment. This method requires the patient to weigh himself/herself to determine the fluid to be used. The patient connects a bag of dialysate fluid to the peritoneal catheter site near the abdomen and allows solution to drain into the peritoneal cavity. Once the fluid has remained in the peritoneal cavity for a certain period of time, the fluid is drained back into the bag that originally contained the fluid. This procedure usually takes about 30 minutes to accomplish and must be done four to five times daily.

RESEARCH

Objective:

The objective of this research was to design an efficient, yet biocompatible dialysis unit for internal use in individuals with renal failure. In continuation with the previous year's work, we attempted to better conceptualize the design and functions of the unit by addressing issues such as biocompatibility, size, location, and the dimensions of the unit. The design of the model was to incorporate the functions and components of traditional dialyzers into a miniaturized unit, with a focus on membrane fabrication. Initially, it was intended to fabricate the membrane material in the Howard University Materials Science Research Center of Excellence. However, our research revealed that the optimum materials and membrane could not be fabricated in the MSRCE laboratory. Therefore, a theoretical model of an internal unit was designed; however, the actual performance of this unit requires physical experimentation.

Membrane Materials:

The membrane permeability and the design of the dialyzer determine performance characteristics of dialyzers. The most intrinsic component of the hemodialysis process is the membrane used to filter the blood.

The membrane permeability is determined by the designation "low-flux" or "high-flux." High-flux membranes allow the passage of larger molecules and display higher water permeability than the low-flux membranes thus necessitating the use of machines with volumetric fluid control to ensure safe fluid removal. An idea membrane would be semipermeable, allowing only certain sized molecules or electrolytes to pass through and biocompatible. A biocompatible material would make up this membrane to prevent possible complications due to the body's natural defenses against foreign materials.

A determining factor of the membrane's efficiency is its pore size. The pore size is dependent upon the size range of the molecules in a given solution to be filtered. Eurethrocytes range from 7.2-17.1 microns, leukocytes can range from 6.7 to 12 microns, and platelets vary from 2 - 4 microns in diameter. This permits a general variance range of 0.5-2 microns for most membranes, allowing most of the waste and some nutrients to filter through, but not the blood cells.

Currently, the dialyzers used in most hospitals have low-flux cellulose acetate (CA) membranes. Cellulose acetate is an inexpensive, easily manufactured material, but not inert, which may be the cause of some adverse reactions. In fact, Dr. Steven E. Lerner & Associates reported that the less biocompatible a membrane is, the more likely an incidence of clinical infection will occur. One complication is the drop in white blood cell and platelet count during the first hour of dialysis. It returns to the normal count towards the end of the procedure. This change tends to be clinically insignificant, but a more serious complication is an inflammatory response, that initiates a "first use" reaction. Symptoms include chest pain, back pain and shortness of breath that occurs 20 to 40 minutes after the hemodialysis process begins. Such reactions occur less often with a more biocompatible membrane because of their attenuated ability to activate complement.

Also, amyloid and amyloid bone diseases are more frequent, particularly with patients kept on CA dialyzers for longer periods of time. Production and retention of B_2 microglobulin is believed to be the cause of this disease. Synthesis and release of B_2 microglobulin is stimulated by the recurrent complement activation that occurs with each dialysis. CA dialyzers cannot sufficiently clear the membranes of the B_2 microglobulin. Therefore, the best option, for the patient's sake, is to change to a more biocompatible membrane. A study conducted by Steven E. Lerner & Associates revealed that an increased biocompatibility could lead to increased metabolism (especially on the days of hemodialysis) and therefore have an adverse effect on the patient's nutrition. Furthermore, it could lead to decreased mortalbility and morbidity among the chronic hemodialysis population, but these possibilities have not been statistically verified.

Out of the dozens of different chemically formulated membranes tested for hemodialysis, four withstood the rigors of clinical testing: cellulose, cellulose acetate, polyacrylonitrile (PAN), and polysulfone (PS). The cellulose membrane, Cuprophane PT-150, produced by a Western German firm, Enka-Glanstoff, has become the standard to which all other membranes are evaluated because of its uniform quality, clinical effectiveness, and low cost. It is fabricated into sheets, hollow fibers, and coils. Standard membranes have solute and water permeabilities approximately equal to PT-150. High-flux membranes have vitamin B_{12} and water permeabilities three or more times greater than the PT-150. Prescribed dialyzers material is based on cost and convenience rather than uncertain scientific evidence demonstrating the merits of one material over another. However, if lower cost and convenience is resulting in higher mortality rates, usage of better materials is the only logical answer.

PAN and PS materials are polymers, long chains of repeating monomers, which are more biocompatible than CA materials. Polymers have a higher flux than CA, better clearance, and are synthetic materials. They are obviously a better choice than the presently used CA material, but their higher cost is an unfortunate but major determining factor for its usage. Other polymers just as efficient include polyurethane, polyethylene, polymethylmethacrylate (PMMA), and polytetra-flouroethylene (PTFE).

A six month experiment was conducted by Dr. James McCarthy and fellow peers that compared the preservation of residual renal function in CA dialyzers to PS dialyzers (Division of Nephrology and Internal

Medicine, Mayo Clinic). All patients tested were well matched in regards to sex, age, initial renal clearance, predialysis blood pressure, and hemodynamic stability during hemodialysis. They concluded from the experiment that a polysulfone dialyzer delivered a higher Kt/V (1.34 + 0.30 [mean + SD]) than the CA dialyzer (1.06 + 0.20). The PS dialyzer patients also had a higher average urea clearance than the CA patients after four to nine months of dialysis. Their findings provided further evidence that the choice of dialyzer membrane may have an effect on intrinsic renal function, and PS is a better material than CA.

PTFE, better known as TEFLONR [CF_2-CF_2], is an inert, synthetic, leak proof, autoclaveable, high recovery, easy to use, white, linear polymer that is typically used for coatings (i.e., frying pans), wire and cable installations, motors, and generators. It is produced by the free-radical polymerization of tetraflouroethylene (a colorless gas). Its carbon-fluorine bonds make it one of the most interesting, unique polymers used in industry and everyday life. It has a high crystallinity (90%) as manufactured, is insoluble in most solvents, non adhesive, low friction properties, and constant electrical and mechanical properties from 20-250°C. The low friction properties are due to the tendencies of PTFE molecules to repel other molecules, which results in its excellent non-stick properties. The strong, carbon-fluoride bonds make it highly inert and the prime choice for storing chemicals. TEFLON's popularity is a result of its fine, quality properties that is idea for an internal dialysis unit.

Polyethylene, $[C_2H_4]n$, is the main ingredient for plastics. It has three different densities: high (HDE), low (LDE), and linear low density (LLDE). At a high density, it's at its most rigid and toughest state, and at a low and low linear densities, it is a soft, flexible, thin film material and melts at temperatures of 110-150°C.

PAN is derived from acrylonitrile, CH_2=CHCN, a colorless, volatile, combustible liquid used in polymerization of acrylic fibers, plastics, and rubbers. The AN_{69} PAN dialyzer membrane is associated with anaphylactic reactions in patients taking ACE (angiotensin converting enzyme) inhibitors, drugs that are used for treatment of hypertension and congestive heart failure. Anaphylaxis is an allergic reaction mediated by an antigen antibody complex, and occurs within the initial five minutes of dialysis. These AN_{69} dialyzers tend to be associated with higher bradykinin levels in patients on ACE inhibitors, in comparison to other membranes.

Another possible cause of anaphylactic reactions is ethylene oxide (ETO), a frequently used sterilizer for most dialyzer units. The reactions results from the conjugation of antibodies to ETO and human serum albumin (ETO-HSA). Coating the membrane with plasma proteins or washing out the residual ETO will reduce the chances of a reaction. PMMA, polyurethane, and PAN are possible polymers for dialysis use, but there is research still being done on them. They have some good properties, such as biocompatibility, and because most are synthetic, there would not be a shortage of materials; however the anaphylaxis reactions associated with the PAN membrane tends to pose a problem for its future use.

Membrane Configurations:

Another vital aspect of the membrane is its design or configuration. The design of the membrane determines how much blood can be filtered and how sufficiently. There are presently 3 different types of membrane designs: hollow fiber, parallel plate, and coil. Each one has a disadvantage and advantage over the other, but all carry the same ultimate purpose.

The hollow fiber is a composite of capillary, small, hollow membranes held together at each end by a clay-like potting material, and housed by a cylinder. These hollow tubes are approximately the size of a strand of hair, and combined provide a large surface area. Due to its large surface area, it provides for better filtration, making this design the best one of the three. Its pros include no membrane compliance, low blood flow resistance, controlled and predictable diffusion and ultrafiltration, vacuum creation capacity, countercurrent flow, and large surface area. Its only con is its difficulty of fabrication, especially in the Howard University Materials Science Research Center of Excellence (MSRCE) lab.

Parallel plate dialyzers have two or more sheets of semipermeable membranes enclosed between support structures. The components of this dialyzer are housed into a plastic container. In parallel dialyzers, blood flows between membrane layers while the dialysate flows over the membranes in the opposite direction in which is a counter current flow. It also has capacity for vacuum due to negative pressure. This membrane is easily fabricated, permits predictable ultrafiltration, is more firmly supported than the coil membrane, and

has a lower resistance to blood flow than the coil design. However, this membrane gives way to slight compliance.

The coil configuration is a long spiral tube of semipermeable membrane that is wound around a central core, much like a paper towel roll. A mesh screen material that supports the membrane separates the membrane layers. Blood flows horizontally through the membrane while the dialysate flows vertically, creating a crosscurrent flow instead of counter current like the other membranes. The filtration of the blood depends solely on positive pressure in which excess fluid (i.e. water) is pushed through the membrane. It efficiently removes waste, and the positive pressure pushes excess water in the blood through the membrane and into the dialysate. It is also easily fabricated. However, its high blood flow resistance, unstable support, and the blood compartments tending to have compliance expansion due to the high blood pressure of compliance makes this design futile.

Conceptualized Unit:

The design of our unit was based on research into various materials and concepts of dialysis treatment in order to provide an optimum model for internal use. However, difficult to design without actual experimentation, the design of this unit addresses many of the issues related to nephrological and material research. Based on our conceptualized design, further research and actual experimentation is possible.

The housing of the conceptualized unit will be made of Teflon polymer and divided into top and bottom casings to enclose the unit's components. Teflon was chosen due to its biocompatibility and durability. Also, Teflon is used in many biological technologies such as artificial heart valves and joints. The housing will contain compartments for both the dialysate and blood pumps, generators, and the filtration membrane. The dimensions of the unit will be approximately 7cm x 7cm x 3cm which is small enough to fit into the body without being so heavy as to inhibit the individual's normal functions. The membrane used will be fabricated of polysulfone (PS) polymer as opposed to the more commonly used cellulose acetate (CA) membranes using the hollow fiber membrane configuration. PS was chosen as the membrane material due to its biocompatibility and easy fabrication. In lieu of these properties, a study conducted at the Mayo Clinic's Division of Nephrology and Internal Medicine found that "patients with chronic renal failure requiring maintenance hemodialysis retain intrinsic renal function longer when using reprocessed polysulfone membrane hemodialyzers [as opposed to] single-use cellulose acetate membrane hemodialyzers" (McCarthy). PS dialyzers provided better filtration results; in fact, the study showed that "patients with parenchymal renal disease (glomerulonephritis or nephrosclerosis) had markedly better retention of intrinsic renal function with PS than with CA dialyzers" (McCarthy). The hollow fiber configuration was chosen for this unit because it provides a large surface area within a small space. The surface area of the unit's membrane will vary pending the needed substance clearances of the patient. Although they are much smaller than the external dialyzer, the pore size of the membranes in the internal unit will remain .5-1.5 μm in diameter. The fibers themselves will have an inner diameter of 200 μm and a thickness of 15 μm. Micro pumps will be used in the unit to which will regulate blood and dialysate flow. A definite type of micro pump to use in the unit has not been determined for there exist various types. The difficulty in choosing a pump configuration is due in part to the high flow rates and pressures required of such small pumps inside the body.

However, of particular interest to the MSRCE lab, scientists at the University of Washington have fabricated fixed valve micro pumps etched on silicon wafers that operate "solely by the differential pressure characteristics in each flow direction" (Forester and Burdell). As an intrinsic part of our unit, these type of pumps are good candidates for usage due to their use of etched valves as opposed to moving parts which may become jammed, thus causing pump malfunction. Generators within the unit will serve as the power source for the pumps pending the pump configuration used. The unit will be fastened onto the femur for support; from here the femoral artery will lead into the unit where it will be connected to tubing leading into the membrane. The femur was chosen as the region of attachment because of its size and strength.

Also, this location places the unit in an area where there is less likely to be an incidence of damage due to the patient's daily functions (i.e. exercise, job). The fact that this area is away from vital organs also lends to the practicality of this location. The blood exiting tube will be connected to the femoral vein, thus continuing normal blood flow. Another tubing from

the unit will be connected to the bladder to collect waste. Dialysate will be introduced into the unit via catheter tubing leading into the body from an external pump, much like the technology used with insulin pumps. This idea originated from the problems with finding a location within the body for the storage of the dialysate. About two liters of dialysate is needed daily for effective dialysis treatment; this large amount of fluid is very cumbersome within the body, thus external introduction of dialysate was determined to be a more feasible option. The demonstration model is a hollow fiber membrane of which the membranes are fabricated of cellulose acetate polymer made by Baxter International Inc. However, some manufacturers distribute dialyazer membranes made from other synthetic polymers. The dialyzer model will be connected to two pumps (one for substance to be filtered and one for dialysate). When used clinically, the dialyzer is used along with a dialysis machine that pumps blood and dialysate through the membrane. In observation of the basic components of the two models, there is no significant difference except the sizes of the units and that the internal unit houses all of its components. However, these *small* differences are what set the two apart considerably in terms of its convenience for the patient.

CONCLUSIONS

Problems:

While conducting this research a number of issues presented problems in our design. One of the major issues that had to be addressed was the introduction of the dialysate into the unit. Due to the large amount of dialysate that needs to be introduced daily (2 liters), it was difficult to determine where it would be stored. At first, it was decided to have a bag of dialysate within the body that would serve as the reservoir for dialysate introduction. However, we determined that a bag holding that much fluid would require too much space. As a result we decided to use insulin pump concepts to introduce dialysate. Another major issue that had arisen in our research was that of the location of the unit within the body. Upon deciding where in the body to place the unit, firm support and accessibility to major arteries, veins, and the bladder, had to be considered. Charles Jones (graduate student) determined that the most feasible location for the unit was the femur bone. Another problem that we faced in this research was the membrane fabrication. The hollow fiber configuration used in our model could not be fabricated in this lab, therefore we had to obtain a commercial dialyzer (Baxter International). Overall these problems didn't greatly hinder our conceptualization of this unit. In fact, these problems led us to more innovative ideas to be used in our design.

Suggestions for Future Research:

In conducting our research, we felt that certain issues that were not able to be addressed because of the time factor, should be considered for future research. Issues such as membrane durability within the unit, blood leaks and pump malfunction, and membrane fabrication should be addressed in order to improve on this idea. Also, surgical techniques should be considered when conducting this research. These issues, again, were unfortunately somewhat ignored due to time limitations, however they should be taken into account in further research.

References:

All information was obtained from various World Wide Web sites, and Shirley Clark, Head RN for the Dialysis Unit of Howard University Hospital.

REU Project Title:

Characterization of Polyethylene Wear Particles from Artificial Implants Using Atomic Force Microscopy

REU Intern, Major, Home Institution:

Catherine McPherson, Mechanical Engr, Princeton University

REU Principal Investigator, Dept, Institution:

Mohsen Mosleh, Mechanical Engineering, Howard University

REU Principal Investigator Email Address:

spencer@msrce.howard.edu

Abstract:

Previous study of the wear particles from artificial hip and knee implants has been performed to gain an understanding of the mechanisms that lead to failure. Atomic Force Microscopy has been used in this analysis. In order to gain a better simulation and understanding of implant wear which ultimately causes failure, it is necessary to gain not only topographic information on the wear particles, but information on the mechanical properties as well, such as hardness, adhesion and viscosity. Previous A.F.M. use has been limited to topographic data only. Different A.F.M. techniques have been researched examined and used in order to overcome this limitation. While the initial problem has been solved, research has uncovered previously unknown limitations that have yet to be resolved.

Introduction:

In artificial implants, the contact and continuous sliding motion between parts create small wear particles, which may be a life-terminating factor for the implant. These wear particles infect the surrounding tissue and cause a condition known as osteolysis. As a result of wear, cracks form and the implant may loosen, ultimately causing total failure. In order to improve the lifetime of these implants, an understanding of the wear mechanisms must be reached through a characterization and analysis of these wear particles.

In previous research, the implant has been simulated using distilled water as a lubricant. A small drop of the lubricant, containing wear particles, has been removed and deposited on a silicon wafer. After evaporation, the remains were analyzed using Atomic Force Microscopy. The conclusion was that the particles are mostly submicron in size. However, there are major limitations to the approach used for the analysis of the wear particles, which I have been trying to solve. Since only topographic data could be obtained, possible contamination may be mistaken for Polyethlylene particles. Also, water is really not a good model for the synovial fluid found in the joints of the body. Bovine serum would provide a better simulation, but contains proteins and long-chained molecules, which could be mistaken for wear particles using traditional A.F.M. techniques. I researched different A.F.M. techniques that would permit us to differentiate between phases, and to analyze mechanical properties of a substance, such as adhesion, hardness, and viscosity, thus being able to tell what is a wear particle, protein, long-chained molecule, or contamination.

A.F.M. Techniques:

In Contact Mode, I generated a number of Force/ Distance curves of different points on a surface. After the scan, this technique is used to measure forces on the A.F.M. tip as it approaches and retracts from the surface. The outcome is a plot of the deflection of the cantilever versus the extension of the piezo scanner, and gives insight into the mechanical properties at different points. If the lines are parallel, two different points have similar properties. A greater slope will imply a relatively greater hardness. A constant slope

indicates constant properties throughout the sample thickness. A change in slope implies a layer of contamination over the sample. If the approach and retraction follow the same line, there is no adhesion between the tip and the surface. A difference in the actual slope between approach and retraction give information on the plastic deformation of the sample. It is extremely important to remember that these results are relative to each other. A different tip will yield a similar pattern, but the actual numbers will be different.

In addition, there is a technique known as "Phase Imaging", which is an extension of the Tapping Mode. In this mode, the cantilever is oscillated at resonant frequency and scanned over the surface. When analyzed, there is a phase lag between the periodic signal, which are sent to drive the oscillation of the cantilever and the detected oscillation signals. Variation in the phase lag at different points on the surface reflects differences in viscosity along the surface. One is therefore able to tell differences in composition or phase. This may be executed in a few select spots by vibrating the surface and monitoring the phase lag yourself. This phase-imaging technique may be implemented into the software so that the phase image may be mapped simultaneously with topographic data throughout the scan.

Conclusions:

On top to typical problems with A.F.M., I have come across numerous problems and limitations. Initial characterization of the Polyethylene particles available in the lab showed them to be on the magnitude of 200 microns, which is TOO big to be scanned. Bovine serum features were also to big for the scanner, which had a 12-micron Z limit. I instead scanned samples of 3 micron Iron Oxide and 10 micron Aluminum Oxide in an epoxy matrix. This was very difficult because the epoxy mostly just coated the particles, making analysis nearly impossible. While frustrating, this also revealed a new problem: a lubricant such as bovine serum or synovial fluid will also coat the particles. With phase imaging, it will look like a ball of lubricant, rather than a wear particle coated with lubricant. With the Force/Distance curve, it may be possible to see that there is a layer of lubricant covering the targeted particle, but a characterization of its actual size will be impossible. While a deeper understanding of A.F.M. techniques for analysis of these wear particle has been gained, further work must be done in order to obtain accurate and true characterization of the particle from implant wear.

References:

"Influence of Sterilization Technique on Wear Particles", M. Mosleh, J. Eisenberg, N.P. Suh. Fifth World Biomaterials Congress, May 29-June 2, 1996.

"Wear Particles of Polyethylene in Biological Systems", M. Mosleh, N. Suh. Tribology Transactions, vol 39, 1996, p 843-848.

REU Project Title:

Blackbody Emission from Resistively Heated Thin Films of Silicon Carbide

REU Intern, Major, Home Institution:

Jeremiah Smith, Applied Physics, U of MD, Baltimore County

REU Principal Investigators, Dept, Institution:

Michael Spencer, James Lindasay, Materials Science Research Center of Excellence, Howard University

REU Principal Investigator Email Address:

spencer@msrce.howard.edu

Abstract:

In this experiment we examine the blackbody radiation properties of Silicon carbide. Thin films of silicon carbide are to be isolated and resistively heated. The intensity versus wavelength characteristics of Silicon carbide will be examined at various thicknesses. The incident angle dependence is also examined. Physical difficulties disallowed experimental verification of theoretically predicted tendencies. In particular, the manipulation of Silicon carbide films proved difficult.

Blackbody Radiation:

Blackbody radiation is a natural property of matter capable of occuring in all materials. The intensity of radiation is proportional to the temperature of the matter by the relationship $I = est^4$, where s is the Stephen Boltsman constant and e is the emissivity. Blackbody radiation occurs when a body is in thermal equilibrium [1]. Changing the thickness of a body effects its thermal characteristics and therefore should effect its blackbody radiation characteristics [2]. It is this relationship that is examined.

Experimental Details:

Thin films of Silicon carbide of thickness about 3 microns were grown of silicon wafers for use in the experiment. Nickel-gold was evaporated on the sample to make ohmic contacts for the applied current. 500 and 1000 micron thicknesses were used for the nickel and gold, respectively. The silicon was stripped from the silicon carbide by mechanical and chemical process, specifically sandblasting and etching in a HF : HNO_3 : H_2O solution. Extreme care must be taken in all phases of this process to minimize probability of sample fracture. For support the sample was temporarily bonded to a Pyrex slide during processing. Black tar was used for this temporary bonding and to protect areas not to be etched in the HF solution. After evaporation and etching silver epoxy was used to bond the processed sample to a slide for support. Once in this form, the sample is ready to be loaded into a small vacuum chamber for experimentation. The vacuum chamber is equipped with terminals capable of carrying current to the sample's contacts. It is also connected to a photo detector capable of measuring radiation emitted at different wavelengths.

Results:

Much difficulty was encountered in attempting to isolate the thin films of Silicon carbide for study. Silicon carbide of thickness around 25 microns was easy to work with, however these samples were not available after the technique for sample processing was developed. The samples used during the duration of the research were of thickness about three microns and were very difficult to work with. These samples were extremely weak and the Silicon carbide film had to be supported at all times. Convenienences such as blow-drying and tweezer handling were not possible with such fragile films. With extreme care and use of supporting structures, the problem of frailness of the

film could be overcome. Most of the films also exhibited geometrical stress fractures. These fractures were caused by the lattice spacing difference between silicon and silicon carbide and were worsened by the differential lattice expansions between silicon and Silicon carbide when the wafer is heated and cooled [3]. Despite much effort, this problem was never solved and no technique was developed to decrease probability of these inherent fractures occuring.

References:

[1] Physics for Scientists and Engineers, Fishbane, Gasiorowicz, and Thornton.

[2] Fundamentals of Statistical and Thermal Physics, Reif. F.

[3] Journal of Nuclear Science, R. B. Matthews, vol. 51, no. 2, pg. 203-208.

The Pennsylvania State University

Electronic Materials and Processing Research Lab

1998 REU Participants

REU Participant	Home Institution	Prinicipal Investigator
Front Row:		
Jackson Lee	Cornell University	Stephen Fonash
Mahima Santhanam	Boston University	Robert McGrath
Jeremy Rowlette	The Pennsylvania State University	Robert Davis
Glenn Deardorff	The Pennsylvania State University	David Allara
Back Row:		
Robert Davis	Director, EMPRL, PSU	
Andrzej Mieckowski	PSU Staff Engineer	
Isaiah Williams (No report given)	California State University Sacramento	Darrell Schlom

REU Project Title:

UV–Ozone Development Steps for Contrast Enhancement in Electron Lithography Using Ultrahigh Resolution Monolayer Resists

REU Intern, Major, Home Institution:

Glenn Deardorff, Chemistry, Pennsylvania State University

REU Principal Investigator, Dept, Institution:

David Allara, Chemistry and Materials Science, Pennsylvania State University

REU Principal Investigator Email Address:

dla3@email.psu.edu

Abstract:

An IR spectrometer was calibrated to conduct real time measurements of the chemical changes occurring during UV-ozone treatment of octadecylsiloxane (ODS) self-assembled monolayer (SAM) resists on Si wafers before and after e-beam doses typical for lithography. High quality ODS films were prepared in a controlled humidity chamber. Preliminary studies of e-beam damage were conducted using an SEM and associated problems were identified. A cell was built for use in the IR instrument, but actual runs were not able to be completed during the project time.

Introduction:

Previous work, in collaboration with H. Craighead (Cornell NNUN facility), has shown that a UV-ozone development step can improve etch contrast in e-beam patterning of Si using SAM resists [1]. Currently, the resolution available in lithography using polymer resists is limited by the range of scattered electrons in the resist (so called "proximity effects"). Scanned low-energy beams reduce these effects but result in a shorter electron range in the resist. ODS SAMs have been shown to yield feature sizes as small as 5 nm. Also, as these monolayers have a thickness on the order of 25 Å, the shorter electron range present with low-energy beams is not a problem. Monolayers in general are densely packed, highly organized, can be prepared in a reproducible manner, and are stable. Thus, they would make an ideal substitute for current polymer resists.

Fundamental studies of e-beam damage in ultrathin layer resists were done by D. Allara and K. Seshadri of Penn State and H. Craighead and M. Lercel of Cornell [2]. They determined that electrons striking the ODS molecules broke C-H bonds, causing the carbon atoms to form double and triple bonds with each other. Thus, the irradiated portion of the monolayer becomes more carbonaceous. This damaged area is more susceptible to the attack of a gas-phase oxidant like O_3, which removes the carbonaceous deposit, leaving a bare area in the monolayer. Since O_3 works slower on the undamaged portions of the monolayer, one is left with a mask formed of ODS molecules. As the SiO_2 layer on the target wafer can be attacked immediately by hydrofluoric acid, a quick dip will now yield an improved etch contrast [3].

The prior UV-ozone development studies involved the repeated halting of the process for characterization purposes. This continuation of the project was done in order to conduct real time studies on the UV-O_3 step, that is to leave the wafer in constant contact with the O_3 environment. Analysis of the resulting spectra would show if the carbonaceous deposit was removed linearly (i.e. at a constant rate).

Experimental Procedures:

In a chamber maintained at 15 to 20 % humidity, an ODS solution consisting of 40 mL of anhyd hexadecane, 10 mL of anhyd CCl_4, and 50 mL of vacuum-distilled octadecyltrichlorosilane (OTS), was

prepared. A double-sided polished, IR-grade (111) silicon wafer, previously cleaned using a combination of sonication, UV-O_3, and "piranha wash" (H_2O_2 + H_2SO_4), was placed into the ODS, with the monolayer forming in 20 to 90 min. The presence of the monolayer was confirmed by observing that the wafer completely repelled the solvent when taken out of the solution. The wafer was sonicated in CCl_4, and was characterized using ellipsometry (26 Å) and water (114°) and hexadecane (43°) contact angles. Infrared spectroscopy was performed in the transmission mode using a Bruker Vector 22 instrument. Spectra were recorded for blank wafers with no surface film other than native oxide.

To assure that a similar area on both sides of the wafer could be analyzed after irradiation, an aluminum foil covering was placed over the wafer, exposing a 1 cm x 1 cm area on each side. A dosage of 180 mC was delivered to the exposed area on each side of the wafer using a SEM with a probe current of 1 mA. The wafers were then rinsed with acetone and ethanol and were characterized as before. Prepared wafers were also irradiated with dosages of 490, 800, and 3600 mC/cm^2.

Results and Conclusions:

The spectra of the initial ODS films reproduced the earlier results [2,3]. The figure shows a typical spectrum. For all of the wafers, characterization of the irradiated areas did not show the expected behavior. While the hexadecane contact angle dropped below 10°, as expected, the water contact angle remained high (over 100°, versus the expected sub-90° result). Since the wafers were exposed to doses consistent with previous work, the changes must have been due to the sources. Perhaps the difference arises from different contamination levels in the two experiments. Further studies in which a PMMA-coated wafer was irradiated in a similar manner to that outlined above were planned to check the reproducibility with this well-known resist.

References:

[1] "Self-assembled monolayer electron-beam resists on GaAs and SiO_2", M. J. Lercel, R. C. Tiberio, P. F. Chapman, H. G. Craighead, C. W. Sheen, A. N. Parikh, and D.L. Allara, J. Vac. Sci. Technol. B 11(6), Nov/Dec 1993.

[2] "Electron-Beam-Induced Damage in Self-Assembled Monolayers", K. Seshadri, K. Froyd, A. N. Parikh, D. L. Allara, M. J. Lercel, and H. G. Craighead, J. Phys. Chem., v. 100, pp. 15900-15909, 1996.

[3] Kannan Seshadri, PhD Thesis, Pennsylvania State University, Spring 1998.

REU Project Title:

An Approach to Electron–Beam Induced Non–Epitaxial Crystallization of Amorphous Si Thin Films

REU Intern, Major, Home Institution:

Jackson Lee, Electrical Engineering, Cornell University

REU Principal Investigator, Dept, Institution:

Stephen Fonash, EMPRL, Penn State University

REU Principal Investigator Email Address:

Fonash@emprl.psu.edu

Abstract:

While most e-beam crystallization experiments have dealt with the solid-phase epitaxial crystallization of amorphous zones created in single crystal Si films, our research focused on studying the direct crystallization of PECVD amorphous Si films on glass, specifically Corning 7059. We used 50 keV electron energy in our experimentation, which is significantly lower than electron energy levels used in most earlier work, and found the a-Si samples had to be dehydrogenated for successful crystallization. We also used a wider matrix of current densities and dosages than previously reported. By using a Leica EBPG5-HR e-beam writer, we produced an array of 0.5 micron diameter crystallized spots separated by 10 microns. After distinguishing crystallized areas through tests in reflectance and transmission, SEM pictures and profilometer readings proved the topography of the spots to be elevated, possibly due to heating of the glass substrate. Electron-beam induced crystallization of materials is a subject that has received much attention in the last several years due to its application in making selected area crystallized regions. With the crystallized spots produced, there is a potential of creating microsized areas in which electronic devices can be built and of creating seeds to control nucleation in solid-phase crystallization. The latter can be used to make larger grains and grain boundaries smaller, which help in lowering intragrain defect density and providing better stability and higher carrier mobilities.

Introduction:

Over the last few years, the crystallization of amorphous Si precursor films to create polycrystalline Si has been extensively studied due to its potential in providing materials for electronic devices, with its high carrier mobilities, potential of good stability, low intragrain defect density, and high doping efficiency when compared to amorphous Si. However, in crystallizing amorphous Si, many problems occur, the most important ones being thermal budget, crystallization time, and grain growth in nucleation. Whereas thermal budget and crystallization time have been reduced due to such advancements as metal induction, grain growth and the development of granular regions are especially important for higher carrier ability and good stability. Due to these problematic areas, different processes for crystallizing Si have been developed. Two of these processes, furnace annealing and rapid thermal annealing, have dealt with the heating of entire Si films, while two others, laser annealing and e-beam crystallization, have dealt with the crystallization of specific areas on a Si film.

E-beam crystallization is different than laser annealing in a few major aspects, such as the fact that e-beam crystallization operates at lower power densities and produces larger grains. [1] In the process of e-beam crystallization, there have been two main factions, one dealing with zone melting crystallization with a low energy e-beam causing heating, and the other dealing with the creation of point defects at an amorphous – crystalline interface on epitaxial Si films. Zone melting crystallization is achieved with rapid

thermal processing caused by a line electron beam operating at voltages that range between 6 - 15 keV. [2] In contrast, solid-phase epitaxial crystallization of Si films is generally induced with a TEM e-beam irradiation operating from 80 to 300 keV. [3] This crystallization occurs at the atomic level with the migration of the a-c interface due to point defects created by the nuclear elastic collisions stimulated by electrons. Also, in order for the creation of point defects to occur, a high dosage must be used, usually in the order of 10^5 C/cm^2. In this project, with the purposes of controlling nucleation or crystallization and of hopefully creating microsized areas for TFT devices and solar cells, we report on the use of electrons to induce crystallization of amorphous silicon in a process different from the two previously mentioned.

Procedure:

Amorphous silicon samples were prepared through plasma enhanced chemical vapor deposition at 170 degrees of amorphous hydrogenated Si on Corning 7059 glass substrates until a thickness of 1000 Angstroms was reached. A sample was treated with a Leica EBPG5-HR e-beam writer operating at 50 keV to create a pattern of 400 by 400 spots with a spot diameter of 0.5 microns. The current was approximately 1000 nA, with a spot size of 0.5 microns, and a dosage of 1,000,000 μC/cm^2. With the help of an optical microscope to look at reflectance patterns, it appeared that 'crystallization' was observed in the spots exposed. In order to prove crystallization, this dehydrogenated pattern was exposed to UV light at 237 nanometers and reflectance was measured.

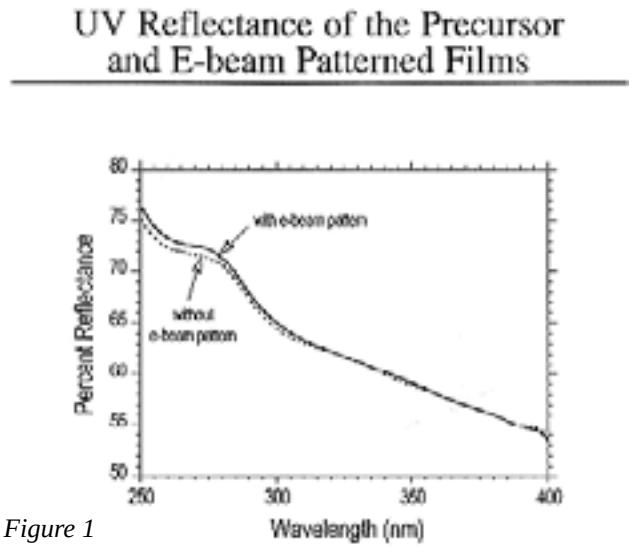

Figure 1

Cracks were also observed along with the patterns seemingly being crystallized, and led to the dehydrogenation of amorphous Si film in a furnace for 1 hour at 600 degrees, to test the effect of hydrogen in the films. Next, the pattern was reproduced on two a-Si films, one hydrogenated, and another dehydrogenated, and it was observed that hydrogen seemed to cause the cracks in the Si film. The dehydrogenated sample was placed under a Leica 440 scanning electron microscope, and protrusions were observed. This was verified with the use of an Alpha-Step Model 500 surface profilometer.

The dehydrogenated Si sample, with the 'crystallized' pattern on it, was then annealed at 680 degrees for 8 minutes. This temperature and time was used because of a previous test which used a regular amorphous Si sample as a control, and at 8 minutes, the film was about 80 percent crystallized. Next, the e-beam current and dosage parameters were changed, and a threshold was observed at 1000 nA, and 200,000 μC/cm^2.

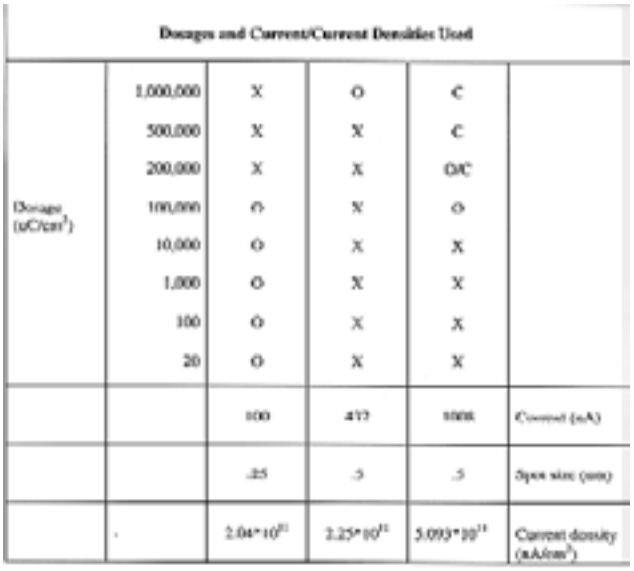

X - test not attempted
O - test not successful in crystallization
C - test successful in crystallization
O/C - test not successful in crystallization, successful in creating hills

Figure 2

Though no pattern became visibly crystallized, on the 200,000 μC/cm^2 sample, spots were still observed, and crystallization occurred at the dosage of 500,000 μC/cm^2. Finally, regular Corning 7059 glass was exposed under the e-beam with 1,000,000 μC/cm^2 dose at 1000 nA to help elucidate the effects of e-beam exposure on the glass substrate.

Summary:

With the different dosages and current / current densities tested, a threshold in the dosage and current needed for crystallization in the sample could be considered. That dosage, analyzed to be around 200,000 μC/cm^2 for a 1000 nA beam, is much smaller than dosages commonly used for the creation of point defects in epitaxial crystallization. Also, the only successful crystallization in varying currents and current densities occurred at 1000 nA, or 5.093x10^{11} nA/cm^2, which is significantly higher than current densities recorded in previous work for either high energy epitaxial crystallization or low energy zone melting crystallization. The fact that the energy used in this experiment was 50 keV as opposed to 6 - 15 keV used in zone melting crystallization and 100-300 keV generally used in point defect crystallization indicates that neither process previously documented is the case in this experiment.

The cracks appearing on the hydrogenated Si film seem to be due to hydrogen evolution of the original Si:H sample, which indicates heating at some point in the sample. Along with this hydrogen evolution, SEM pictures show that the actual crystallized spots seemed to be protruding from the surface of the film, as shown by images of 58.5 and 80 degrees tilt.

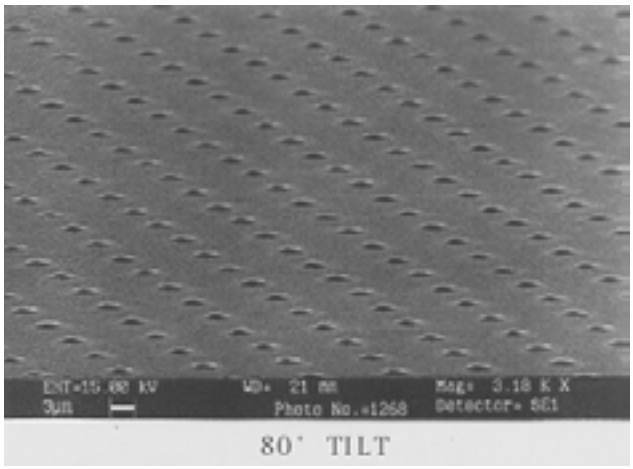

Figure 3

Profilometer readings for 1,000,000, 500,000, and 200,000 dose arrays show the elevated areas to be around 4000 - 6000, 2000 - 3000, and 600 - 800 Angstroms high respectively. However, due to the curve-like shape of these 'hills' created, these measurements, unless luckily measured at the exact center of each spot, is less than the actual height of each spot. By making a comparison to the actual diameter and measured diameter of each spot and measuring the height of the spot at 80 degrees tilt on the SEM picture, the law of sines can be used to estimate the height of each spot to be around 6770 Angstroms high for a 1,000,000 μC/cm^2 dose array. The profilometer readings are useful in suggesting growth in height, however, and with pictures taken with an optical microscope, it is obvious that the hills increase in diameter as well as in height. For the 200,000 μC/cm^2 pattern, even though no crystallization was actually observed, the pattern is still easily visible with an optical microscope. Accordingly, when the glass substrate is exposed to e-beam treatment at 1,000,000 μC/cm^2 dosage, with an optical microscope it is clearly evident that these hills in fact form in the glass substrate, as opposed to the Si film. Also, profilometer readings show that the glass substrate had 'hills' of at least 3000 - 4000 Angstroms, which demonstrate similar readings as in the crystallized 1,000,000 μC/cm^2 Si film.

In theorizing the mechanism of crystallization, first, previous work must be analyzed. Since the dosage in our work is much lower than previous e-beam experiments, it makes the creation of point defects impossible in our case. Also, in previous work, a threshold of 80 keV has been theorized as the energy needed for solid-phase crystallization to occur through point defects of thin films, which again proves the point. [4] For the case of rapid thermal processing, or the actual heating of the Si film with the e-beam, with a variation of Bethes' stopping formula, the maximum temperature change is 33.4°C, which is surely negligible in crystallizing Si thin films, and thus disproves the case of the e-beam annealing the Si film. And since even without the Si film, the protrusions are visible through observation with an optical microscope, it is then speculated that the actual heating of the glass substrate causes the protrusions and with the right current density and dosage, causes crystallization of the Si film covering the glass substrate.

In annealing one of the dehydrogenated Si samples exposed with a dosage of 1,000,000 μC/cm^2, the spots do not appear to grow much in diameter. However, the regular crystallization of the amorphous Si film remaining seems to center around the spots exposed by the e-beam, which indicates possible control over grain nucleation and growth with this process.

Applications:

The most important application of this research is the possible use of the protrusions created on a glass substrate by an e-beam to produce patterns for nanoprinting. By using a pattern-creating program along with an e-beam writer at the right parameters, a mask can be created without the use of lithography and etching. With the protruded patterned surface, any metal can be deposited onto the glass substrate through evaporation, and thus, the steps of lithography and stripping of the metal are unnecessary and avoided. Since, in this research, the 'hills' created seemed to have a reasonable height of at least 3000 - 4000 Angstroms, and due to the fact that it appears controllable, it is conceivable to create metal masks with specific patterns on it by simply exposing a glass substrate to an energetic electron beam. Another application is the controlled nucleation of certain areas of an amorphous Si thin film by using an electron beam to seed grains. Since annealing causes crystallization around the spots exposed, specific patterns can be produced on a thin film to contain the grain growth of crystalline Si to certain areas, and also for the possible reduction of grain boundaries. Along with that point, by using a higher dosage, in the magnitude of 10^6 uC/cm^2, a whole selective area can actually be crystallized, which is useful, if a specific crystallized pattern or area is needed on an a-Si film to create TFTs and solar cells. With this process, the energy can remain at relatively lower levels, around 50 keV, rather than the high energies (100 - 300 keV) needed to induce point defect solid-phase epitaxial crystallization. Next, textured glass surfaces can be created by using an e-beam exposure. Since 'hills' were created in this experiment, the possibility of creating a textured surface is practical. With this process of e-beam induced protrusion, this surface, with optical absorption due to light trapping properties, is useful and often used in the creation of solar cells and photodetectors.

References:

[1] M. Pauli, G, Dahn, and J. Muller, "Comparison of laser and line-electron beam recrystallization of thin polycrystalline silicon films", Applied Surface Science 54 (1992), pp. 386-391.

[2] M. Pauli, M. Doscher, and J. Muller, "Zone Melting Crystallization of Silicon Films of Graphite Substrates", 11th E.C. Photvoltaic Solar Energy Conference (1992), pp. 525-528.

[3] I. Jencic, M. W. Bench, I. M. Robertson, and M. A. Kirk, "Electron-beam-induced crystallization of isolated amorphous regions in Si, Ge, GaP, and GaAs", J. Appl, Phys. 78 (2) (1995), pp. 974-982.

[4] M. W. Bench, I. M. Robertson, and M. A. Kirk, "Energetic Electron Beam Induced Recrystallization of Ion Implantation Damage in Semiconductors", Mat. Res. Soc. Symp. Proc. Vol. 235 (1992), pp. 27-32.

REU Project Title:

High–Resolution Dry Etching of Si–Based Dielectrics Using a Chemically Amplified Electron–Beam Resist

REU Intern, Major, Home Institution:

Jeremy Rowlette, Electrical Engr, Pennsylvania State Univ

REU Principal Investigator, Dept, Institution:

Robert Davis, Applied Research Laboratory, Pennsylvania State University

REU Principal Investigator Email Address:

rjdavis@emprl.psu.edu

Abstract:

As feature sizes in modern ICs shrink into the submicron (nanometer) range, reactive ion etching (RIE) processes are complicated by phenomena such as molecular transport, ion angular distribution effects, and image potential effects, among others. This project explores the etching of deep submicron trenches in spin-on-glass and silicon nitride using the combination of direct-write electron beam lithography and magnetically enhanced reactive ion etching (ME-RIE). In our process we explore the use of Shipley's XP8943 e-beam resist, a negative tone, novalk-based, chemically amplified resist, for the patterning of deep submicron features.

Introduction:

With the advent of ultra-large-scale integration (ULSI), feature sizes in modern integrated circuits have steadily reduced far into the nanometer range. This reduction in minimum feature size below the one micrometer threshold has brought with it significant complications in pattern transfer techniques requiring reactive ion etch (RIE) processes. Such phenomena as molecular transport, ion angular distribution effects, and image potential effects become more apparent in the submicron range resulting in etch rates and etch profiles that are strongly dependent upon such factors as absolute feature size, aspect ratio, and pattern density [1] [2] [3]. In the manufacturing of application-specific integrated circuits (ASICs) where process parameters are subjected to a wide range of design specifications, the development of new RIE processes can be costly and time consuming. Thus a greater understanding in the relationship between etch rates and etch profiles on such factors as absolute feature size, aspect ratio, and pattern density at the submicron level is extremely valuable to the microelectronics industry.

This project studies the effects of such phenomena in the etching of deep submicron trenches in spin-on-glass (SOG) and Si_3N_4. The etching of submicron trenches and vias in Si-based dielectrics will provide a basis for creating multi-layer copper interconnects in high-density microelectronics [4].

Experimental Procedure:

5" Silicon wafers were used as substrates for the multiple layering of Filmtronics 300F spin-on-glass (SOG). As much as three layers of SOG were deposited with each layer having an average thickness of 1400 A upon final curing. In addition, 4" Silicon wafers with 1100 A of Si_3N_4 deposited using Plasma-Enhanced Chemical Vapor Deposition (PE-CVD) were obtained. Trench patterns were generated using L-Edit software and were converted to GDS file format for direct-write electron beam lithography. Both the SOG wafers and Si_3N_4 wafers were cleaved into 36mm x 36mm samples and coated with Shipley XP8943 negative tone, novolak based e-beam resist. The XP8943 resist and substrate were spun at a rate of 4000 rpm for 40 sec yielding an 1850 A resist film thickness. The sample was soft-baked at a temperature of 106° C. The resist was then exposed with a 25 nm beam at 50 KeVand a current density of 15 $\mu C/cm^2$ using a Leica EBPG-5 beam-writer. Samples were then baked at 115°C for 60 seconds immediately following exposure. The post exposure bake thermally activates an acid catalyst that

promotes cross-linking of the resist polymers. Samples were developed in a 1:1solution of Shipley's 312 Developer and DI water. Patterns were then transferred into the underlying dielectric film using an Applied Materials P5000 magnetically enhanced reactive ion etch (ME-RIE) system with CHF_3/Ar gas chemistries with a 1:1 ratio at 70sccm for 120sec. RF power and magnetic enhancement were maintained at 600 W and 80 G respectively. Samples were then coated with approximately 90 A of Gold and cleaved along crystal planes running normal to the trench orientations. Trench profiles were then viewed under a scanning electron microscope.

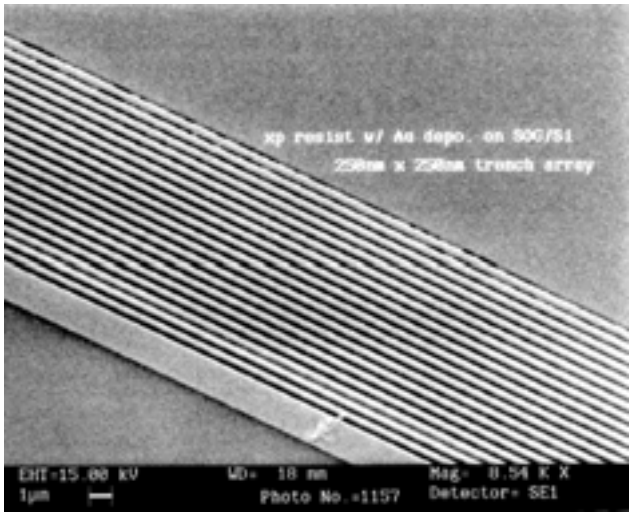

Figure 1. SEM image of 250 nm trenches in XP8943 e-beam resist on SOG after development and prior to ME-RIE processing

Results and Conclusions:

Significant progress was made in the process development and characterization of Shipley's XP8943 e-beam resist. This novalak-based chemically amplified resist was found to have excellent resolution down to 100 nm and exceptional stability in hydrocarbon/ argon RIE plasmas. The robust nature of the resist resulting from acid-enhanced polymer cross-linking allowed for deep sub-micron etching without the need of metal deposition and subsequent lift-off methods. However, due to it's stability in plasma chemistries and it's resistance to typical removal chemicals, lengthy oxygen plasma etches were required in the removal of the resist. The resist was found to have exceptional resolution when exposed with a 25 nm beam at 50 KeV and a exposure dose of 15 $\mu C/ cm^2$.

SEM images were taken of trench profiles along with other feature patterns etched into the underlying dielectric films (SOG and Si_3N_4). Figure 2 shows a sample with 250 nm x 250 nm crosshatching etched into a Si_3N_4 film. Further SEM analysis is necessary to accurately determine the dependence of etch rates on the various trench dimensions and trench densities.

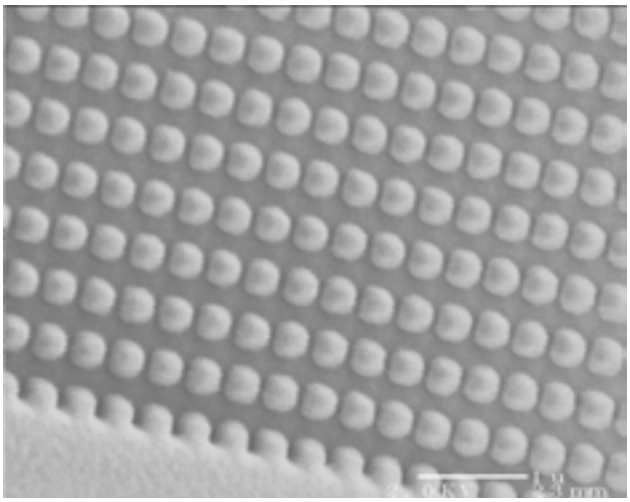

Figure 2. SEM image showing 250 nm x 250 nm crosshatching etched into Si_3N_4 film using Applied Materials P5000 ME-RIE system

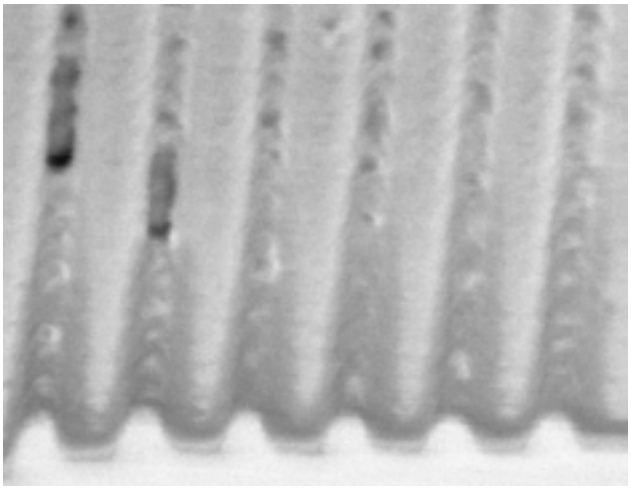

Figure 3. SEM image of 150 nm wide trench profiles etched into Si_3N_4 film

References:

[1] J.W. Coburn and Harold F. Winters, Appl. Phys. Lett., Vol. 55, No. 26, 2730 (1989).

[2] Richard A. Gottscho and C. W. Jurgensen, J. Vac. Sci. Technology. B 10(5), 2133 (1992).

[3] S. Ohki, M. Oda, H. Akiya, and T. Shibata, J. Vac. Sci. Technol. B 5(6), 1611 (1987).

[4] Z. J. Radzimski, W. M. Posadowski, S. M. Rossnagel, and S. Shingubara, J. Vac. Sci. Technol. B 16(3), 1102 (1998).

REU Project Title:

Etching of SiO_2 High Aspect Ratio Trenches

REU Intern, Major, Home Institution:

Mahima Santhanam, Biomedical Engr, Boston University

REU Principal Investigator, Dept, Institution:

Robert McGrath, Materials Science & Engr, The Pennsylvania State University

REU Principal Investigator Email Address:

mcgrath@engr.psu.edu

Abstract:

Reactive ion etching (RIE) was used to etch high aspect ratio trenches on silicon dioxide substrates. Reactive ion etch tools provide highly directional (anisotropic) ion fluxes for definition of high-aspect-ratio features used in integrated circuit manufacturing. A computer aided design (CAD) program was used to define various patterns for both photolithography and direct-write electron beam lithography masks. Patterns defined contained trenches 2 mm in length so as to allow for easy subsequent analysis of the trenches that were etched. With photo-lithography, trench widths were varied from 2000 nm to 250 nm. After transferring the initial pattern to a photoresist covered SiO_2 wafer, the wafer was etched in an Applied Materials ME-RIE tool operating with a CHF_3 gas discharge. Subsequent to the etch step, samples were placed in a scanning profilometer for measurement of SiO_2 etch rate and etch rate selectivity to resist. Etch times were varied between 30 and 120 seconds, and the SiO_2 etch rate was measured to be ~1000 Å/min.

Experimental Procedure:

Silicon wafers (6 inches in diameter) covered with a 2000 Å oxide blanket layer were used to pattern high aspect ratio trenches using photolithography and electron beam lithography. A pattern was produced using CAD techniques with trenches varying in size from 2μm to .25μm in width. The wafer was then coated with a standard, Shipley 1813 photoresist before the pattern was transferred onto the wafer using photolithography. The SiO_2 wafer was then scribed and cleaved into several smaller pieces before being placed in the RIE tool. The RIE tool operated with a CHF_3 gas discharge. Several etch parameters were altered in efforts to vary the etch rates. The etch parameters that were varied included time, power and pressure. Subsequent to etching, the resist was stripped from the wafer samples by dipping them in acetone and running it through a sonicator. Next, the wafer pieces were examined under the profilometer in order to measure the etch depths. Some of the wafer samples were also scribed and cleaved by hand, coated in gold and examined under the SEM for trench definition.

SiO_2 wafers were also used to perform direct-write

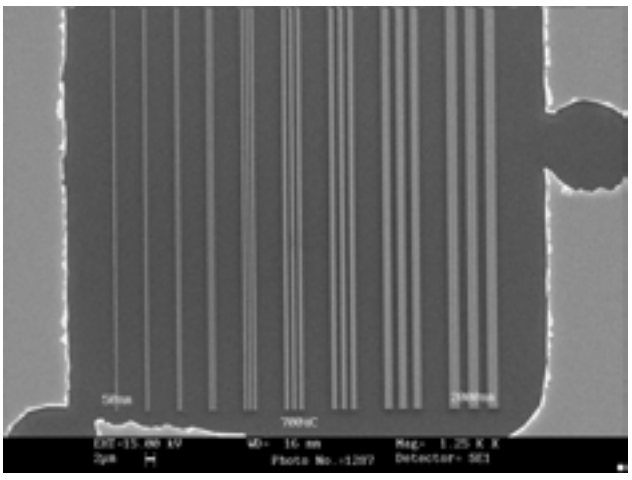

Figure 1: SEM image of trenches of varying widths resulting from direct write E-beam Lithography

electron beam lithography. The SiO_2 wafers were coated with a standard 3% PMMA resist. The trench pattern for this procedure was slightly different from that of the photolithography step.

The trench sizes varied in width from 2000 nm to 50 nm. A dose array, as seen in figure #1, was created to detemine the best charge and energy deposition per unit area for optimal resolution. These samples were also placed in the RIE tool for etching.

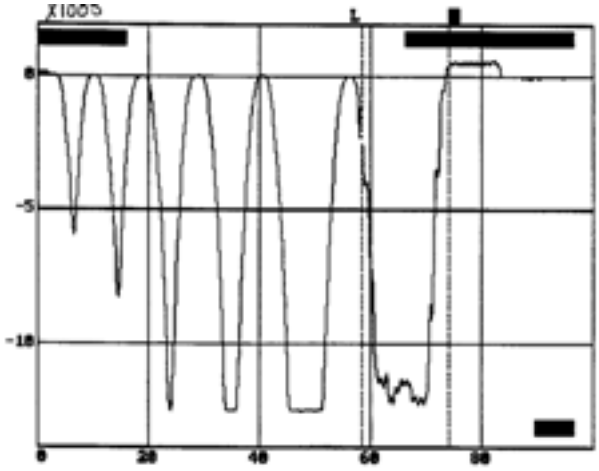

Figure 2: Profilometric measurements of trench depths after RIE etch.

Results and Conclusions:

Pattern transfer using photolithography did not produce the most refined features. This was possibly due to problems in the exposure and development times of the SiO_2 wafer. But, after careful examination under the profilometer (as seen in figure #2), an average etch depth of approximately 1000 Å/min was noticed.

Variation of time, power and pressure provided insight into the workings of the RIE tool. Errors in pattern transfer resulted in the loss of patterns after stripping the resist off of some of the wafers.

Electron beam lithography proved to be an efficient method for directly writing fine line features on a wafer. The dose array showed that beam energies in the region of 675-800mC/cm^2 provided the best resolution. It was noticed that the trench lines 75 and 50 nm in width proved to stretch the limits of the e-beam tool.

Further work is intended to perfect the methods of pattern transfer and plasma etch in order to obtain smaller and more refined features with a greater etch depth.

Stanford NanoFabrication Facility

1998 REU Participants

REU Participant	Home Institution	Prinicipal Investigator
Front Row:		
Sam Bishop	University of Washington	James Harris
Blair Irwin	Princeton University	Mary Tang
Kyndall Barry	Bethune-Cookman	Jim Gibbons / Judy Hoyt
Phyllis Chen	California Technology	James Plummer / Mike Deal
Chancy Schulte	Swarthmore College	Blas Cabrera
Yuri Dancik	Princeton University	James Plummer / Peter Griffin
Middle Row:		
Nin Loh	Pomona College	Krishna Saraswat / James McVittie
Tanja Cuk	Princeton University	Rick Kiehl
Joe Altepeter	Washington University	James Plummer / Peter Griffin
Ashish Ahuja	Columbia University	Shan Wang
Adam MacBeth	Swarthmore College	James Harris
Corina-Elena Tanasa	Bard College	Mark McCord
Back Row:		
Mike Deal	SNF Staff	
Mary Tang	SNF Staff	

REU Project Title:

Fabrication of Sub-Micron Spin-Dependent Tunneling Junctions Using E-Beam Lithography

REU Intern, Major, Home Institution:

Ashish Ahuja, Dept of Applied Physics, Columbia University

REU Principal Investigators, Dept, Institution:

Manish Sharma, Department of Electrical Engr,
Shan Wang, Dept of Mat Sci and Engr, Stanford University

REU Principal Investigator Email Address:

plummer@ee.stanford.edu

Abstract:

Using a soft ferromagnet/dielectric/hard ferromagnet structure it is possible to take advantage of an effect called spin-dependent tunneling (SDT) to give relatively high MagnetoResistive (20%) effects. A bilayer process has been optimized so that the lead/SDT junction contact area is minimized. By using SNR-200 negative photoresist and PMGI SF6 positive resist, 0.4 micron junctions with sufficient throughput have been fabricated with the specified procedure.

Introduction:

In today's memory cells, a continual read/write refreshing process is used in order for data to be stored for sufficient periods of time. In an effort to produce more reliable memory devices, SDT junctions provide non-volatile memory. The large observed MR effects also allow SDT junctions to serve as read heads in magnetic recording devices. Both of these applications are possible due to the unique method of electron transport within the device.

By using two ferromagnet films which differ in their coercivities it is possible to change the magnetization of one magnet with an external magnetic field while leaving the other relatively constant. This control of the "density of states" allows for control of the tunneling current. When the two magnets have parallel spin orientation, for example, and a sufficient voltage is applied, the tunneling current across the barrier is maximized. It is at this time that the ferromagnet on one side of the barrier has enough "space" for the majority spin electrons from the other side of the barrier and tunneling is allowed.

Process:

In processing the SDT devices control of the feature sizes was crucial in order to (1) minimize the contact area between the actual junction and the lead and (2) to prevent electron conduction through the barrier via pinholes and other defects. A bilayer process with SNR-200 negative DUV resist and PMGI SF6 positive resist was used. By taking advantage of the different etch rates of the two layers the desired undercut was achieved.

Using silicon <100> wafers, the PMGI was spun on first at 7000 rpm for 60 seconds giving a thickness of 2500 angstroms. (Although in making the actual devices the resist would be spun on the ferromagnet/dielectric/ferromagnet SDT structure, for our experimental purposes we were able to spin directly on the Si wafer.) The softbake was then done on a hotplate for 120 seconds at 250°C. The SNR-200 was then thinned with type P thinner and spun on at 4000 rpm's also for 60 seconds. The wafer was baked for 120 seconds at 110 degrees C.

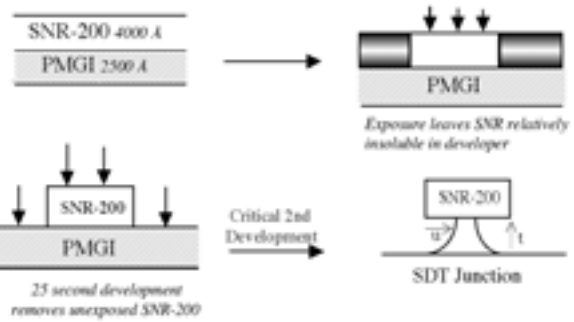

figure 1

The first exposure was done using electron beam lithography techniques (Figure 1). A dosage of 5 microCoulombs/cm^2 was used. Etching of the SNR-200 layer was done in CD-14 for 25 seconds. The second PMGI exposure was then done with a deep UV lamp and an exposure dose of 96.

The crucial step of etching the underlying PMGI was then done. It was important to maximize the undercut while still keeping the structure stable so that it did not lift-off entirely. This constituted the primary part of our investigation.

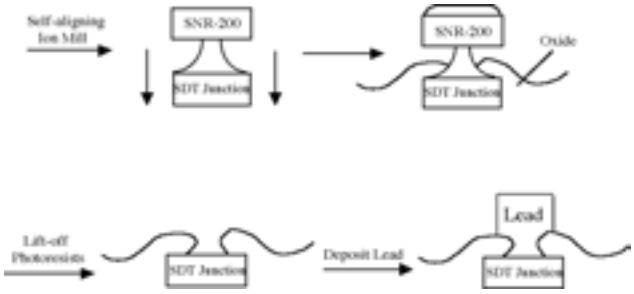

Figure 2 shows how the actual SDT junction joins with the upper lead so that a device can be completed and a voltage can be applied. Here, it is possible to see why such a structure and undercut was necessary in the first place.

A self-aligning ion mill is done to etch out the junction area. It is self-aligning because it will automatically align the junction with the original SNR block saving an alignment step. After this an oxide will be deposited, as shown, and the resist layers will be lifted off. Finally, the lead itself will be deposited. Because the final contact area between the lead and the junction is the major controlling parameter in terms of how small the SDT junction itself can be, it is clear why the undercut size was of utmost importance.

Results and Conclusion:

Boxes and lines 0.4 microns on a side with sufficient undercut and good throughput have been achieved (figure 3). Using the specified process, actual devices will be fabricated and characterized by testing the MR effects. The process itself will also be further developed in an effort to obtain 0.2 micron junctions. (For example, a thinner PMGI with less solvent content may be used.) Finally, the junctions will allow the study of switching in ultra-small magnetic devices.

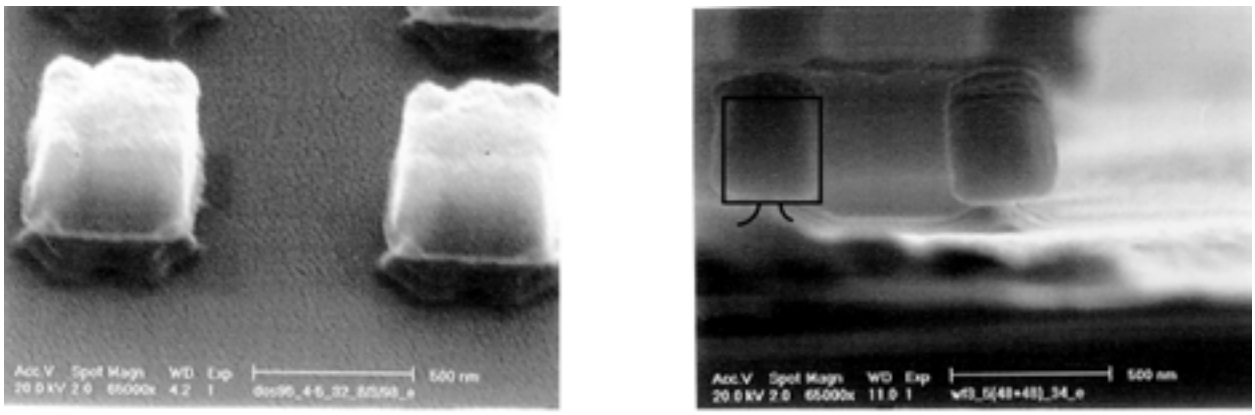

0.4 micron boxes and lines with undercut

figure 3

REU Project Title:

Inducing Protein Crystallization Using the Electric Field from an Atomic Force Microscope

REU Intern, Major, Home Institution:

Joe Altepeter, Physics, Washington University

REU Principal Investigator, Dept, Institution:

Peter Griffin, Stanford University

REU Principal Investigator Email Address:

griff@cascade.stanford.edu

Abstract:

The goal of this project was to deliberately induce the crystallization of proteins in solution. Crystallized proteins of sufficient size can be studied using x-ray diffraction. While conventional methods have some success in crystallizing proteins, the methods are unreliable and ineffective in many cases. The driving theory behind our approach to crystallization is that an electric field may have some effect on the highly polar protein molecules and promote spontaneous crystallization. The primary tool used to both study protein growth and apply the electric field was the Atomic Force Microscope (AFM). Due to lack of time, the results of these trials were inconclusive.

Introduction:

A crystal is an ordered array of atoms or molecules in a three-dimensional repeating structure. More specifically, a protein crystal is an ordered array of protein molecules, stabilized by the polar charges of the proteins. These protein molecules are quite large (on the order of 100 Å), and do not easily begin crystallization in many cases. In almost all cases, however, it is trivial to promote continued crystallization once an initial crystal seed is added to a solution of uncrystallized proteins. This initial crystal nucleus is formed by the collision of several protein molecules at the correct angle and under the correct conditions for crystallization. This initial nucleation is currently performed by adding a number of proteins to a solution at an experimentally determined ideal pH and hoping for the necessary collisions to occur. This random method leads to results that are difficult to reproduce or unsuccessful. It is for this reason that a deliberate method of protein crystallization would be useful.

Protein molecules are the building blocks of living structures, and it is important to find the geometry and structure of many protein molecules. The primary method used today to investigate this structure is x-ray diffraction which requires a protein crystal of sufficient size to function correctly. X-ray diffraction functions on the basic principle of Bragg's Law of Diffraction: $\lambda = 2d \sin\theta$ (d = spacing in the crystal lattice, λ = wavelength of the x-rays, θ = angle of incidence with which the x-rays strike the lattice surface). By varying the wavelength of x-rays used and the angle of incidence, researchers can find the spacing d between a simple crystal lattice. (When the equation above is satisfied, a diffraction pattern appears on a detector.) While this equation results from a simple lattice using point molecules or a regular array of identical holes, the same mathematical theory can be applied to discover information about more complex molecules, such as proteins.

To test our alternate method of protein crystallization, we decided to use the AFM. The AFM is not only a superb imaging tool with sub-nanometer resolution, it is capable of applying a reproducible, controllable, and localized voltage. AFM imaging is based on the intuitive concept of dragging a point across a surface and measuring the change in height based on the deflection of the point. In the AFM, this tip is commonly Silicon Nitride and oxide sharpened. At

the point, it has a radius of 10 - 25 nm. This tip is attached to the underside of a 10 micron by 25 micron rectangular cantilever, which is dragged across the surface with the tip in actual contact.

As the tip is pushed up "hills" or drops into "valleys" on the surface, the angle of the cantilever changes. A laser from above the cantilever is constantly being reflected from the its upper side to a photodetector. This photodetector registers the change in height through the change in laser deflection.

The method of AFM imaging described above is called contact mode, as the tip actually touches the surface for the duration of the scan. Unfortunately, many softer materials are destroyed or damaged during scanning because of the force of the tip dragging across the surface. Tapping mode is a less destructive alternative. Using this method the cantilever is oscillated vertically at a resonant frequency. At the low end of the oscillation, minuscule forces can be detected without destructively contacting the surface. Interruptions in the oscillations are detected without need of excessive contact. Tapping mode is in general more difficult to use, but far more valuable because of its capability to image with no force.

While imaging was an important part of this project, applying a voltage with the AFM was more vital. Special MESP metal-coated AFM tips allowed a voltage to be applied from the tip to the substrate. We first studied this voltage in air, through the oxidation of hydrogen-terminated silicon. This silicon was produced using diffusion-clean silicon wafers dipped in a 180 second 6:1 buffered oxide etch. The process of using a voltage to oxidize silicon was modeled after the anodic oxidation of silicon in fluid. A voltage from the AFM oxidizes hydrogen-terminated silicon leaving raised areas of SiO_2, detected by AFM image scan. This may be caused by the dissociation of ambient water vapor in the air into H^+ and OH^-, and/or from the propagation of electron holes in the silicon crystal. Oxidation tests were designed to more thoroughly understand the voltage applied by the AFM.

Summary:

From oxidation trials, we concluded that the voltage could produce oxide lines reproducibly in air. The speed with which the tip passed over the surface was inversely proportional to the width and height of the oxide lines. The magnitude of the voltage used was directly proportional to the width and height of the oxide lines. Only negative voltages had a significant or reproducible effect. In order to apply a voltage in fluid, a 12V variable current / variable voltage power supply was used to apply the voltage, as the AFM was not equipped to apply a voltage in fluid.

Due to lack of time, the application of voltages to protein solutions was not possible. Preliminary attempts to produce oxide lines in fluids showed that the mechanism of oxidation in fluid was significantly different than oxidation in air, and the method by which we applied this voltage was not thoroughly tested.

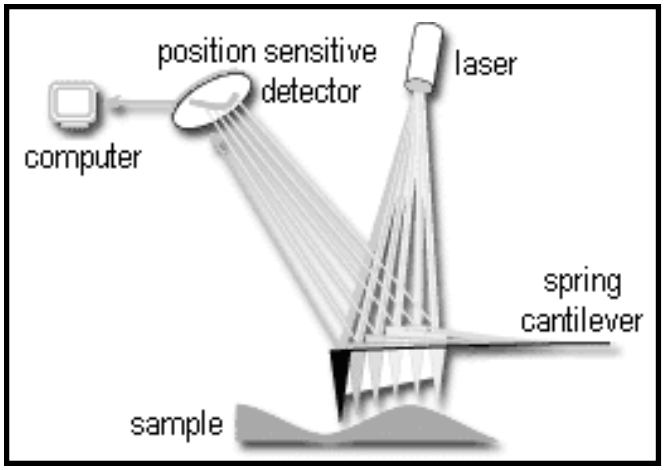

REU Project Title:

Studying Si/$Si_{1-x-y}Ge_xC_y$ Band Offsets using MOS Capacitors

REU Intern, Major, Home Institution:

Kyndall Barry, Physics, Bethune-Cookman College

REU Principal Investigator, Dept, Institution:

James Gibbons and Judy Hoyt, EE, Stanford University

REU Principal Investigator Email Address:

gibbons@ee.stanford.edu, hoyt@ee.stanford.edu

Abstract:

In this study, SiGeC wafers grown by two different methods, Molecular Beam Epitaxy (MBE) and Chemical Vapor Deposition (CVD), were processed into n-type metal-oxide-semiconductor (MOS) capacitors. The resulting capacitors were used to compare conduction band offsets in Si/$Si_{1-x-y}Ge_xC_y$ heterojunctions for CVD and MBE grown epitaxial layers. By comparing measured and simulated MOS capacitance vs. voltage (C-V) curves, conduction band offsets can be extracted. not yield any conduction band offsets. Since electronic properties of materials depend on the growth process, it is possible that Si/$Si_{1-x-y}Ge_xC_y$ heterojunctions grown by MBE show conduction band offsets, whereas CVD grown material does not. In order to test this, we have performed MOS C-V measurements simultaneously on MBE and CVD grown samples. The MBE samples were similar to the one's used for admittance spectroscopy. The two sets of samples underwent identical post-epitaxial processing, in order to ensure uniformity in fabrication conditions.

Introduction:

Si-based heterostructures involving alloys of C in Si and SiGe further expand the range of device applications for Si-based heterostructures. The exceptional properties of SiO_2 in conjunction with the possibility of "band gap engineering" make Si heterostructures promising candidates for future high-speed VLSI applications.

In this project, Si/$Si_{1-x-y}Ge_xC_y$ layers with a nominal Ge concentration of 20 at. % and carbon fractions up to 1.9 at. % were studied because it is a new alloy and not much is known about its electronic properties. The incorporation of substitutional C in Si and Si1-xGex has been of considerable interest, since it is expected to provide additional flexibility for device applications. The addition of carbon to $Si_{1-x}Ge_x$ compensates some of the biaxial compressive strain. This relaxes the film thickness constraints for pseudomorphic growth, enabling the growth of thicker layers. In recent experiments, conduction band offsets were reported in MBE grown Si/$Si_{1-x-y}Ge_xC_y$ heterojunctions using Admittance Spectroscopy [1]. MOS C-V measurements [2] on separate CVD grown Si/SiGeC samples, however did

Experimental Technique:

MBE growth is a physical process in which solid sources of the elements are evaporated onto the Si substrate. The MBE wafers in this work were grown at Hughes Research Labs. CVD growth is a chemical technique in which gases such as silane, germane, and methylsilane react and deposit Si, Ge, and C on the Si substrate. The CVD wafers were grown at Stanford University.

MBE and CVD epitaxial wafers were provided for thermal oxidation and fabrication into test structures. The gate oxide was grown by wet oxidation at 750°C for 40 min. Aluminum was deposited on the oxide, and patterned to define the MOS capacitor. After device fabrication, temperature dependent C-V measurements were performed in the CIS Measurements Lab using an HP4275A LCR meter. A Lakeshore MTD-130 cryostat was used to vary the temperatures between room temperature and 100K.

Typical n-type, MOS capacitors will produce C-V characteristics similar to the solid line in Fig. 1. However, if a potential energy well has formed in the conduction

band due to the buried SiGeC layer, electrons will accumulate in the well and additional voltage is required to free them. This extra voltage to deplete the electrons shows up as a plateau on the C-V curve. In Fig. 1, plateaus

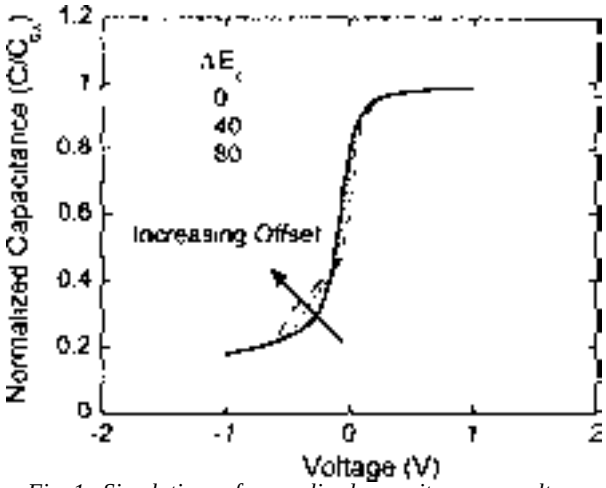

Fig. 1. Simulations of normalized capacitance vs. voltage curves in which plateaus appear due to conduction band offsets.

associated with increasing well depths are represented as dotted and dashed lines. By comparing measured and simulated MOS capacitance vs. voltage (C-V) measurements, conduction band offsets can be extracted.

Results and Conclusions:

For C-V curves, the capacitance is plotted against the DC gate voltage. At room temperature, both the CVD and MBE capacitors exhibit well-behaved C-V characteristics. There is no evidence of a capacitance plateau to indicate a potential energy well in the alloy layer. This C-V behavior is expected at room temperature. At low temperatures, it is easier for the electrons to be confined in the well and produce a capacitance plateau.

Fig. 2 shows the high frequency C-V characteristics of the MBE MOS structures at 100K. Samples with 20 at. % Ge and C concentrations of 0.8 and 1.2 at. % exhibit typical Si MOS capacitor behavior; however, the 1.9 at. % C sample shows lack of electron accumulation which indicates that traps are present and the material is non-ideal. Fig. 3 shows the high frequency C-V characteristics of the CVD MOS structures at 100K. These samples also exhibit behavior of a typical Si n-type MOS capacitor.

No plateaus were observed in the samples which is in agreement with previous studies done at Stanford. MOS C-V measurements in conjunction with 1D simulations using a Poisson solver suggest that the conduction band offset is < 30 meV for Si/$Si_{1-x-y}Ge_xC_y$ containing 20 at. % Ge and up to 1.9 at. % C.

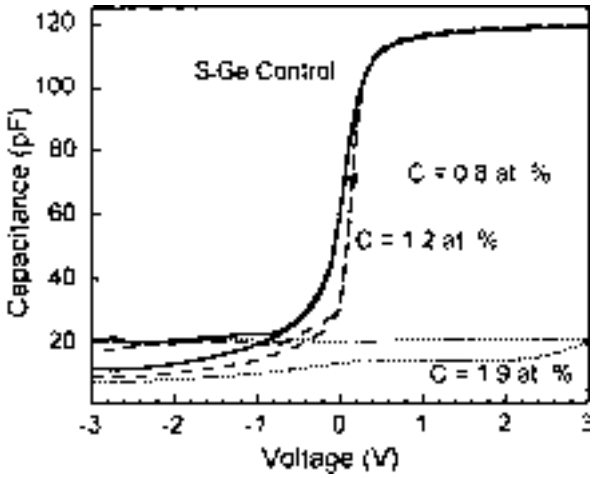

Fig. 2. Capacitance vs. voltage curves for MBE grown Si/$Si_{1-x-y}Ge_xC_y$ MOS capacitors at 100K.

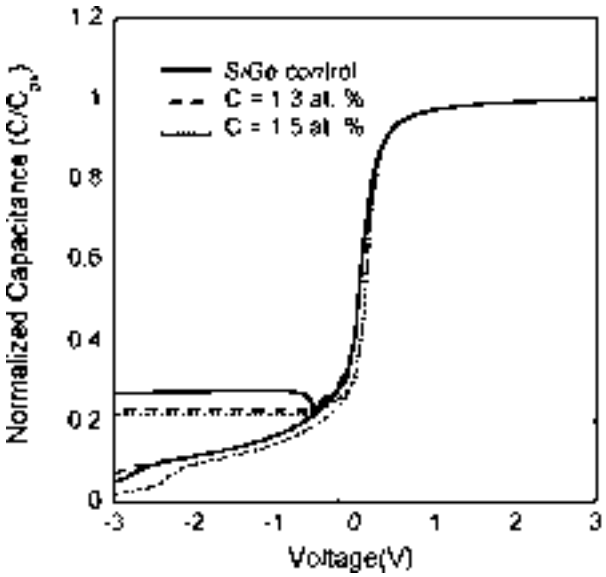

Fig. 3. Capacitance vs. voltage curves for CVD grown Si/$Si_{1-x-y}Ge_xC_y$ MOS capacitors at 100K.

References:

[1] B.L. Stein, E.T. Yu, E.T. Croke, A.T. Hunter, T. Laursen, A.E. Blair, J.W. Mayer, C.C. Ahn, Appl. Phys. Lett. 70(25), 3413 (1997).

[2] D. Singh, K. Rim, T.O. Mitchell, J.L. Hoyt, and J.F. Gibbons, "Measurement of the Conduction Band Offset Si/$Si_{1-x-y}Ge_xC_y$ Heterostructures using Metal-Oxide-Semiconductor Capacitors." Submitted to the J. Appl. Phys.

REU Project Title:

Process Development of Chlorobenzene and LOL2000 Liftoff Processes with Stable Overhang Structures

REU Intern, Major, Home Institution:

Samuel Bishop, Chemical Engr, University of Washington

REU Principal Investigator, Dept, Institution:

James Harris, Electrical Engineering, Stanford University

REU Principal Investigator Email Address:

harris@ee.stanford.edu

Abstract:

The key feature of a practical lift-off process is undercutting in the resist profile. However, forming resist patterns using positive photoresist alone does result in undercut profiles. Two processes were developed to induce undercutting in the resist. The first process involved soaking photoresist covered wafers in chlorobenzene either before or after exposure. The second process places the resist layer on top of a layer of the chemical LOL2000. Appropriate undercut profiles were achieved for chlorobenzene soaking before and after exposure using Shipley 1813 photoresist.

Introduction:

In a lift-off process for lithography, a resist pattern is formed prior to evaporating metal for wiring. The metal on top of the resist pattern is lifted off during a stripping step. Previous techniques subtractively etched off metal before stripping the resist [1]. A lift-off process eliminates the metal etching step. The key feature of a practical lift-off process is undercutting in the resist profile. However, forming resist patterns using positive photoresist alone does not result in undercut profiles.

Two processes were developed to induce undercutting in the resist. The first process involved soaking photoresist covered wafers in chlorobenzene either before or after exposure. The chlorobenzene diffuses into the resist and lowers the development rate of the top portion of the resist layer [2]. The second process places the resist layer on top of a layer of the chemical LOL2000. LOL2000 is not photosensitive and has a faster development rate than the resist. In both processes, the difference in development rates leads to undercutting.

Experimental Procedure:

First, the Headway Resist Spinner was used to coat wafer pieces with photoresist, e.g. Shipley 1813 or 3612. Next, the coated wafer is baked in order to drive off solvents and influence solubility to chlorobenzene. For the first series of experiments, wafer pieces were soaked in chlorobenzene for 30 minutes directly before exposing. For the second series of experiments, wafer pieces were soaked for 30 minutes directly after exposing. Exposure was done on a Karl Suss exposer/aligner. Exposure times ran from 1s - 7s, but nominally fell in the range 2-5 s. Finally, the exposed wafer was developed in the appropriate developer solution, e.g. Microposit Developer Concentrate or LDD 26W. The resulting resist pattern was then imaged to evaluate the resolution and undercutting.

The process variables to control and optimize were resist baking time, chlorobenzene soaking time, exposure time, and development time. Chlorobenzene soaking and development times were kept constant for all samples. Variables were first visually optimized for the 1.0 micron linewidth resolution to obtain appropriate exposure time. An optical microscope was used to evaluate the exposure level of each sample. A scanning electron microscope was used to analyze the resist profiles.

The chlorobenzene soak time was set at 30 minutes leaving the bake and development times as the key variables to manipulate. Increasing the development time thinned the neck of the resist profile, while increasing the bake time decreased the amount of overhang. Soaking longer would have had the effect of creating a thicker "cap" region due to the chlorobenzene soaking further into the resist.

The LOL2000 process is a two layer procedure where a thin layer of the chemical LOL2000 is put down underneath the photoresist. The LOL2000 is not photosensitive and has a higher development rate. It is able to produce undercutting without using the toxic and carcinogenic chlorobenzene. There are now two bake steps to control prior to exposure and development. Note that the "cap" region would be much larger in the LOL2000 process due to the fact the LOL2000 layer is only a fraction of a micron thick.

Results and Conclusions:

Appropriate undercut profiles were achieved for chlorobenzene soaking before and after exposure using Shipley 1813 photoresist. The details of the recipe for the samples soaked in chlorobenzene prior to exposure were: a 10 minute bake, a 3.2 second exposure time, a 2 min 15 s development time, and a 30 min chlorobenzene soak time. Figure 1 shows the profile of a representative sample soaked prior to exposure. For the samples soaked subsequent to exposure the details were: a 20 min bake, a 5 second exposure time, a 1 min 10 s development time, and a 30 min chlorobenzene soak time. Figure 2 shows the profile of a representative sample soaked subsequent to exposure.

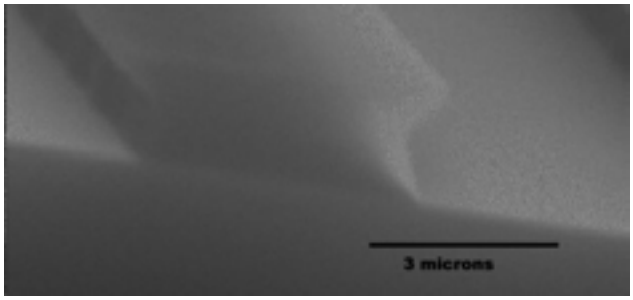

Figure 1. S EM image of photoresist profile for sample soaked in chlorobenzene prior to exposure.

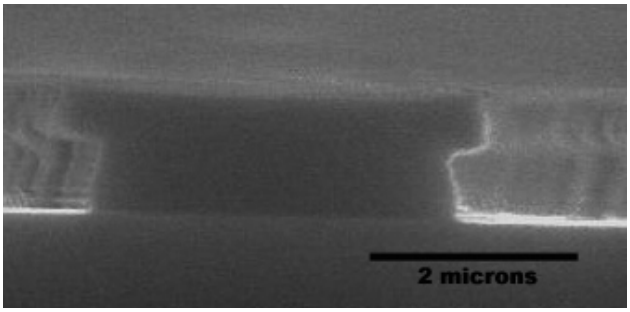

Figure 2. Edge-on SEM image of photoresist profile for sample soaked in chlorobenzene subsequent to exposure.

As expected from similar studies done in the literature, the bake time is the most influential variable because it directly shrinks the overhang region. Also from the literature, lower exposure times give better reproducibility and stability in the photoresist profiles. Finally, soaking after exposure is more applicable to production processes because of decreased contamination risk. Chlorobenzene is a toxic chemical that remains in the photoresist and can only be rinsed out using freon, which for obvious reasons can't be used.

The three areas of work in progress are: conducting similar development on a LOL2000 process, quantifying the overhang using better quality SEM pictures, and applying these recipes to research being conducted in the Harris Group.

References:

[1] "Process Control of the Chlorobenzene Single-Step Liftoff Process with a Diazo-Type Resist",
G. G. Collins, C. W. Halstead. IBM J. Res. Develop., vol. 26, p. 596, 1982.

[2] H. Moritz. Microcircuit Engineering. Academic Press: London, 1985.

REU Project Title:

Grain Structure in Thin Polycrystalline Silicon Lines

REU Intern, Major, Home Institution:

Phyllis Chen, Chemical Engr, California Inst of Technology

REU Principal Investigator, Dept, Institution:

James Plummer, Mike Deal, Joseph Tringe, Electrical Engineering, Stanford University

REU Principal Investigator Email Address:

plummer@ee.stanford.edu, deal@ee.stanford.edu, jtringe@leland.stanford.edu

Abstract:

In today's trend toward smaller, faster microelectronics, there is a strong push to understand the constituent material properties at a micron scale. The structure of polycrystalline silicon grain boundaries influences the electrical properties of the material at this length scale. It is our goal to identify a correlation between the crystallographic orientation of neighboring grains and consequent electrical properties. We measure the resistance of lines approximately the width of individual grains, then physically characterize the structure of the grain boundaries with a transmission electron microscope (TEM). The TEM can image crystal lattices of individual grains, and electrons diffracted by these lattices give distinct patterns that correspond to specific crystal orientations. By taking TEM diffraction patterns of adjacent grains, we can resolve the misorientation angle between these two grains. We recreate this angle of misorientation with a computer program and then use this simulation to calculate the atomic density of geometry of the grain boundary. With this information, we can find the correlation between the grain boundary structure and the resulting electrical resistivity.

Introduction:

Polycrystalline silicon is widely used today in microelectronic circuits. As these devices shrink to the micron scale, the constituent material properties become even more important. Grain boundaries in polysilicon influence the electrical properties at this scale. The goal of this project is to find a correlation between the grain boundary structure in polysilicon and the resulting electrical resistivity.

A grain boundary occurs at the intersection of adjacent crystals and marks a discontinuity in the lattice structure. There are two angles of rotation associated with the misorientation of the crystals: tilt and twist. Joe Altepeter, another REU student at Stanford, wrote a computer program in Mathematica that rotates a lattice through two arbitrary angles and then measures the atomic density of a plane of intersection with the original lattice position.

Experimental Procedure:

Blanket films are non-ideal for testing the properties of grain boundaries since the nonuniform grain size and inhomogeneous boundary structure lead to nonuniform current flow. The unpredictable current path makes it impossible to discern which grain boundaries are being crossed. Instead, thin lines of polysilicon approximately the width of a grain boundary were used. Previous work with an atomic force microscope (AFM) revealed the average grain size was approximately 0.1 μm. The smallest lines tested were 0.12 ?m in width and 0.4 μm in length, about the size of four grains in series. The height of the lines was 1.0 μm.

To test the electrical properties of these lines, current was passed through the horizontal pads, and the resulting voltage drop was measured across the vertical pads. The resistance follows an Arrhenius rule. By measuring the resistance at several temperatures, the activation energy for the tested sample can be found.

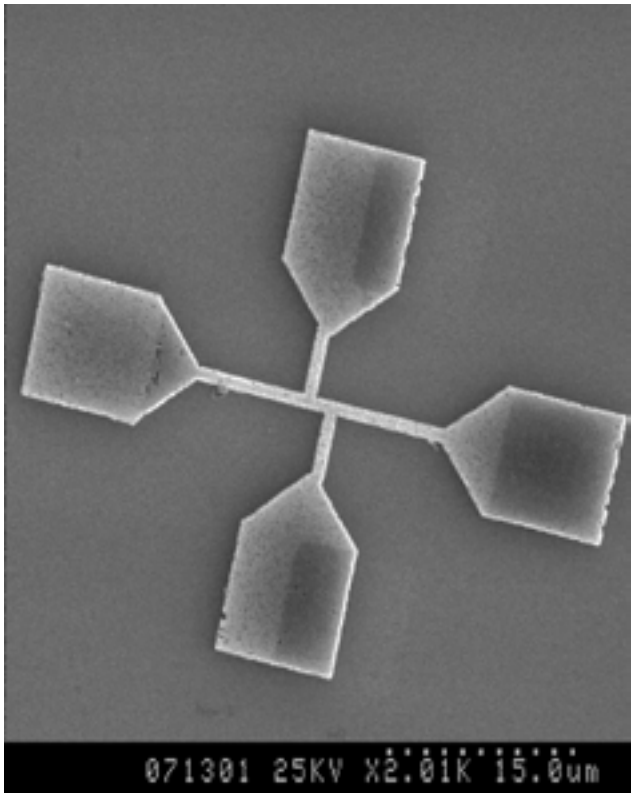

Figure 1. SEM image of the device used, plan view. The area of interest is between the two vertical arms.

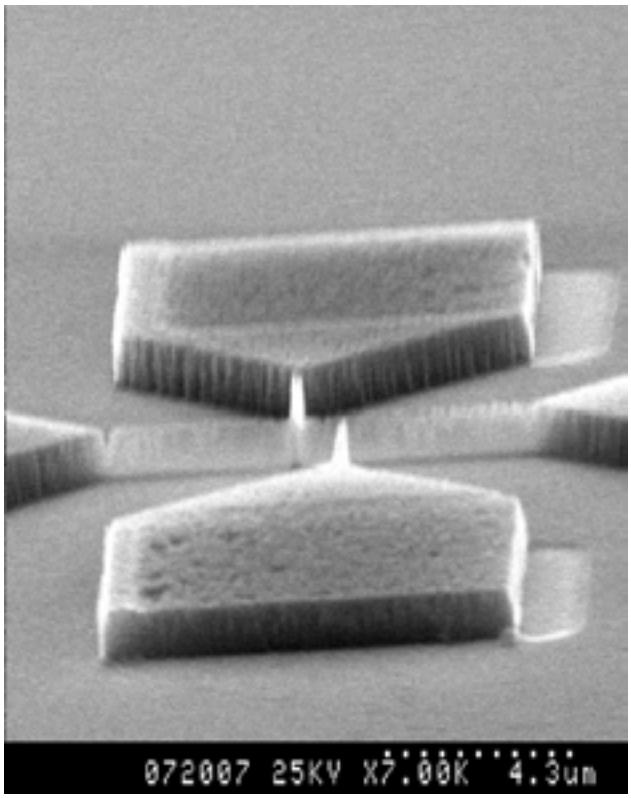

Figure 2. SEM image of device used, angle view. The height of the structure can be seen.

Once the electrical properties are known, certain devices are chosen to have their grain boundary structures characterized using a TEM. In order to be imaged, the specimen has to be electron transparent, less than 0.2 μm in thickness. The devices are viewed along the plane of the wafer. Since the width is 0.12 μm, no further preparation of the area of interest is necessary.

An image of the device serves as a map of the individual grains. Then, diffraction patterns are taken on either side of the visible grain boundaries. The crystallographic orientation can be discerned from these diffraction patterns. By knowing the relative misorientation of the adjacent crystals, the angles of rotation are calculated. To recreate the grain boundary, these angles are then used in the computer program which also calculates the atomic density of the intersection.

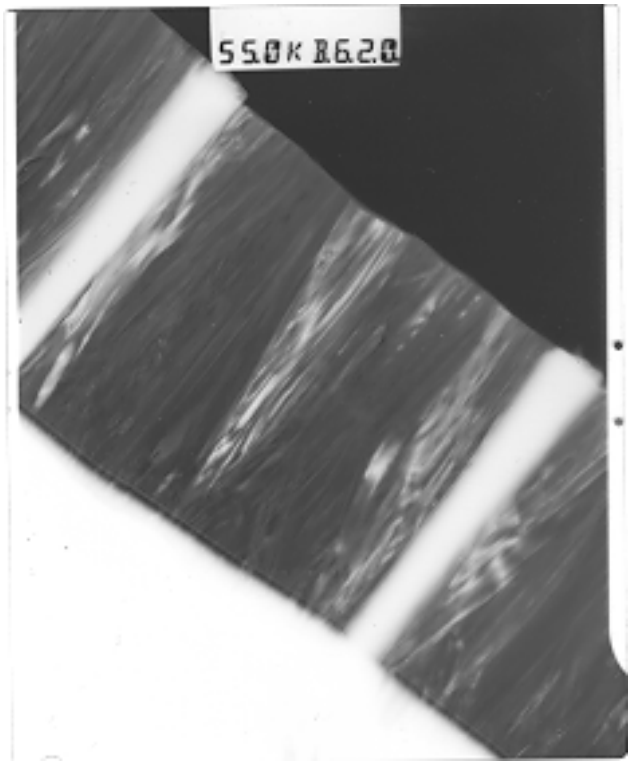

Figure 3. TEM image with the area of interest between the dark bands. Columnar growth of the grains is apparent.

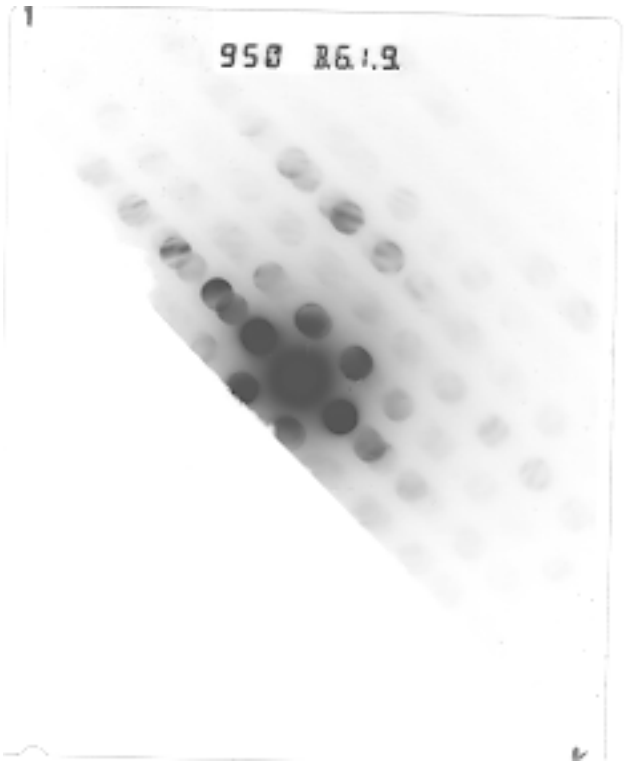

Figure 4. TEM diffraction pattern showing a (011) orientation.

Summary:

Data from previous electrical testing was analyzed in order to calculate the activation energy. Certain devices with interesting electrical properties were selected to be physically characterized. Due to complications, these devices could not be imaged. However, the TEM method of crystal orientation characterization was performed on sample devices. This method, in conjunction with the Mathematica program, shows promise in helping to find a correlation between certain grain boundary structures and the consequent electrical properties.

References:

[1] V. Randle, The Measurement of Grain Boundary Geometry (Bristol, UK: Institute of Physics, c1993)

[2] V. Randle, Microtexture Determination and Its Applications (London, UK: Institute of Materials, 1992)

[3] J.W. Edington, Practical Electron Microscopy in Materials Science (New York: Van Nostrand Reinhold Co., 1976)

[4] D. Sands, Introduction to Crystallography (New York: Dover, 1993)

REU Project Title:

Fabrication of Nanostressors for Patterned Self–Assembly of SET Junctions

REU Intern, Major, Home Institution:

Tanja Cuk, Electrical Engr, Princeton University

REU Principal Investigator, Dept, Institution:

Cheng Hung, Materials Science, Richard Kiehl, Electrical Engr, Stanford University

REU Principal Investigator Email Address:

cyhung@snowmass.stanford.edu, kiehl@ee.stanford.edu

Motivation and Background:

Cheng-Yu Hung and Richard Kiehl are interested in patterning InGaAs stressors on top of an AlGaAs/GaAs quantum well to position nanometer scale Arsenic precipitates for use in Single Electron Tunneling Junctions. So far, stressors have been placed in lateral arrays, successfully positioning the precipitates in lines. The next steps are to pattern squares to position precipitates in both x and y directions and rings to detect possible directionality in the strain field. In this project, several resists and doses were tried on test samples to pattern squares small enough to locate a single precipitate and rings thin enough to locate a single strand of precipitates. The resists were patterned using Electron Beam Lithography and the samples were viewed under the Scanning Electron Microscope.

Experimental Procedure:

Resist is spun onto GaAs pieces and then exposed under the electron beam. Depending on the type of resist, the beam energy strengthens (negative resist) or loosens (positive resist) the polymer bonds. Developing clears areas written upon in positive resist, while it clears everything but those areas written upon in negative resist.

Several recipes for positive and negative ebeam resist were tried. A recipe especially developed at the Stanford Nanofabrication Facility for a thinned negative ebeam resist, SNR200—0.5: type P thinner, gave the only reportable result [1]. In order to facilitate the adhesion of SNR to the GaAs surface, the procedure includes three bakes and spins an adhesion promoter before the resist. The final resist coat is 2000A thick. The recipe is as follows:

Before Exposure:	*After Exposure:*
15min Bake at 120°C	2min Bake at 110°C
Spin Hexamethyldisilazane (HMDS) at arbitrary speed and time	develop in CD-14 for 20 sec
Spin SNR—thinned at 5500 RPM for 30 sec	rinse in DI water for 60sec
2min Bake at 110°C	

Since negative resists are not very robust, the resist should be spun as close to the exposure time as possible and developed right after.

Two factors are critical in obtaining the desired pattern on the resist — one is the develop time, the second is the dose ($\mu C/cm^2$). The higher the dose or the longer the develop time, more of the resist gets strengthened or loosened. Hence, in the case of negative resist the feature size is bigger than expected for higher doses or longer develop times. Since ebeam dosage is a more accurate measure than develop time, most experimenters play with the dosage and keep the develop time fixed. The dosage can be varied in an "exposure matrix," in which each line corresponds to a different dose. For 2000Å thick SNR200, a dose of 16 is recommended [2].

Common Problems Encountered:

A common problem in Electron Beam lithography is the scattering of electrons, caused by atoms in the resist, electrons bouncing off the hard substrate, and by secondary electron emissions. Electron scatter effects the pattern in three ways: a. sharp edges round off, especially in small features; b. the dose of a given feature increases depending on the spacing between features (commonly called the proximity effect); c. small features need higher doses than larger features because of added exposure in larger features [3].

As mentioned above, a common problem with negative resists is adhesion to the substrate. Even though the recipe took this into consideration, the problem persisted. In the first and last samples, markers put around the patterns floated around — some rotated with respect to the substrate, others even collided into one another. More common, however, was for features to "pop" off the surface and lower the density of squares/rings.

Results and Conclusions:

In the first pattern, 50nm, 100nm, and 150nm squares are spaced 250nm apart in separate three by three arrays with 1 μm spacing between arrays. The rings have 200nm inner diameters, 300nm outer diameters, and 1 μm spacing between rings. The dose varies between 16 and 88 with a stepping of 2.

The first time that the sample was looked at under the Scanning Electron Microscope (SEM), no dots (originally intended to be squares, but because of electron scatter turn out like dots) were seen below 30μC/cm^2. Only after a second viewing, 150nm dots could be detected at 16μC/cm^2. The 100nm dots were even less dense than the 150nm dots and the 50nm dots could not be seen at any dose. These results indicate that adhesion is poorer for lower doses and smaller dots. Perhaps, the added dose firms up the connection between the resist and substrate; added electron scatter in larger features could have the same effect. Above 30μC/cm^2, the dose becomes too big for the spacing between features. The proximity effect can be seen in fig 1a (88μC/cm^2), where all of the dots in the 3x3 array form a big square, and fig 1b (45μC/cm^2), where the dots are connected by thin lines. The rings turned out like filled circles at all doses, also because of the proximity effect—see fig 2a (45μC/cm^2).

In the next pattern, the spacing between dots was increased in the hope of getting a regular pattern of unconnected dots at higher doses. In the hope of getting unfilled rings, the inner diameter was increased. The 150nm dots are spaced 1 μm apart in the three by three arrays, with 1.5 μm spacing between arrays. The inner diameter of the rings is 1 μm, while the outer diameter is 1.15 μm. The dose varies between 30 and 57, with a stepping of 3.

The results show a more regular pattern of unconnected dots. Fig 1c shows 150nm dots at 45μC/cm^2; fig 1d shows 150nm dots at 30μC/cm^2. Comparing the dot density of the two pictures well-documents poorer adhesion at lower dosages. In fig. 1e, two dots are zoomed in to show the approximate size. At 30μC/cm^2, the picture shows the dots to be around 170nm. This means that a lower dosage is needed to achieve 150nm dots and yet, at lower doses the dots are much more rare.

The rings turned out as unconnected lines, shown in fig 2b. In the software used to make the patterns, rings have to be composed of small triangles and squares; some parts of the ring may be thinner then others. Perhaps, the "diagonals" of the rings did not show up because they weren't thick enough.

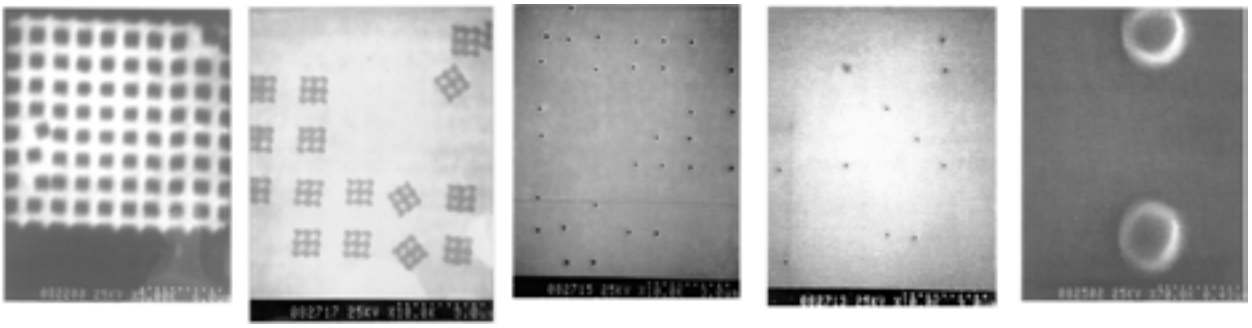

Fig1a *Fig1b* *Fig1c* *Fig1d* *Fig1e*

Progression of 150nm Dots: ***1a)*** *0.25 μm spacing in 3x3 arrays, 88 μC/cm^2.* ***1b)*** *0.25 μm spacing in 3x3 arrays, 45 μC/cm^2.* ***1c)*** *1μm spacing in 3x3 arrays, 45μC/cm^2.* ***1d)*** *1μm spacing in 3x3 arrays, 30μC/cm^2.* ***1e)*** *high zoom, 1μm spacing in 3x3 arrays, 30μC/cm^2*

The next pattern could not be fully tested because of gross adhesion problems, possibly caused by using a new bottle of HMDS. The detectable features are "box shaped" rings, some of 1 μm inner squares (Fig. 2c, 62μC/cm) and others of 0.5 μm inner squares (Fig. 2d, 62μC/cm^2); both have ring widths of 100nm. Thick rectangles were used to pattern the rings in the hope of getting unbroken rings with the edges rounded off by electron scatter. Unfortunately, the results do not indicate that the edges are rounded off enough. However, the inner square of the 0.5 μm rings does look more like a circle.

In the hope of getting well-sized and regular dots, the spacing and dose were varied. However, with increasing regularity the dots become bigger than desired. A suggestion for future research is to strengthen the adhesion in the processing prior to exposure instead. Rings, in general, were more regular—a good pattern needs to be chosen so that they remain unfilled and unbroken. Adhesion, however, may represent a problem for thinner rings.

References:

[1] Basic Recipe: Janet Rock at IBM; Modifications at SNF by: Jim Schneider, Joe Tringe, Theresa Kramer, Vivek Subramanian, Esin Terzioglu.

[2] H.I. Liu, Fabrication and Properties of Silicon Nano-Structures, Stanford PhD Thesis (1995).

[3] Williams, Ralph E., Gallium Arsenide Processing Techniques. Dedham: Artech House, 1984, pp.155-158.

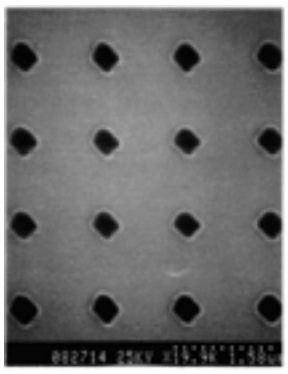

Fig 2a

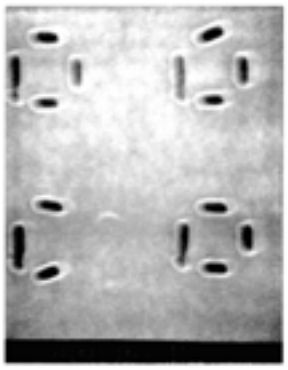

Fig 2b

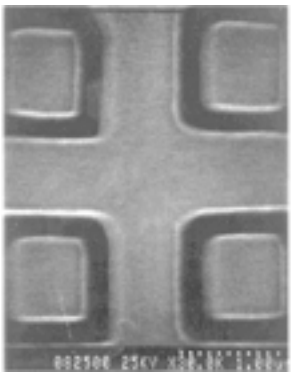

Fig 2c

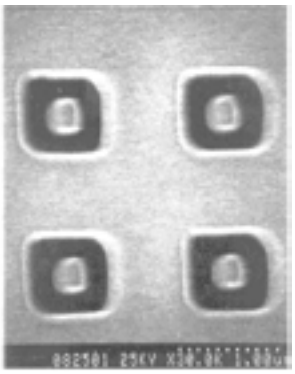

Fig 2d

Progression of Rings: ***2a)*** *200 inner diameter, 45μC/cm^2.* ***2b)*** *1 μm inner diameter, 45μC/cm^2.* ***2c)*** *"box rings," 1μm inner diameter, 62μC/cm^2.* ***2d)*** *"box rings," 0.5 μm inner diameter, 62μC/cm^2.*

REU Project Title:

Protein Crystal Growth on Rough Silicon Surfaces

REU Intern, Major, Home Institution:

Yuri Dancik, Chemical Engineering, Princeton University

REU Principal Investigator, Dept, Institution:

Peter Griffin, Center for Integrated Systems, Stanford University

REU Principal Investigator Email Address:

griffin@stanford.edu

Abstract:

Protein crystals are often used to determine the atomic structure of a protein through X-ray diffraction. However, the conventional ways of growing protein crystals require a large amount of trial and error. For some proteins, crystals will not grow under any conditions. The goal of this project is to induce protein crystallization in a systematic fashion by creating structures on a Si wafer surface that are essential for nucleation — the first step in the growth of crystals — to take place. Terraces, steps and valleys were created on the Si surfaces by etching the wafers in 45% KOH solution and viewed with the Atomic Force Microscope (AFM). Drops of solution of noncrystallizable protein were deposited on etched Si wafer pieces. The trials are still underway. In addition, AFM pictures of a crystal of ATPase were taken and show the occurrence of terrace and step-like structures on the crystal surface.

Introduction:

The surface of a crystal observed at an atomic scale displays features which are essential for crystal growth: terraces, separated by steps; the latter composed of ledges and kinks.

The first step in the formation of protein crystals out of a protein solution is nucleation. At a high enough solute concentration, a nucleation energy barrier is overcome and a few protein molecules diffuse out of the solution and aggregate, thus forming a seed crystal. The formation of this seed crystal is essential for the subsequent crystallization process. Further molecules diffuse out of the protein solution onto the terraces of the seed crystal. They then diffuse towards the ledges. The kink site thus moves in the positive X direction (fig. 1) until it reaches the edge of the crystal. In turn, the entire step moves in the positive Y direction, until it reaches the edge of the crystal, at which point a new terrace is begun. Thus a crystal with a repeated lattice structure is formed [1].

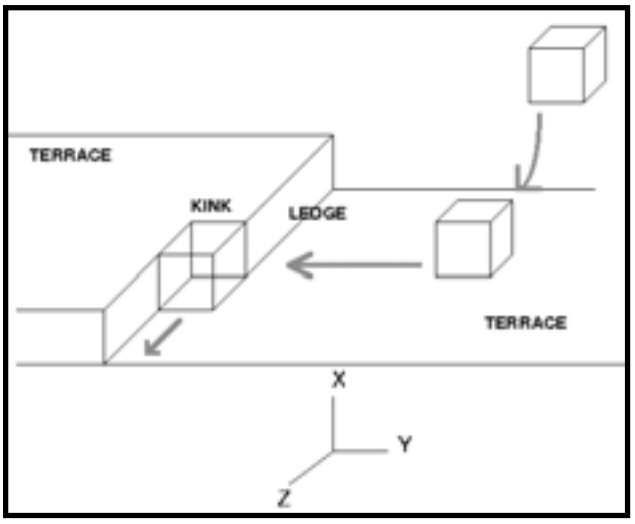

Fig. 1: Schematic Terrace-Ledge-Kink model of crystal growth.

The most common method used to make proteins crystallize is the Hanging Drop Technique. A few milliliters of a protein solution are mixed with an aliquot of a salt solution and deposited onto a glass cover slip. The glass cover slip is inverted so as to cover a reservoir, which contains the same salt solution at a specific concentration and pH. Since the salt

concentration is greater in the reservoir than in the drop, water evaporates out of the drop. The protein solution concentration in the drop increases, making it possible for protein molecules to diffuse out of the solution and form the initial seed crystal [2]. The disadvantage of this method lies in the fact that the protein molecules must "find each other" in order to form the initial seed crystal. In addition, large amounts of time are required to discover the right salt concentrations and pH values for any given protein.

The etching of Si wafers in KOH creates structures on the Si surfaces which approximate terraces and steps on a crystal surface. Pieces of etched Si wafers are used to replace the glass cover slip in the Hanging Drop Technique. The first molecules to diffuse out of the protein solution should bind to the terraces and steps and thus be able to "find each other" and aggregate faster. This should speed up the nucleation process and make the crystal growth of non-crystallizable proteins much more likely to occur.

EXPERIMENTAL PROCEDURE

ATPase Crystal Preparation:

ATPase crystals were grown and provided by Prof. David McKay of structural biology using the Hanging Drop Technique.

Wafer Preparation:

3" and 4" <100> wafers were RCA cleaned and etched in 45% KOH solution for 3 to 5 min, at 80°C. This etching produced pits of depths ranging from 60 Å to 100 Å (fig. 2). After imaging the wafers were sawed into 1 cm^2 pieces (Micro Dicing Service, Sunnyvale, CA) to be used instead of glass cover slips. Some Si pieces were oxidized to make the surface hydrophilic. They were dipped in a 5:1:1 H_2O:H_2O_2:HC_l solution at 80ßC for 30 min so as to produce a thin oxide coating about 20 Å thick. Other Si pieces were silinated. A third set of Si wafer pieces was left bare.

AFM Imaging:

All images were taken using a Digital Instruments Nanoscope 3000 Atomic Force Microscope. The wafer images were taken in deionized water in Tapping Mode, using a fluid cell and DNP tips obtained from Digital Instruments. The driving frequency was chosen at a peak between 8kHz and 12kHz and the root mean square amplitude range was 0.3-0.6V. The setpoint was kept to about half the value of the RMS amplitude. The ATPase crystal images were taken in the protein solution in Tapping Mode using the same fluid cell and DNP tips. The ranges for the drive frequency and the RMS amplitude were the same as for the wafer imaging. The optimum setpoint was found to lie in the 0.09-0.18 V range.

Results And Conclusion:

Figure 2 is a 1 µm x 1µm scan of the surface of a glass cover slip used in the Hanging Drop Technique. The glass surface is relatively smooth and does not provide any site for protein molecules to bind to and aggregate. Figure 3 is a 200 nm ¥ 200 nm scan of a KOH etched wafer surface. The surface consists of 60-70 Å high hillocks and valleys which should serve as nucleation sites.

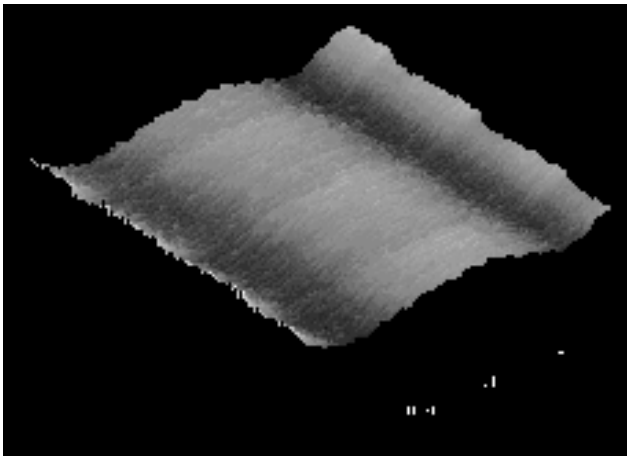

Fig. 2: AFM image of a 1 µm x 1 µm section of a glass cover slip.

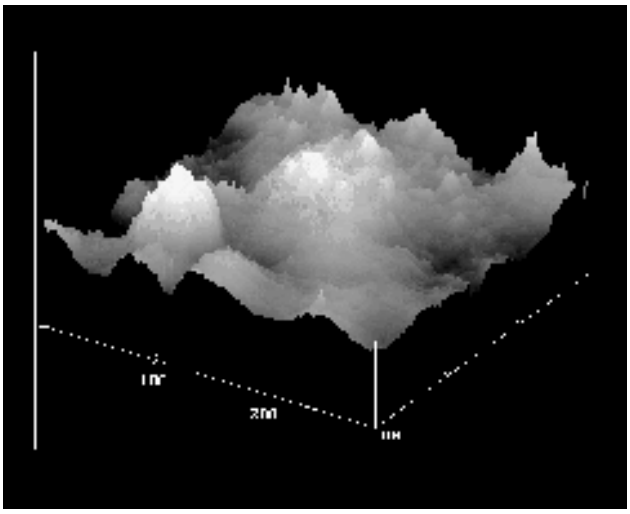

Fig. 3: AFM image of a 200 nm x 200 nm section of an etched Si wafer.

Figure 4 represents the surface of an ATPase crystal. Terrace and step-like structures are easily recognizable. The steps are about 135 nm high. The steps' width alternates, with the larger steps being about 1μm wide and the smaller ones about 0.5 μm wide. The distance between each step is roughly 0.5 μm. However, these alternating step widths were found on different areas of this particular ATPase crystal only. Another ATPase crystal displayed steps of equivalent heights, but the steps were sharp and did not noticably vary in width. The distance between each step on the second crystal surface was approx. 0.5-0.7 μm.

Silicon wafers have been etched in 45% KOH solution to create structures on the surface which should facilitate and accelerate the formation of an initial seed crystal. Trials are currently underway using oxidized, silinated and bare etched Si wafer pieces instead of the conventional glass cover slip. The method is being tested with solutions of proteins which have as yet never yielded crystals using traditional methods.

References:

[1] R. Ghez, "A Primer of Diffusion Problems", John Wiley and Sons , pp. 70-72, 1988.

[2] A. McPherson, "Preparation and Analysis of Protein Crystals", John Wiley and Sons, pp. 97-98, 1982.

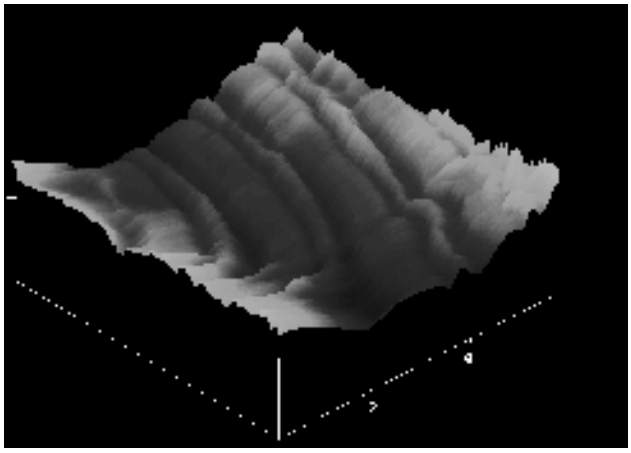

Fig. 4: A 6 μm x 6 μm AFM scan of an ATPase crystal surface.

REU Project Title:

Microstamping Mazes onto Glass Substrates for Separating Integral Membrane Proteins

REU Intern, Major, Home Institution:

Blair Irwin, Chemistry, Princeton University

REU Principal Investigator, Dept, Institution:

Mary Tang, Dept. of Electrical Engineering,
Curt Frank, Dept. of Chemical Engr, Stanford University

REU Principal Investigator Email Address:

mtang@snf.stanford.edu

Abstract:

All living beings are made of cells surrounded by a plasma membrane. The plasma membrane is composed of a double layer of lipids studded with proteins which are essential to cell survival [1-4]. The most widely used method for isolating integral membrane proteins from the bilayer is solubilization by detergents which often results in a loss of native structure [5, 6]. Our research involves developing a more efficient method for isolating integral membrane proteins in their native state. Our proposal combines two recent scientific developments: microstamping and polymer-supported lipid bilayers. Microstamping a chemically reactive ink on glass slides allows us to locally define specific areas to which lipids, modified with reactive polymer head groups, can attach. The result is a two dimensional matrix of immobile and fluid domains through which protein separation by electrophoresis can occur. This summer we have succeeded in making a microstamp which contains the desired patterns which will later make up our maze. Our plans for the future are to perfect the inking process, lay down the bilayer, and perform micro-electrophoresis.

Introduction:

Most current methods of integral membrane protein separation result in protein denaturization. My project this summer was to work on a new method of separating integral membrane proteins from the lipid bilayer while at the same time preserving their native state. We devised a new separation technique which not only prevents denaturization, but also uses a smaller quantity of reagents and a shorter amount of time than previous methods. Unlike current methods, our new method will also allow one to differentiate between proteins which have the same amino acid sequence but different folded structures within the bilayer. Our new method will also provide insight as to how proteins interact with one another in the bilayer.

Method:

Our new technique combines two recent scientific developments: microstamping and polymer-supported lipid bilayers. Microstamping is a process which uses an elastomeric stamp with relief on its surface to produce a pattern of ink on a substrate (Figure 1) [1]. The first step in microstamping is the production of a wafer with a pattern of photoresist. This patterned wafer is produced through the use of photolithography. The next step is to pour polydimethylsiloxane or PDMS on the patterned wafer and allow it to cure. The PDMS is then peeled off the wafer and inked. The inked stamp is then brought into contact with a glass substrate, forming an inked pattern which is the negative of the patterned wafer. In our project, we used aminopropyltriethoxysilane or APS as the ink. We think that the APS reacts with the hydroxide groups on the surface of the glass and produces amine-terminated propane groups. To see if the inking worked we used a flourescent probe, flourescin isothiocynate, which reacted with the ink and could be viewed under a flourescent microscope.

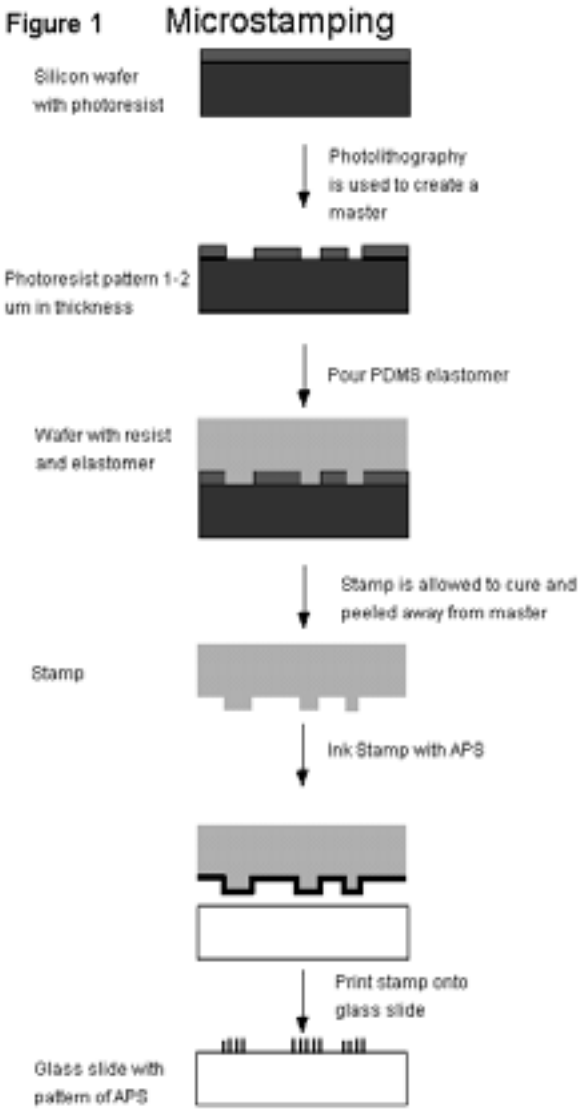

There are several advantages to microstamping. One advantage is that microstamps are relatively inexpensive and easy to make. Another advantage is that several stamps can be made from a single master wafer and stamps can be used repeatedly. A final advantage is that stamps can be produced under ambient conditions.

In addition to microstamping, the other recent development we plan to use in our project is polymer-supported lipid bilayers. Polymer-supported lipid bilayers are artificial cell membranes which maintain the structural and dynamic properties of free membranes [2]. These membranes can serve as a model system to study the basic interaction mechanisms responsible for the structure and function of biological membranes. One can control their composition and reorganize them using an electric field [3]. The polymer support is needed because it prevents the denaturing of the proteins [4]. We create the polymer support by using lipids with functional groups bound to their heads. These functional groups react with the ink on the surface of a glass substrate, immobilizing the bottom layer of lipids in the inked portions. We will apply the lipid bilayer to the substrate through vesicle fusion [5].

Our plan is to apply an electric field to a supported lipid bilayer and sort the proteins in the bilayer by their size and charge. We can not just apply this electric field to a uniformly supported bilayer because the proteins would get caught in the polymer cushion. To prevent this entanglement, we plan to use microstamping to create a pattern of ink and therefore a pattern of polymer barriers on a substrate (Figure 2).

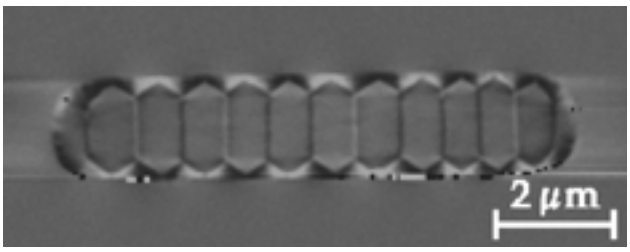

Figure 2

By having a pattern of polymer barriers, the proteins will only be able to move in the channels between the barriers when the electric field is applied. Proteins will congregate at certain regions of the maze depending on the ease at which they move through the maze.

Results:

I made significant strides on this project this summer. I learned how to do scientific research on the web and in journals while researching current methods of protein separation. The research I did will become part of a grant proposal to fund this project. I also learned how to use the program L-edit to design a mask with 14 different patterns for sorting proteins. A large part of my summer was spent researching which patterns to use. One interesting pattern I used was one used previously to sort white blood cells [1]. Some of the other patterns we chose were staggered bars, circles, ice-cream cones, chevrons, and rectangles (Figure 3). We varied the spacing, symmetry, and sizes of all our patterns. We used features as small as 2 μm. After creating these masks, we made wafers and stamps from the masks. Making the stamps required me to learn

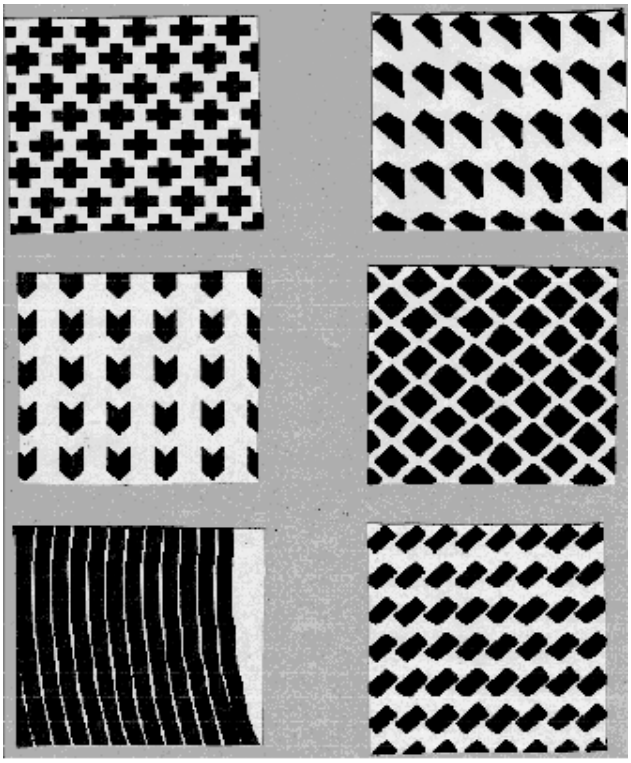

Figure 3

how to use the headway resist spinner, the Karl Suss developer, the dektak, the sputterer, the wet bench, in addition to many other pieces of equipment in the nanofabrication facility. We managed to use these facilities successfully and make stamps which preserved the geometries on the wafer. We also made strides in developing a way to ink the stamps (Figure 4). I made several inked samples and learned how to use the fluorescent microscope to analyze them.

Although much progress was made this summer, there is still work to be done on this project. We must perfect the inking process. We need to optimize the drying time of the ink, the amount of ink used, and the method of application of the ink. We also must learn how to apply the lipid bilayer and perform microelectrophoresis. Once these tasks are accomplished, we will have devised an easier, cheaper, more efficient way of separating integral membrane proteins. Perhaps our new method will be used in drug development to devise new drug treatments which will improve the health and welfare of mankind.

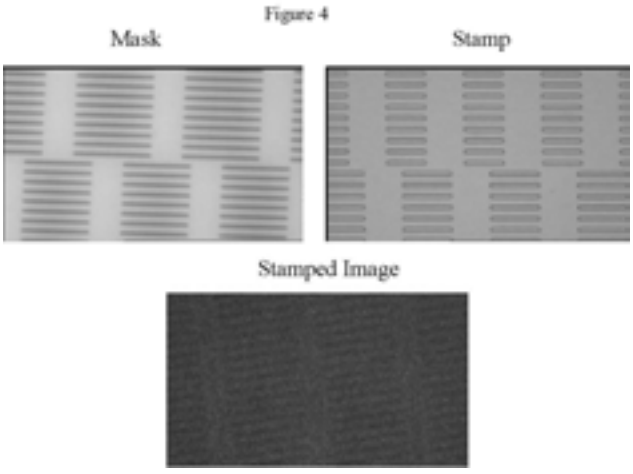

Acknowledgements:

I would like to thank Mary Tang, Alice Gast, Curt Frank, Jane Edwards, Nina Silverman, the Stanford Nanofabrication Facility, the National Nanofabrication User Network, and the Research Experience for Undergraduates program for giving me the opportunity to participate in this project. I especially want to thank Mary Tang, who answered my endless questions and taught me a great deal not only about nanofabrication and integral membrane proteins, but also about research in general.

References:

[1] Pamela M. St. John and H. G. Craighead. 1995. Microcontact printing and pattern transfer using trichlorosilanes on oxide substrates. Appl. Phys. Lett. 68: 1022-1024.

[2] Tampe, R., C. Dietrich, S. Gritsch, G. Elender, and L. Schmitt. Nanofabrication and Biosystems. Cambridge: Cambridge University Press, 1996.

[3] Groves, J.T., S. Boxer, amd H. McConnell. Electric field reorganization of two-component supported bilayer membranes. Proc. Natl. Acad. Sci. 94: 13390-13395.

[4] Tampe, R., C. Dietrich, S. Gritsch, G. Elender, and L. Schmitt. Nanofabrication and Biosystems. Cambridge: Cambridge University Press, 1996.

[5] Sackmann, E.. Supported Membranes: Scientific and Practical Approaches. Science 271: 43-48.

[6] Carlson, R., C. Gabel, S. Chan, and R. Austin. Self-Sorting of White Blood Cells in a Lattice. Phys. Rev. Lett. 271: 43-48.

REU Project Title:

Characterization of Plasma Etching Using Alternative Gases

REU Intern, Major, Home Institution:
Nin Loh, Pomona College

REU Principal Investigator, Dept, Institution:
James McVittie, Stanford University

REU Principal Investigator Email Address:
plummer@ee.stanford.edu

Abstract:

Chlorofluorocarbon (CFC) gases such as C_2ClF_5 (F-115) are used in wafer processing in combination with an etchant like SF_6 to provide a near-anisotropic dry etch. While inert at sea level, these gases can release chlorine atoms which catalyze the dissociation of the stratospheric. Thus ozone-depleting CFC's have been replaced in most etch processes by toxic gases. It is, however, desirable from safety, cost, and flexibility standpoints to find alternative non-toxic gases that will give etch properties comparable or superior to formerly used CFC's and not deplete the ozone. We are characterizing the etching performance of two non-ozone-depleting gases, $CHClF_2$ (F-22) and C_2HClF_4 (F-124) in combination with SF_6. We are studying how their concentration affects polysilicon-to-oxide and polysilicon-to-photoresist selectivities and the profiles of polysilicon etched lines and spaces. Dry etching experiments were performed on a parallel-plate plasma etcher operating in plasma mode and analyzed using a Nanospec thin film measurement system and a scanning electron microscope (SEM). We compared our results to those of the standard process of 50% C_2ClF_5. Our results show that using 20-25% of $CHClF_2$ (F-22) at 400 W and 150 mTorr will provide selectivities and etch profiles comparable to those attained with the standard process.

Introduction:

Chlorofluorocarbon (CFC) gases were once widely used in plasma etching to provide a near-anisotropic etch. These gases accomplish this by depositing a passivation layer of polymer on the sidewalls while the material is being etched. Unfortunately, chlorofluorocarbons have been found to deplete the ozone that protects the Earth from harmful ultraviolet light. The inertness of conventional CFC's allows them to rise to the stratosphere and release chlorine atoms that catalyze the dissociation of ozone. For this reason, these gases have been banned from production and replaced by toxic gases such as chlorine and hydrogen bromide. Because machines using toxic gases require additional leak protection and care in adjusting flows, operating them is more expensive and affords less flexibility in terms of changing process recipes. This is fine for commercial purposes in which machines are normally used for one process. But at multi-user laboratory such as the Stanford Nanofabrication Facility, a plasma etcher may see a dozen different recipes in one day. It is therefore desirable to develop processes that use non-toxic gases so that users may have more flexibility in their research.

Our objective was to replace a near-anisotropic polysilicon etch process that will soon be obsolete because of a decreasing supply of the CFC. The current process uses 50 sccm of the CFC gas C_2ClF_5 (known commercially as Freon 115), in combination with 50 sccm of the etchant SF_6. The process is run at a pressure of 150 mTorr using and RF power of 375 W. We studied the etch characteristics of two gases, $CHClF_2$ (F-22) and C_2HClF_4 (F-124), in order to develop a new process with equal or higher selectivities and equal or lesser degrees of undercutting. These gases were chosen by for their chemical similarity to C_2ClF_5 and their

hydrogen component. The hydrogen is removed by hydroxyl ions in the atmosphere, making the freon unstable and reducing its chances of reaching the stratosphere.

Apparatus and Procedure:

The current process is run in a Drytek DRIE 100 parallel-plate plasma etcher operating in plasma mode (where the wafer is on the grounded electrode). Because we connected the test freon gases to the line calibrated for CF_4, we had to find the flow of each gas in terms of the indicated CF_4 flow. This was accomplished by comparing the rate of pressure rise in the etch chamber at a given flow for each gas. Throughout all our test etches, the pressure and RF power remained at 150 mTorr and 400 W (and 0 reflected), respectively while the test gas concentration varied from 0% to 80%.

First we examined how the etch rates of silicon dioxide, polysilicon, and Shipley 3612 positive photoresist varied with test gas concentration. We etched quarter 4-inch wafers with about 0.1-micron blanket film of silicon dioxide for about 2.5 minutes. We then etched away about 0.1 micron (using laser reflectivity as a gauge) from quarter wafers with about 0.4 microns of polysilicon. Next we etched 0.2 microns away from wafers with a 1.0-micron blanket of photoresist. All thicknesses were measured using a Nanospec thin film measurement system.

To examine the etch profiles of the gases, we exposed a fine line mask onto wafers with Shipley 3612 photoresist over polysilicon over oxide. We etched, with a 25% overetch, these wafers using the standard process and 0%, 15%, 25%, and roughly 40% of each gas. After etching, the samples were cleaved, sputtered with gold, and examined under a Hitachi S-800 scanning electron microscope.

Results and Analysis:

We found that the average ratios between the pressure rise rate of CF_4 and the pressure rates of F-22 and F-124 are 0.965 and 1.62 respectively. As expected the etch rates of oxide, polysilicon, and photoresist decreased with decreasing concentrations of the etchant SF_6. We fitted 3rd and 4th order polynomials to our etch curves and used the resulting curves to determine how selectivities vary with freon concentration. The selectivities also dropped with increasing freon concentration. We found the polysilicon-to-oxide and polysilicon-to-photoresist selectivities of the standard process to be 14.8 and 5.6, respectively. Our selectivity curves show that we can achieve the selectivities of the standard process using up to 20% of either F-124 or F-22.

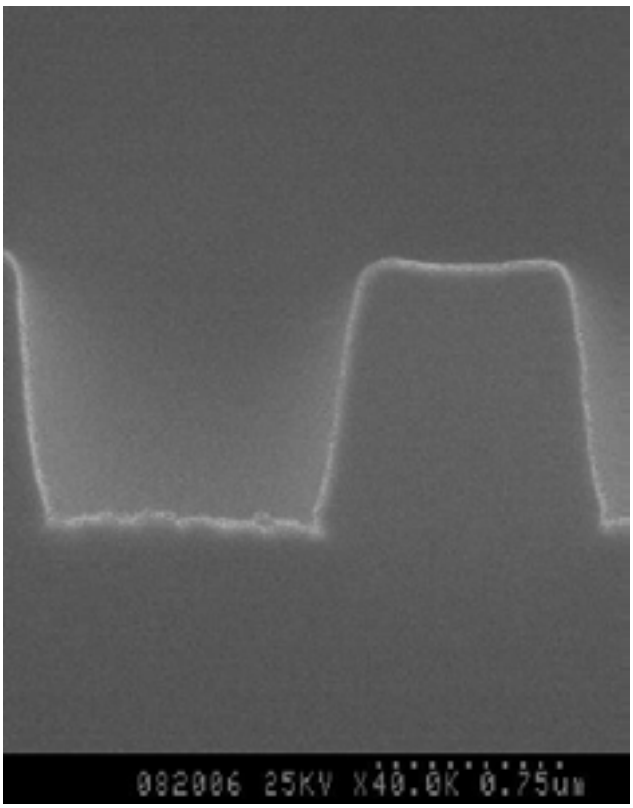

Figure 1. 2.25 micron Line/Space in Photoresist.

The SEM revealed a surprising effect of each gas. Figure 1 shows the photoresist profile of a 2.25-micron line and space structure before etching. Figure 2 shows an analogous structure after it was etched with the standard process giving an undercut of 0.038 to 0.041 microns. The undercutting was calculated by taking half of the change in the width of a line or space from the width on the resist before etching. As expected, the undercutting was most severe in pure SF_6. But, contrary to our expectations, the degree of undercutting was least overall using 25% of F-22 (0.038 to 0.056 microns in Figure 3) and least for F-124 using 15% (0.056 to 0.075 microns). The undercutting actually increased with the concentration of CFC's! We suspect that a small concentration (15%-25%) of either of the gases is enough to form a polymeric passivation layer on the sidewalls to give a near-anisotropic etch. Additional CFC's slow down the etch rate, perhaps allowing more time for isotropic etching.

Conclusion:

In order to replace a standard polysilicon etch process that uses the ozone-depleting C_2ClF_5 (F-115), we characterized of the etch properties of two non-ozone-depleting CFC's, $CHClF_2$ (F-22) and C_2HClF_4 (F-124). We found selectivities comparable to the standard process using up to 20% of the test CFC's. Furthermore, SEM micrographs show that etch profiles with undercutting comparable to the standard process can be attained using 25% of F-22. Our results suggest that a polysilicon etch run at 400 W and 150 mTorr using 20-25% F-22 and 80-75% SF_6 is the optimum replacement mixture for the standard process.

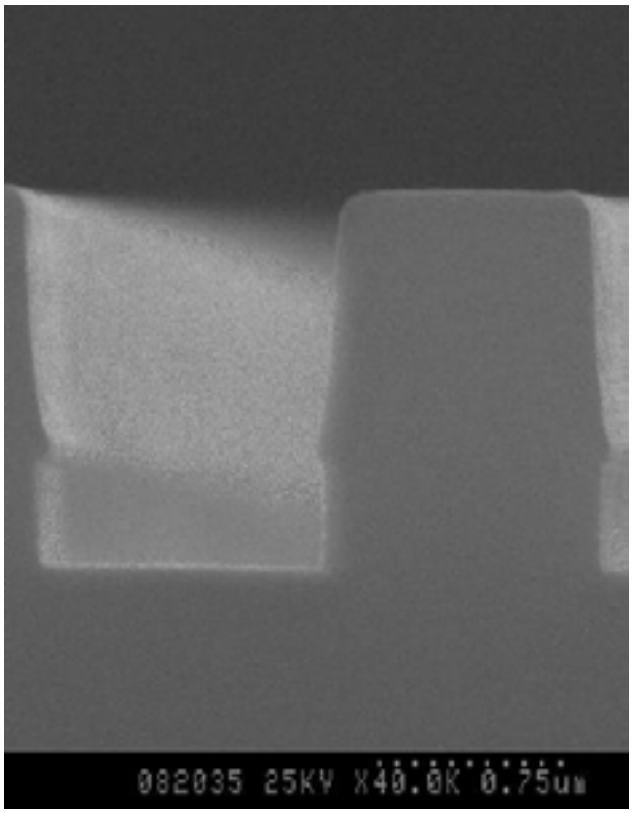

Figure 2. After Standard Etch.

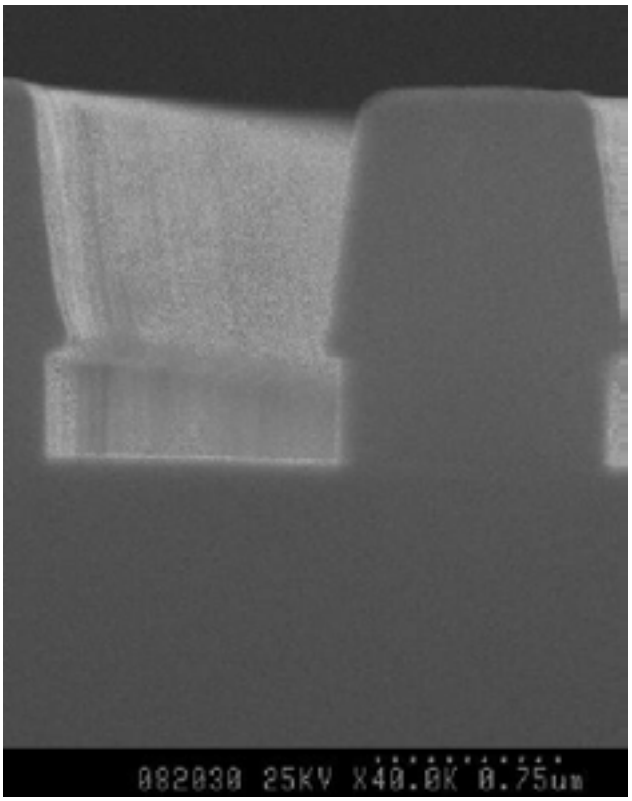

Figure 3. After 25% F-22 Etch.

REU Project Title:

Control of AFM Anodization for Lithography of Single–Electron Transistors

REU Intern, Major, Home Institution:

Adam MacBeth, Electrical and Computer Science, Swarthmore College

REU Principal Investigator, Dept, Institution:

James Harris, Electrical Engineering, Stanford University

REU Principal Investigator Email Address:

harris@snowmass.stanford.edu

Abstract:

A fully operational single-electron transistor (SET) was recently demonstrated at room temperature, though the failure of the device occurred quickly. In order for devices of this type to become feasible for use in integrated circuits, their operational lifetime must be improved considerably. Using a negatively biased atomic force microscope (AFM) tip, thin lines of oxide, on the order of several tens of nanometers in width, can be "written" on thin films of metal. When these lines are written between two areas of conductor, a very small metal island can be formed which electrons can tunnel, creating a transistor. In order to improve the lifetime of these devices, the AFM oxidation process must be studied in detail, so that more robust oxides can be produced. We are currently working on determining the optimal voltages and writing speeds for AFM lithography of titanium, aluminum, copper, and niobium. Once these parameters have been well established, we will attempt to fabricate SETs using the various metals and attempt to measure their electrical properties.

Introduction:

Atomic force microscopy is a technique for obtaining very high magnification images of a material surface. The basic AFM setup includes a finely sharpened tip mounted on a flexible cantilever. This cantilever, or the stage holding the sample, can be precisely actuated by a piece of piezoelectric material. This allows the tip to be scanned over the surface in a racheting fashion. In the contact mode of AFM operation, the tip actually touches the surface, and the movement of the tip over the surface causes a deflection of the cantilever. A diode laser reflected off the back of this cantilever is then deflected from its aligned position on a position-sensitive photo-diode. A computer generated image of the surface is then created using the resulting data.

Using a conductive AFM tip, a voltage can be applied between the tip and a conductive surface. Due to ambient water present between the tip and the surface, oxidation of the surface occurs, a process known as anodization. By moving the tip across the surface, this voltage can be used to "write" lines of oxide on the surface. This method can produce very small line widths and was used to fabricate the first single electron transistor (Figure 1). A SET is a device in which a very small metal island, with a very small capacitance, serves as the gate of a transistor. This island is isolated by insulating oxide lines from two

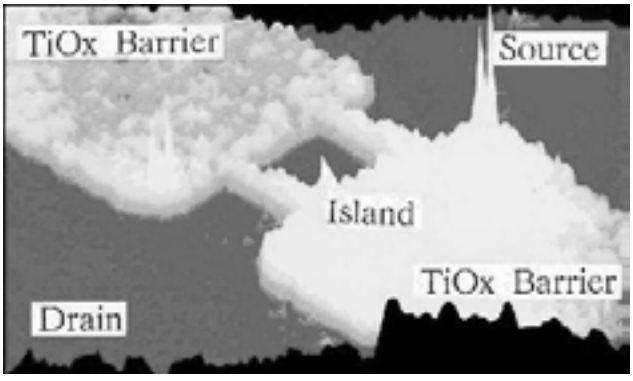

Figure 1. Single-electron transistor fabricated in titanium [1].

larger metal areas, which serve as the source and the drain of the transistor. If the oxide barrier heights are sufficiently large, and the capacitance of the island is sufficiently small (~10-19°C for room temperature operation), tunneling of single electrons to the island can be observed in I-V plots as small steps, known as a Coulomb staircase.

Experimental Procedure:

The initial task for the fabrication of SETs was the calibration of oxide line widths and heights. Si wafers were thermally oxidized to a SiO_2 thickness of ~120 nm. These wafers were then cleaned with a standard diffusion clean of 10 minutes in 4:1 H_2SO_4:H_2O_2, 10 minutes in 5:1:1 H_2O:H_2O_2:HCl. Various thin films were then sputtered onto the surface using a Gryphon sputterer after a 10 sec. dip in 50:1 H_2O:HF. Using the thicknesses given for standard sputter recipes, sputter times were divided down to give the appropriate thickness, assuming a linear relationship between sputter time and film thickness. The sputter conditions were as follows: Ti (~5 nm) 12 sec @ 2.0 kW, Ti (~10 nm) 24 sec @ 2.0 kW, and Al (~10 nm) 6 sec @ 7.5 kW. These film thicknesses were not verified. Copper and titanium at thicknesses of both 5 and 10 nm were also evaporated onto SiO_2/Si samples by Tom Carver of the Applied Physics Department. Using a Digital Instruments Nanoscope 3000 AFM, we then attempted to write oxide lines on these various surfaces. This was performed by writing a simple macro to write one or more lines on the surface. After the macro was run at a certain speed and voltage, the surface was imaged, and the speed and voltage were adjusted for the next run based on observations about the thickness of the oxide. Although we did not attempt to create any SETs, mask patterns were generated and patterned onto a number of wafers. This mask pattern contained a number of structures which could be used for AFM lithography and electrical testing.

Results and Conclusions:

We had trouble getting consistent results in writing of oxide lines, a result which may have been due to variation in humidity or tip quality. Once a firm relationship between parameters and oxidation is established, electrical testing and fabrication of SETs can begin. There are a number of conditions which can be studied in the future such as various metals including Al, Ti, Cu, Nb, and Ni. Other possibilities for control of oxidation include using a humidity controlled chamber or performing oxidation in a fluid.

References:

[1] Matsumoto, Kazuhiko. "STM/AFM Nano-Oxidation Process to Room-Temperature-Operated Single-Electron Devices. Proceedings of the IEEE, vol. 85, no. 4, p. 612., 1997.

REU Project Title:

The Enabling of Germanium Processing and Measurement of Film Uniformity for Dark Matter Detectors

REU Intern, Major, Home Institution:

Chancy Schulte, Engineering, Swarthmore College

REU Principal Investigator, Dept, Institution:

Blas Cabrera, Stanford University

REU Principal Investigator Email Address:

plummer@ee.stanford.edu

Abstract:

Research was done with Professor Cabrera and the Stanford group of the multi-institutional CDMS (Cryogenic Dark Matter Search) experiment. A new class of elementary particle detectors is based on the simultaneous detection of phonons and of ionization in silicon or germanium crystals at temperatures below 100 mK. The sensors are patterned 40 nm thick tungsten and 300 nm aluminum thin-films deposited on 3 inch diameter substrates ranging in thickness from 300 μm to 10 mm. In this work, germanium substrate interactions with aluminum etch (nitric, phosphoric, acetic acids) were monitored. Results from this work show a thin silicon layer on germanium substrate, approximately 10 nm, acts as an effective buffer, enabling etch processing. Thickness of processed tungsten thin-films was characterized using Dektak profilometry equipment. Sputtering was done in Balzers sputter deposition system. Mean film thickness was 464 Å. Minimum thickness was 434 Å and maximum thickness was 512 Å. Standard deviation was 11.4 Å. Evaluation of results shows no predictable variation in film thickness across a substrate. The use of atomic force microscopy (AFM) for future film thickness characterization was explored. Preliminary AFM work shows the equipment to be promising for future thin-film thickness characterization.

Introduction:

Si and Ge detectors are used in dark matter detection in the multi-institutional CDMS (Cryogenic Dark Matter Search) experiment. This new class of elementary particle detectors is based on the simultaneous detection of phonons and of ionization in the silicon or germanium crystals at temperatures below 100 mK. The sensors are patterned 40 nm thick W and 300 nm Al thin-films deposited on 3 inch diameter silicon or germanium substrates ranging in thickness from 300 μm to 10 mm.

Work was done in Stanford's Center for Integrated Systems. In the first part of this research, the problematic interactions of the Ge substrate with processing chemicals, were monitored. In the second part of this work, film thickness uniformity was assessed. Film characteristics must be monitored and controlled to ensure proper operation of detectors. Tungsten films must have a Tc in the range of 50 to 120 mK for the sensors to behave predictably. Tc, and resistance, may be a function of film thickness. In this research, film thickness is measured in conjunction with systematic assessments of Tc of RF magnetron sputtered tungsten films on silicon substrates. Wafers were photolithographically processed using a mask designed for Tc monitoring. W film thickness was measured using equipment including the Dektak Profilometer. The final component of the summer research was the exploration of the use of AFM for possible future use in film thickness uniformity assessments.

Procedure:

A thin Si film, approximately 10 nm, was sputtered on Ge substrate samples using the Balzers DC

magnetron sputter deposition system. Samples were exposed to aggressive Al etch processing. Quality of Ge substrate, Si film, and Ge/Si interface was examined using characterization microscopy equipment and compared to Si/Si sample and Ge sample without buffer layer.

A W thin-film was sputtered on 3" Si substrates using the Balzers system. Samples were photolithographically processed using a uniformity check mask. Films on wafers in the same vertical position on the two row, four column deposition system pallet were characterized using Dektak profilometry equipment.

AFM use for thin-film thickness characterization was explored using wafers used in profilometry.

Results:

A Si 10 nm thin-film on Ge substrate is effective in enabling processing, specifically Al etching.

Dektak film thickness measurements are shown in Figure 1 and Figure 2. Mean film thickness was 464 Å. Minimum thickness was 434 Å and maximum thickness was 512 Å. Standard deviation was 11.4 Å.

Preliminary results from AFM include thickness measurements of three places on wafers used in profilometry analysis. W thin-film thicknesses can be characterized using AFM.

Summary:

Ge substrate interactions with Al etch are buffered effectively by a 10 nm Si film.

There exists thickness variation in W thin-films sputtered in Balzers sputter deposition system. Thickness variation is on the order of 20% across two wafers in same vertical position on deposition system pallet. There is no substantial predictable drop-off in thickness at any edge of wafer.

AFM could be a valuable tool of Professor Cabrera's group in thin-film thickness uniformity assessments. The analysis possibilities available with the AFM system far exceed those of the Dektak profilometry system. Further investigation of uses of this equipment for this group is recommended.

Acknowledgments:

I would like to thank those I worked with at Stanford University: Professor Blas Cabrera, Robert Abusaidi, Roland Clarke, Mike Deal, Shipra Dingare, Jane Edwards, Rick Gaitskell, Robin King, Aaron Miller, Sae Woo Nam, Tarek Saab, and Betty Young. I would also like to thank Professor Lynne Molter of Swarthmore College.

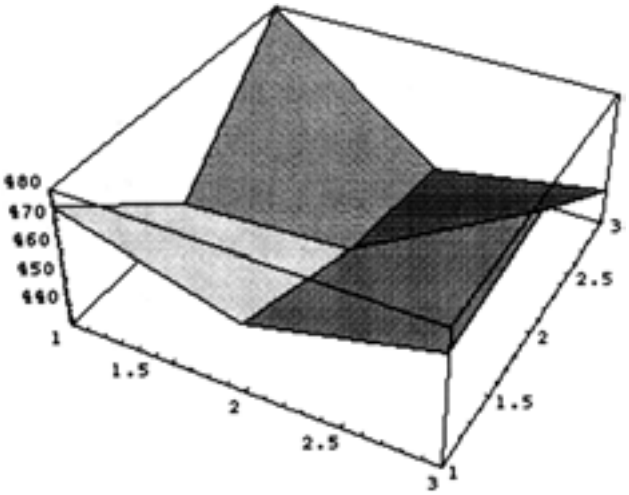

Figure 1: Dektak results for W-T-2: wafer on top row, third column of Balzers pallet.

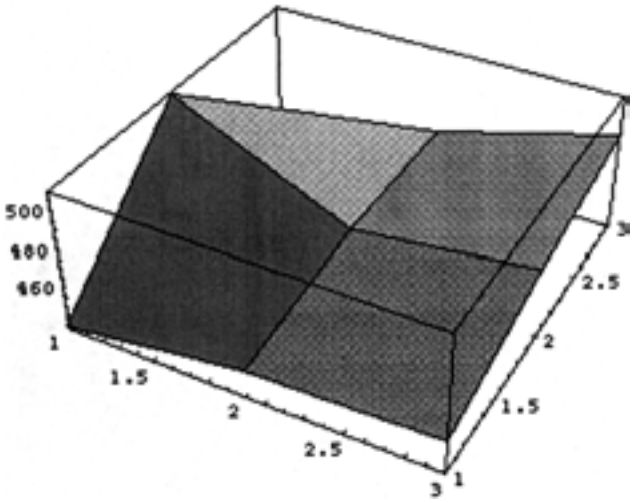

Figure 2: Dektak results for W-T-6: wafer on lower row, third column of Balzers pallet.

REU Project Title:

Resist Charging and Heating in Electron Beam Lithography

REU Intern, Major, Home Institution:

Corina-Elena Tanasa, Physics and Mathematics, Bard College

REU Principal Investigator, Dept, Institution:

Mark McCord, Electrical Engineering, Stanford University

REU Principal Investigator Email Address:

plummer@ee.stanford.edu

Abstract:

Resist charging on masks during electron beam writing degrades overlay performance in lithography by introducing placement errors. To minimize resist charging effects an understanding of the resist charging process is needed. Using the Modular Electron Optical Column we measured the charging of the PBS resist at 10 and 20 KV beam voltage, for resist thicknesses between 0.2 and 1.5 micrometers. The results show that thinner resist charges positively, while thicker resist charges negatively. The surface voltage is energy and thickness – dependent. A model has been proposed for the process of resist charging.

The other part of the project involves testing of the new UV5 and UVN2 resists. Best prebake and postbake parameters, as well as exposure dose have been determined and conclusive SEM images of the exposed pattern have been taken.

Experimental Procedure:

The experimental equipment used in the resist charging experiment was a MEOC, a Modular Electron Optical Column. First the stage holding the resist film on a grounded silicon substrate is moved under the Kelvin Probe for calibration. Then the stage is moved under the electron beam to expose the PBS sample. Finally, the exposed area is moved under the Kelvin Probe to measure the potential of the resist film.

Two sets of experiments were carried out. One was at 10KV beam energy, with 1.2nA exposing current, with a dose of 2mC/cm^2 which corresponds to 100s exposure time. The other experiment was at 20KV beam energy, with 3 nA exposing current, with a dose of 4mC/cm^2 which corresponds to 125s exposure time.

For the characterization of UV5 and UVN2 resists , we exposed wafers covered with thin film of resist in the Hitachi HL-700F Electron Beam machine. The pattern consisted of various arrangements of lines and dots, with feature size between 80 nm and 1 micron.

Charging Model:

The following model was proposed for the process of resist charging. Each electron that goes into the resist creates free electron-hole pairs. The free electrons close to the surface, that is, within 10 to 20 nm depth, escape, leaving behind the positive holes. The beam electrons which penetrate the resist either stop into the nonconductive resist, or arrive at the grounded substrate. The charge distribution is thus negative and approximately constant in the lower part of the resist film and positive and exponentially decaying in the upper part of the resist film. For this charge distribution the surface potential is a second order polynomial function of resist thickness.

Results And Conclusion:

From the two graphs Voltage versus Resist Thickness it follows that the thinner the resist, the more positive is the charging. Also, the higher the energy of the beam, the more positive is the charging of the surface. This is because the more electrons hit the resist film, the more free electron- hole pairs are created and therefore the more holes are left behind after the surface free electrons escape.

The two sets of experimental data are fit by second order polynomials:

$V=1.58-3.88\text{-}10^{-6}(h-154)^2$ for 10KV beam energy, dose 2 mC/cm^2

and

$V=2.86-4.02\text{-}10^{-6}(h-347)^2$ for 20KV beam energy, dose 4 mC/cm^2

Therefore the model proposed describes very well the process of resist charging. There is a thickness of the resist film for which the surface potential is zero.

Concerning the characterization of the UV5 and UVN2 resists, we have determined that optimal prebake parameters are 130°C and 60 seconds, the best exposure dose is $10mC/cm^2$, the postbake parameters are 115°C and 95 seconds, and developing time is 45 seconds. The SEM image with 0.1micron features is shown.

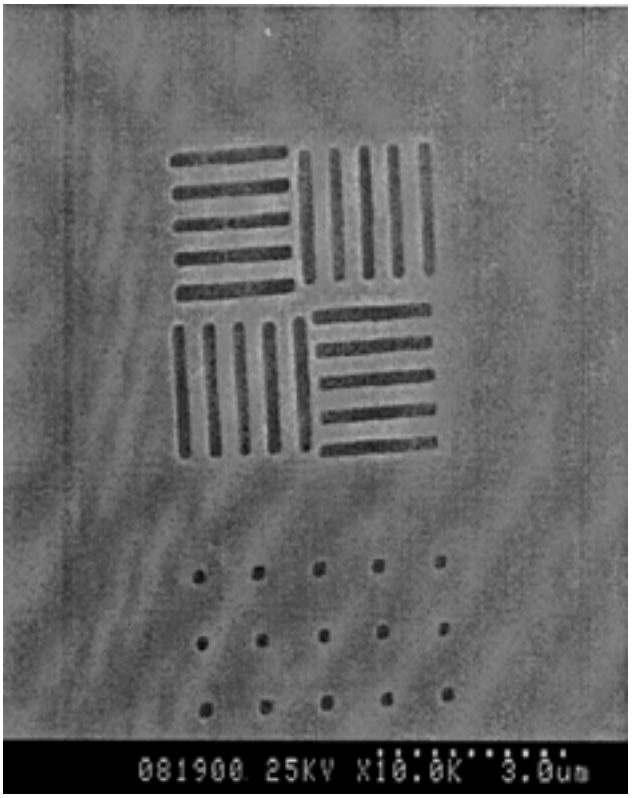

Acknowledgment:

I would like to thank Marnel King for her invaluable help and for the team work we did.

References:

[1] W. Liu, J. Ingino and R. F. Pease, J. Vac. Sci. Technol. B 13(5), 1979(1995).

[2] K. Kanaya and S. Ono, "Electron Beam Interaction with Solids in Microscopy, Microanalysys & Microlithography", pp69-98.

[3] J. T. L. Thong, "Electron Beam Testing Technology", pp177.

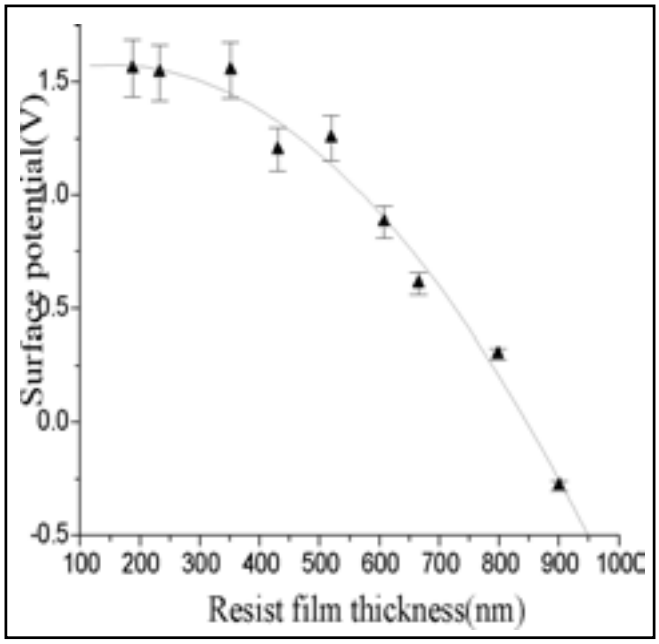

PBS Charging in $2mC/cm^2$ Exposure at 10KV Beam Energy.

University of California Santa Barbara

1998 REU Participants

REU Participant	Home Institution	Prinicipal Investigator
Front Row:		
Brian Wolf	QUEST Staff	
Liu-Yen Kramer	QUEST Staff	
Al Frink	QUEST Staff	
Gavin Scott	UCSB	David Awschalom
Rafael McDonald	Princeton University	Evelyn Hu, Galen Stucky
Lezlie Potter	University of Notre Dame	David Clarke
Back Row:		
Ali Herrera	UCSB	David Awschalom
Helena Holeckova	SUNY of Buffalo	Evelyn Hu
Katie Wooton	Wake Forest University	Geoff Strousse
Ben Werner	UCSB	Pierre Petroff
Patricia Valenzuela	SUNY Albany	Fred Milstein

REU Project Title:

Near Field /Atomic Force Microscopy Using GaN Lenses

REU Intern, Major, Home Institution:

Ali Herrera, Mechanical Engr, UC Santa Barbara

REU Principal Investigator, Dept, Institution:

David Awschalom, Physics, UCSB

REU Principal Investigator Email Address:

liu-yen@engineering.ucsb.edu

I spent the summer at the University of California at Santa Barbara learning about the various properties of the semiconductor gallium nitride (GaN). GaN has been gaining public interest in the last few years because it is an efficient emitter of blue light. Blue light is of interest because it is high-energy and therefore has a short wavelength.

Rising interest in this material has prompted research into better ways of characterizing GaN. Two ways that are currently employed are near field scanning optical microscopy (NSOM) and atomic force microscopy (AFM). The ultimate goal of the project I worked on this summer was to build a new and exciting type of microscope that could combine these two techniques. A NSOM/AFM could produce the same scale of resolution as two separate microscopes and would be an ideal way of correlating light emission with topography.

A conventional near field image is taken using a tapered optical fiber which is placed within a wavelength of light from the surface of the sample. The probe is scanned across the sample surface collecting light through a ~100 nm aperture. This technique allows us to get resolution of a couple hundred nanometers. A conventional atomic force microscope uses a cantilever with a small sharp tip at the end. The cantilever is driven up and down as it moves across the surface of a sample. The smallness of the tip and closeness to the surface allow for atomic scale resolution.

GaN pyramids are the ideal way of combining these two techniques. A GaN pyramid could act as a micron size lens grown on the end of a GaN cantilever. GaN has a high index of refraction, n=2.7. GaN can be used as a cantilever because it has a high piezoelectric constant, which would allow it to be driven up and down by applying an AC voltage. GaN is a hard material so that it would be able to tap on the surface of the sample without incurring any damage unlike a fiber optic tip that would break with any contact with the sample surface.

This summer's research resulted in some interesting conclusions about the prospects of using these GaN pyramids as lenses an NSOM/AFM microscope. We found that the fabrication of the pyramids will allow us to make cantilevers with pyramids at the end with some simple etching processes. The characterization of the pyramids gave us valuable information concerning physical size, material properties, and finally optical properties. Physically the pyramids are the right size and shape for our purposes. The material properties of GaN are ideal for the cantilever tip apparatus we envision. The optical properties of the GaN pyramids were more difficult to classify. We were able to determine with photolithography and near field scanning optical microscopy that the pyramids focused light. In order to compete with current technology the pyramids must be able to focus light down to ~300nm. We did observe the pyramids focusing light down to 2 mm. Further experimentation is necessary to determine if the optical properties of these pyramids are sufficient to replace tapered fiber optic tips. Unfortunately, my part in this project is over; however, I would like to see these pyramids used as lenses in an NSOM/AFM microscope one day. A microscope of this kind would be a major tool in the understanding light emitting samples.

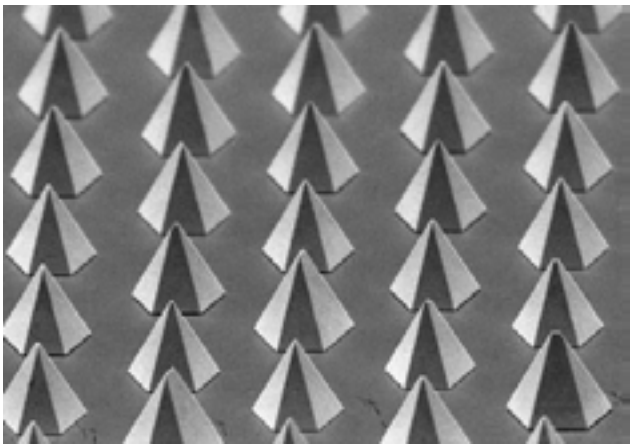

REU Project Title:

Phage Display Libraries Used for Inorganic Material Recognition

REU Interns, Major, Home Institution:

Helena Holeckova, SUNY at Buffalo;
Rafael McDonald, Princeton University

REU Principal Investigators, Dept, Institution:

Galen Stucky and Evelyn Hu, Materials Dept., UCSB

REU Principal Investigator Email Address:

liu-yen@engineering.ucsb.edu

Abstract:

Nature uses unique characteristics, which are desirable for material design and synthesis, including high selectivity, nanoscale self-assembly and precise structure control. Our approach to nanofabrication and pattering inorganic materials, such as metals, magnetic materials and semiconductors, is to use the precise material and structure recognition of biological systems. We are using combinatorial method called phage display libraries to isolate polypeptides that will specifically recognize, bind and nucleate inorganic nanoparticles to interconnect regularly spaced magnetic and electronic materials useful in devices such as electronic circuits.

Introduction:

My goal for the summer was to synthesize magnetic nanoparticles, specifically maghemite (Fe_3O_4), maghemite (g-Fe_2O_3) and hematite(a-Fe_2O_3); also referred to as iron oxide particles. In addition, if time permitted to use the phage display libraries to isolate polypeptides that can recognize and bind to each of the magnetic nanoparticles. An example of how a polypeptide can bind to magnetic particles is the protein hemoglobin, as shown below, each of the four polypeptides is attached to an iron containing heme. The binding between the polypeptide and the heme is based on ionic interactions and van der Waals interactions. We expect that the binding between the polypeptide and our magnetic particles will be based on the same interactions including hydrogen-bonding.

Experimental Method:

The first thing that we have done is to synthesize iron oxide nanoparticles. We are using these before we move on to semiconductor quantum dots, in order to fabricate 2-D highly ordered arrays of ferromagnetic clusters. We are using three different iron oxides: maghemite (Fe_3O_4), maghemite (g-Fe_2O_3) and hematite (a-Fe_2O_3). All the iron oxide particles were analyzed by x-ray diffraction to determine if the correct product was obtained and to determine the size of the particles. Magnetite (Fe_3O_4) was successfully synthesized with sizes ranging from 46 to 113 Angstroms.

Conclusion:

So far, we have been successful in synthesizing magnetite, which is now ready to have polypeptides attached to it. We are now in the position to use the existing iron particles in order to determine which polypeptide will bind to them via the phage display libraries.

If this project does succeed and research continues in this field, then in about 10 to 15 years down the road, we may be able to take a beaker filled with polypeptides or other biological material, dip a inorganic substrate into it and the polypeptides will arrange themselves on the substrate giving us a nano-size electronic circuit.

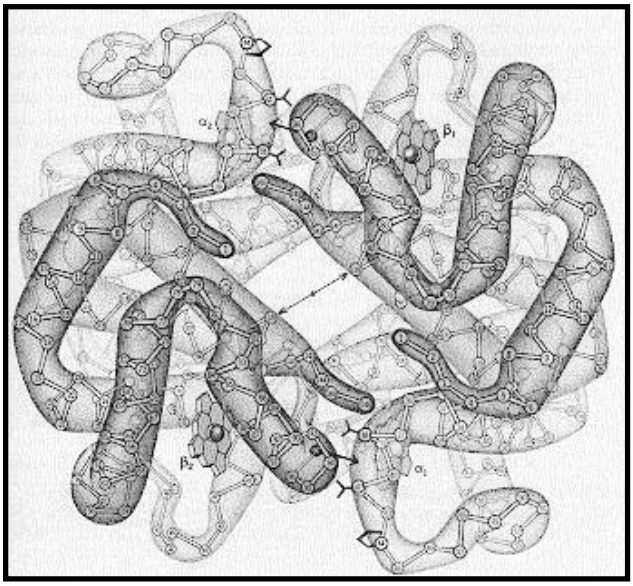

REU Project Title:
Non–Lithographic Nanoscale Fabrication

REU Interns, Major, Home Institution:
Rafael McDonald, Princeton University;
Helena Holeckova, SUNY–Buffalo

REU Principal Investigators, Dept, Institution:
Evelyn Hu and Galen Stucky, Materials Dept, UCSB

REU Principal Investigator Email Address:
liu–yen@engineering.ucsb.edu

The need to make circuits and other electrical devices smaller and smaller has been evident from the birth of the first "computer". Until recently, lithography was the most common method used. This method can etch patterns as small as the wavelength of light that is being used. Unfortunately, this method seems to have hit a plateau: optical lithography can etch only to about 500nm, and other more difficult lithography only to about 300nm. Any method that could pattern inorganics such as semiconductors at smaller length scales would be invaluable. We have looked to nature as our guide, noting that patterns as small as a few nanometers have been observed (Mann, 1996). Not only is nature capable of such small length scales, it does so with self-assembly, allowing a small percentage of proteins to direct the assembly of the majority of inorganic molecules. We wish to take advantage of self-assembly to achieve similar goals.

In these experiments our goal is to use the step edges of off-cut semiconductor materials in order to organize nanoparticles. The first step will be to use the step edges of off-cut gallium arsenide, indium phosphide, and silicon as substrates on which to build a pattern. The semicondutors have a native oxide that is terminate at the surface with hydroxide groups. Due to the two surfaces at the step edge there will be a higher density of hydroxide groups present than on the planar surface. By controlling the kinetics of the reaction at the step edge, we will attempt to preferentially decorate the step edges with silylating agents that terminate with a chemically reactive group, in this case a mercapto group (-SH). This will form a surface with parallel lines of (-SH) groups

After silylation, there were spherical shapes clearly distinguishable on the surfaces of the flat InP and the off-cut InP (Figure below). Silicon, and off-cut GaAs were not studied at this stage because of time constraints. As is shown in Figure, the off-cut InP had slightly more deposition in the regions that were magnified, but there was not a significant difference between the two. They were covered by circles roughly 100 Angstroms in diameter, and 150-200 Angstroms high.

The change in surface appearance after the silylation and gold reactions indicates that the attachment was successful. The fact that the gold will not attach directly to the surface indicates that the silylation worked. More information after the silylation and before the gold attachment needs to be collected. AFM imaging needs to be done in-between these reactions.

As in most research, one question's answer leads to many more questions. Further work needs to be done to assess qualitatively the effects of the concentrations of both the silylation and the gold parts of the experiment. When does the surface appear to be completely covered? Does the gold prevent observing the surface, or the organic, or the combination of the both? Answers to these questions are crucial before further work can be done in this area.

Bibliography:

Mann, Stephen, ed. Biomimetic Materials Chemistry. VCH Publishers, Inc. New York, New York, 1996.

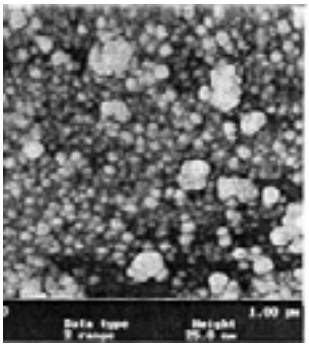

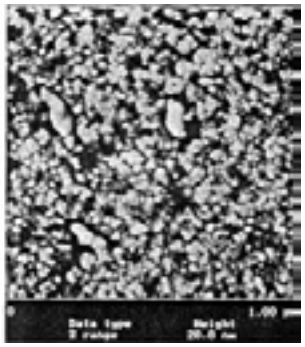

REU Project Title:

Laser Enhanced Debonding of Nitride Semiconductor Films

REU Intern, Major, Home Institution:

Lezlie Potter, University of Notre Dame

REU Principal Investigator, Dept, Institution:

David Clarke, Materials Department, UCSB

REU Principal Investigator Email Address:

liu-yen@engineering.ucsb.edu

Abstract:

Gallium Nitride (GaN) devices have garnered a lot of attention recently because of their use in wide band gap semiconductor applications such as blue LEDs and blue lasers. Many limitations exist in growing device material, however, because of the lack of a matched substrate. Currently, films are grown on Sapphire substrates which have both a lattice constant and thermal conductivity coefficient mismatch, causing stresses and high dislocation densities in the GaN devices as they grow and cool.

Methods:

The ultimate goal of my research group at UCSB is to develop a way to remove thick (100–500mm) GaN films from their Sapphire substrates, releasing the stress caused by the thermal conductivity mismatch. The freestanding film can then be used as a matched substrate for further GaN thin (0.2–2mm) film device growth by Molecular Beam Epitaxy (MBE) or Metal-Organic Chemical Vapor Deposition (MOCVD). On a matched, stress-free substrate, devices should grow with fewer dislocations and defects, resulting in more efficient performance. Another benefit of removing the films from Sapphire, an insulator, is that they can be rebonded to metals such as copper where the material conductivity can dissipate away heat generated during device operation.

Results and Discussion:

Removal was achieved by decomposing the GaN to Ga and N_2 at the substrate interface with pulsed laser energy, separating the film from the Sapphire and allowing the substrate to be lifted off. The laser debonding process setup is shown in the figure below. This debonding process relaxes some of the stress present in the bonded film, as reflected in the Raman spectra of the film before and after its removal. Comparison of the two sets of data reveals that the free standing films have fewer stress-induced lattice vibrations and that the Raman wavelength shift can be calibrated to the film stress.

During the course of my project I was able to optimize a procedure for the lasing and etching removal of thick GaN films from their mismatched Sapphire substrates. I was also able to demonstrate, characterize, and measure the amount of stress relaxation that occurs when the films are lifted off, calculating that for every GPa of stress present in the bonded film, removal relaxes the crystal and shifts lattice phonons to a lower frequency, in addition to narrowing the spectral peaks. Hopefully, my group will be able to use this data to better understand the thermal stress present in GaN films and enable them to grow thicker films to be further used as substrates for growth of high quality, efficient, GaN devices.

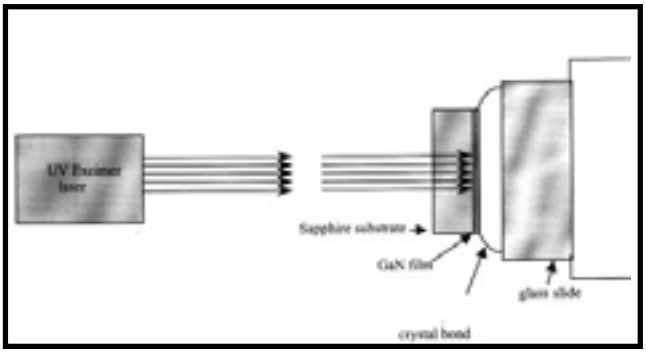

REU Project Title:

The Near-Field Scanning Optical Microscope (NSOM)

REU Intern, Major, Home Institution:
Gavin Scott, UC Santa Barbara

REU Principal Investigator, Dept, Institution:
David Awschalom, Physics, UCSB

REU Principal Investigator Email Address:
liu-yen@engineering.ucsb.edu

Introduction:

Whether it was with a high school biology class or with an at home science kit, just about every single one of us has used a light microscope at some point in our lives. But what do we do if we want to see things that are smaller than the limit allowed by a light microscope?

The answers to that question lies in the realm of near-field optics. The "near-field" of an object (as opposed to the far-field) is the entire region less than one wavelength of light away from that object. When dealing with visible light this is about 400-500nm. I have been involved in a research group that is attempting to build a near-field scanning optical microscope.

The area that most of my research has been devoted to is concerned with the fiber optic waveguides for the near-field microscope. In order to be used for the near-field microscope, the end of the fiber optic probe must be tapered to a small pointed tip. Fabricating these probes to be as efficient as possible has been the focus of my work. With a more efficient probe we will be able to obtain an improved spatial resolution and hence a more efficient near-field microscope.

Experimental Method:

The original procedure we used to taper the fiber we call the "pulling method". In the pulling method we direct a CO_2 laser at a fiber and use a micropipette puller to apply an equal force to either side of the fiber, pulling it into two pieces. The pulling method creates long taper regions and correspondingly small taper angles (the taper angle is measured from parallel to the length of the fiber).

More recently we have switched to the "etching method". In this method we place the fibers in a buffered hydrofluoric acid solution (BHF) with a thin layer of an organic solvent on top. Etching the fibers produced a much larger taper angle than the tapers made by the pulling method. The etched fibers had a taper region approximately one third the length of the pulled fibers.

Analysis/Conclusion:

While experimental data suggests that fibers with etched tips will be significantly more efficient that the fibers with pulled tips, we currently have no quantitative evidence to support this. We plan to perfect our manufacturing techniques until the etched fibers can be consistently reproduced before we begin testing the relative efficiencies of the different kinds of tapered fibers. Once we obtain a higher efficiency fiber tip, we can continue using the near-field microscope with an improved spatial resolution to see things in a way they have never been seen before.

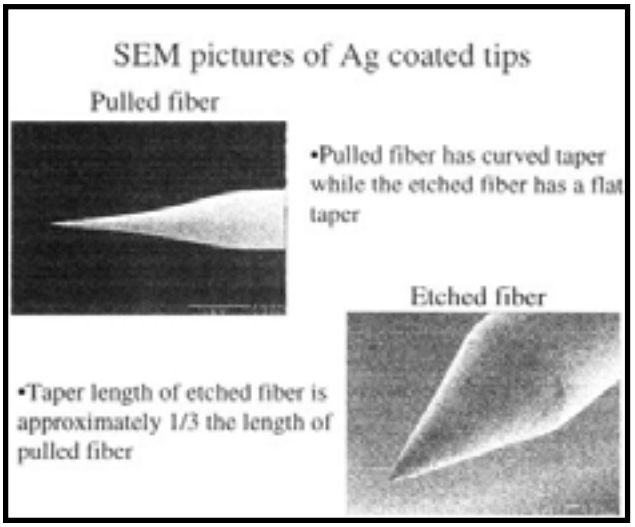

REU Project Title:

The Effects of Adding Emulsion Droplets to a Polyacrylamide Gel

REU Intern, Major, Home Institution:

Linda Steinberger, UC Santa Barbara

REU Principal Investigator, Dept, Institution:

David Pine, Physics, UCSB

REU Principal Investigator Email Address:

liu-yen@engineering.ucsb.edu

Introduction:

Gel electrophoresis is an analytical method used in biology for the separation and characterization of proteins, nucleic acids and subcellular particles such as viruses and organelles. Its works on the principle that charged particles of a sample will migrate in an applied electric field. In polyacrylamide electrophoresis the gel is mounted between two buffer chambers containing separate electrodes. The DNA is then loaded into the wells at the top and once the current is applied the segments migrate downwards.

There are two types of separation that occur during electrophoresis, separation based on charge and separation based on size. Larger fragments have a more difficult time maneuvering through the gel matrix and as a result these strands will travel at a slower rate than the smaller ones. In general, polyacrylamide gels have pore sizes ranging from 20 - 80 nm and are most effective at separating smaller strands ranging up to 10 kb. These are relatively small strands since it is common to work with DNA as large as 300kb. The goal of this project is to produce physically stable polyacrylamide gels that have a large pore size.

Methods and Materials:

Currently, the characteristic pore size of a polyacrylamide matrix is mainly controlled by varying the concentration of acrylamide or bis-acrylamide. In this research we seek to develop an alternative method for creating larger pore sizes while maintaining a physically stable gel. We have been investigating the effectiveness of creating larger pores by adding emulsion droplets to the aqueous solution of the polyacrylamide gel and allowing the gel to polymerize around them. An emulsion droplet is basically a mixture of oil and water with surfactant at the interface in order to maintain kinetic stability and avoid coalescence. It has a structure similar to that of a micelle except that the center is composed of oil (see figure below).

In this experiment the emulsions are composed of SDS and isooctane. I have investigated three methods of removing these emulsions from the gel phase of the polyacrylamide. Various concentrations of alcohol and SDS were used to solubize the emulsions. In addition, an electric field was applied to a number of gels in SDS in an attempt to drive out the emulsions.

Results and Conclusions:

The first two methods that were used to remove the emulsions, simple diffusion using either alcohol or SDS, did not give promising results. The best results I achieved occurred using the third method, which was applying a voltage to a gel in a buffered solution containing SDS. The emulsion droplets migrated downwards cleaning out the gel from top to bottom.

I would like to see further attempts made at removing the emulsions using an electric field. The gels should be run in higher concentrations of SDS. In addition, the buffer/SDS solution should periodically be changed. I believe it would be advantageous to use a transparent porous plastic, which allows for the diffusion of water and also covalently bonds polyacrylamide. I also think it would be beneficial to attempt to remove the emulsions using a salt solution. The particles of such a solution are relatively small and therefor would have an easier time diffusing through the medium. I would also like to see the use of radioactive sulfur to produce the SDS. Using radioactive SDS either in the emulsions themselves or in the SDS bath would allow for a more rigorous and quantitative method for determining the level of cleanness of the gel.

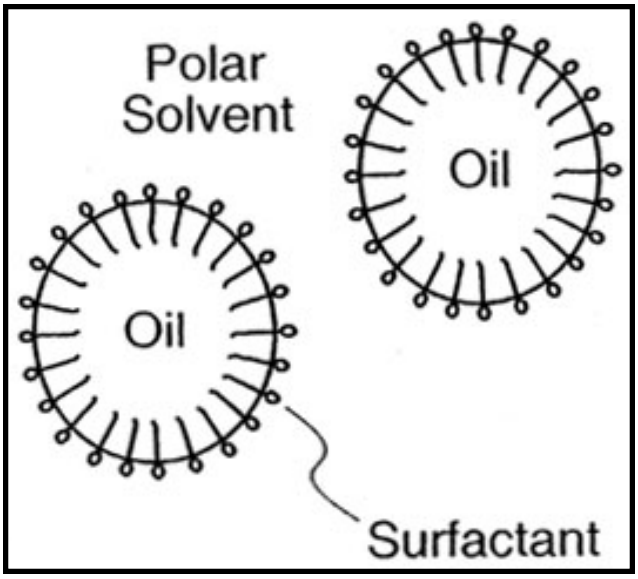

REU Project Title:

Mechanical and Microstructural Properties of Lightweight Ceramic Ablators

REU Intern, Major, Home Institution:

Patricia Valenzuela, Rensselaer Polytechnic Institute

REU Principal Investigator, Dept, Institution:

Fred Milstein, Mechnical Engineering, UCSB

REU Principal Investigator Email Address:

liu-yen@engineering.ucsb.edu

Introducation:

High temperature and high strength heat shields are needed for proposed manned exploration of other interstellar planets. These missions will experience severe heat loads and high shear loads during the descent into a planet's atmosphere. Traditional ablative materials that have worked well in protecting the vehicle from a high heating environment have not been mass efficient.

Lightweight Ceramic Ablators (LCA's) were recently developed at NASA Ames Research Center using a low-density fibrous substrate impregnated with polymeric resin as an ablative heat shield that can withstand very high heating rates and shear loads while providing the necessary thermal protection for the interior of the vehicle. The three types of ablative material that fall under the LCA family are Phenolic Impregnated Carbon Ablator (PICA), Silicone Impregnated Reusable Ceramic Ablator –Fibrous Refractory Composite Insulation (SIRCA-FRCI), and Silicone Impregnated Reusable Ceramic Ablator-Ames Insulation Material (SIRCA-AIM).

Methods:

In order to optimize the development and use of LCA's, it is necessary to measure the properties and behaviors of these materials, including the thermophysical, thermochemical, mechanical, and microstructural characteristics. The thermal properties have already been tested. Therefore, this project consists of understanding the mechanical and microstructural properties. These tests include such tests such as shear, hardness, compression, and tension and possibly others if needed.

Arc-jet tests, which bombard the material with ions, are used to simulate conditions when entering an atmosphere. These tests have been conducted to analyze the thermal performance and ablation characteristics of the LCA's in high enthalpy, hypersonic flow environment. After arc-jet tests were performed there was a formation of a char layer on the surface of the material, which will begin to spall from the base material. Both the charred and non-charred (virgin) states were tested in order to determine how the strength of the material changes when it re-enters an atmosphere.

Results and Conclusions:

In-plane results indicate that SIRCA-F has the highest mean compressive strength, followed by SIRCA-A, and then by PICA. Results from PICA tests in the out-of-plane direction differ significantly from that of the in-plane. The out-of-plane PICA had a compressive strength four times that of the in-plane. The secant modulus (E50%,E90%) of the material identifies the stiffness of the material as it reaches its compressive strength. In comparison, Cork has a range of compressive strength of 0.54 - 2.0 MPa and a hardness range of 0.8-3 MPa, which is quite similar to that of the LCA's.

During the course of this project, the Scanning Electron Microscope was used to understand the effects of testing on the LCA's. Particular attention was paid to the fiber orientation. Also, the stressed fibers gave a microscopic view on the fractured surfaces (figure below).

The next step in this project will be to test these materials mechanically while they are being heated, in order to learn more about the mechanics during this charring process. In the meantime, we recommend adjusting the fiber to polymer ratio to make the LCA's stronger. Also, it may be wise to consider using other kinds of polymers to impregnate the material.

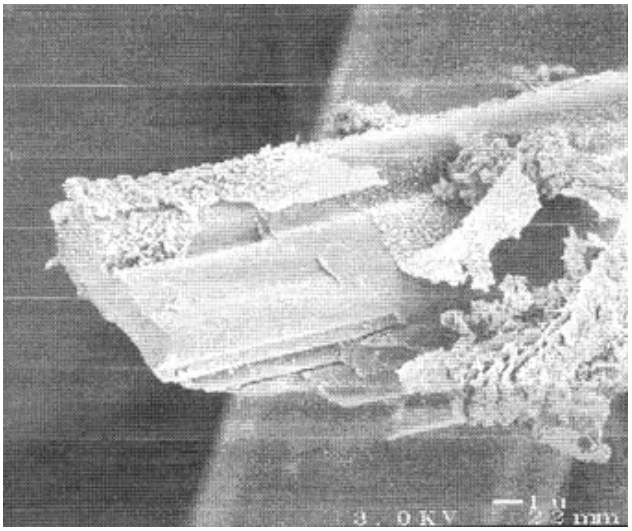

REU Project Title:

Annealing Behavior of Ar+ Plasma–Damaged InAs Quantum Dots & InGaAs Quantum Wells

REU Intern, Major, Home Institution:

Ben Werner, UC Santa Barbara

REU Principal Investigator, Dept, Institution:

Pierre Petroff, Materials Dept., UCSB

REU Principal Investigator Email Address:

liu-yen@engineering.ucsb.edu

Abstract:

Quantum wells (QWs) and quantum dots (QDs) are semiconductor structures grown using molecular beam epitaxy (MBE) which allows deposition of atomic monolayers. QDs and QWs are grown small enough such that quantum behavior such as confinement of single electron-hole pairs in QDs and a "tunable" emmission/ absorsion wavelengh or bandgap in QDs and QWs is exhibited. The issue of radiation resistance is relevant to the performance of many semiconductors since plasma radiation is used in device fabrication. A previous study by Winston Schoenfeld has shown that QDs are more resistant to Ar+ radiation than QWs, however we can't account for the presence of radiation-induced damage at the depths of the active regions in the QD and QW samples. We are prompted to examine more closely the dynamics of radiation-induced point defect migration in these devices.

Samples:

Our QD and QW samples were grown using molecular beam epitaxy (MBE) while the various elements (In, Ga, As, Al) are evaporated onto the substrate. Our QDs are self-assembled dots (SAD), which means that they form without manipulation in the MBE growth chamber. Our QDs are InAs on a GaAs substrate. Since InAs has a larger lattice constant (atoms spaced farther apart) than GaAs, at about 1.7 mono-layers (ML) of deposition the InAs finds it more energetically favorable to "bead up" into islands, It is this lattice mismatch that sets up the strain field that we have proposed has some influence on defect migration.

Experimental Techniques:

In our experiments we anneal Ar+ plasma-damaged QD and QW samples using the rapid thermal annealing (RTA) technique which facilitates point defect migration. We then measure the photoluminescence (PL) of the samples which gives us the wavelengths and intensities at which the sample is absorbing and emitting light. Comparing the PL of the damaged and annealed samples to control samples can tell us whether or not the point defects are propagating into the active regions. Considering the structure of the our QD and QW samples we can make an inference as to mechanism for point defect migration in these and similar devices.

Results/Error Analysis:

Measuring the PL of the same sample on separate occasions allows us to determine how much error is represented in our data. When we were conducting our data analysis we discovered that there was significant error, which invalidated any trend we might hope to see from one data point to the next. We proposed two principle sources of error; the sample is not homogeneous, and, the laser power isn't high enough to consistently excite the reference well and the upper QD/QW to the same proportion.

Conclusions & Recommendations:

It appears that our samples, particularly the QDs, are not homogeneous enough to resolve trends in an experiment such as this. It might be useful to vary the MBE growth conditions (such as the temperature or QD layer thickness) and then take the PL of these samples in order to compare the error represented in each. Homogeneous growth of QDs is already a primary focus in quantum electronics research, so it may be that new growth techniques will soon solve this problem.

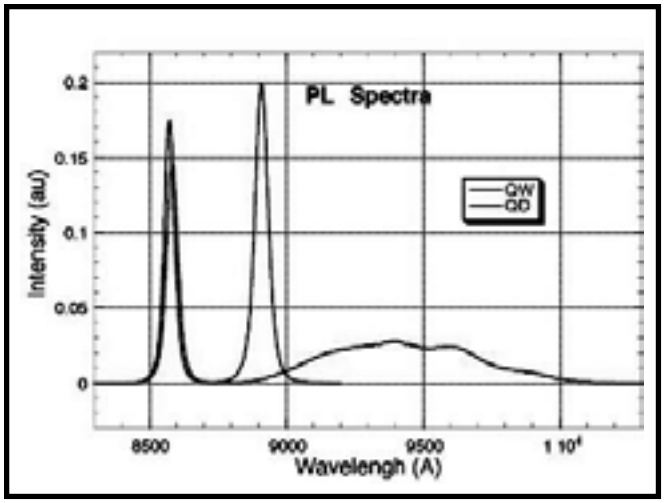

REU Project Title:

II–VI Semiconductor Nanocrystals Synthesized in Solution Phase

REU Intern, Major, Home Institution:

Katie Wooton, Wake Forest University

REU Principal Investigator, Dept, Institution:

Geoffrey Strouse, Department of Chemistry, UCSB

REU Principal Investigator Email Address:

liu-yen@engineering.ucsb.edu

Introduction:

Semiconductor nanocrystals have received much attention lately because of the size-dependence of their physical and optical properties. The wavelength of light absorbed and emitted by a semiconductor nanocrystal can be tuned by varying the size of the crystal. As cluster size increases, the energy of the lowest optical transition decreases due to quantum effects, causing a red shift in optical absorption. This property has been used to develop light-emitting diodes (LEDs) that can emit light in the blue-green range. If conducting organic molecules could be used to link the clusters, a nanometer-sized circuit could be fabricated from self-assembly methods. The purpose of this project was to investigate the synthesis and optical properties of ZnS and CdS nanocrystals of varying sizes, as well as related compounds made by substituting the capping groups of the clusters.

Methods and Results:

The first goal of the project was to synthesize discrete-sized, monodispersed ZnS and CdS clusters of the type $M_x(SPh)_y$ (M = Zn, Cd; x = 4, 10; y = x + 6). The next step was to control the substitution of the capping groups with organic molecules and to connect multiple clusters into a lattice. The long-range goal of the project is to assemble multiple clusters into a working circuit connected with organic conducting molecules.

Several discrete sizes of ZnS and CdS clusters were successfully synthesized in solution. Two methods for cluster modification were explored: halide substitution and pyrolytic routes. The small clusters (Cd_4 and Zn_4) were substituted at apical positions by halides (I and Br). On the large clusters (Cd_{10} and Zn_{10}) pyrolytic routes were used to replace the four apical phenylthiol groups with 4-aminophenylthiol. These clusters were identified by electrospray mass spectrometry (ESMS) in both positive and negative ion modes. Absorption spectra were gathered to determine the relationship between cluster size and wavelength of light absorbed.

Conclusion:

Monodispersed ZnS and CdS clusters of various sizes may be synthesized in solution. The size of the cluster may be controlled by changing stoichiometry, temperature, and solvent conditions. It is possible to substitute halides or 4-aminophenylthiol for phenylthiol capping groups. Optical absorption varies with cluster size, as predicted by theory. One recommended future course of study is the reactivity of 4-aminophenylthiol capping groups with organic acids to connect ZnS and CdS clusters into a lattice by dehydration synthesis. It is of interest whether polypeptides or DNA could be used to facilitate or direct this process. The figure below shows an example of a completed lattice of clusters. Note that the assembly of clusters is an adamantanoid formation, as is the structure of each individual cluster.

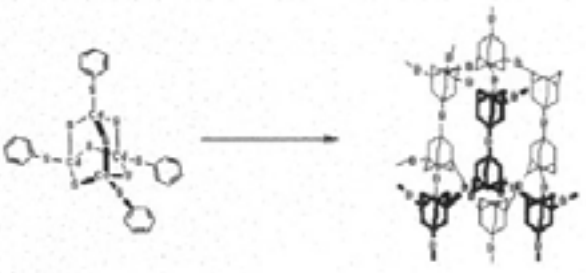

Crystal engineering ZnS and CdS clusters into a lattice

Index of Interns and Principal Investigators

A

Ahuja, Ashish 53, 55
Allara, David 43
Altepeter, Joe 53, 57
Awschalom, David 87, 91

B

Barry, Kyndall 53, 59
Bekker, Sigal 1, 3
Bishop, Samuel 53, 61
Blakely, Jack 17

C

Cabrera, Blas 80
Calderon, Raiza 29, 31
Carr, Dustin 23
Carroll, Sarah 1, 5
Chen, Phyllis 53, 63
Clarke, David 90
Craighead, Harold 19
Cuk, Tanja 53, 66

D

Dancik, Yuri 53, 69
Davidsmeier, Thomas 1, 7
Davis, Robert 41, 49
Deal, Mike 53, 63
Deardorff, Glenn 41, 43

E

Engstrom, James 25

F

Fonash, Stephen 45
Frank, Curt 72
Frink, Al 85

G

Gibbons, James 59
Griffin, Peter 57, 69
Gutman, Michael 1, 9

H

Harris, James 61, 78
Hayduk, Eric 1, 11
Herrera, Ali 85, 87
Holeckova, Helena 85, 88, 89
Hoyt, Judy 59
Hu, Evelyn 88, 89
Hung, Cheng Yu 66

I

Irwin, Blair 53, 72
Isaacson, Michael 21

J

Jochum, John 1, 13
Jones, Kimberly 31
Jones, Philip 1, 17

K

Kiehl, Richard 66
Kornegay, Kevin 9
Kramer, Liu-Yen 85

L

Landwehr, Diana 1, 19
Lavoie, Erick 1, 5
Lee, Jackson 41, 45
Lindasay, James 38
Loh, Nin 53, 75

M

MacBeth, Adam 53, 78
Mallison, Melanie-Claire 1
Marshall, Tavia 29, 31
Mayer, Marc 1
McCord, Mark 82
McDonald, Rafael 85, 89
McGrath, Robert 51
McPherson, Catherine 29, 36
McVittie, James 75
Meyer, Marc 21
Mieckowski, Andrzej 41
Milstein, Fred 93
Mosleh, Mohsen 36

N

Neves, Hercules 3, 13

O

Ober, Christopher 11

P

Petroff, Pierre 94
Phillips, LaRon 29, 31
Pine, David 92
Plummer, James 63
Potter, Lezlie 85, 90

R

Rowlette, Jeremy 41, 49

S

Santhanam, Mahima 41, 51
Schulte, Chancy 53, 80
Scott, Gavin 85, 91
Sharma, Manish 55
Slinker, Keith 1, 23
Smith, Jeremiah 29, 38
Spencer, Michael 38
Steinberger, Linda 92
Strouse, Geoffrey 95
Stucky, Galen 88, 89
Sturm, Ben 1, 25
Suzuki, Yuri 7

T

Tanasa, Corina-Elena 82
Tang, Mary 53, 72
Tien, Norman 5
Tringe, Joseph 63

V

Valenzuela, Patricia 85, 93

W

Wang, Shan 55
Werner, Ben 85, 94
Williams, Isaiah 41
Wolf, Brian 85
Wooten, Katie 85, 95

KEY:

Interns

Principal Investigators

Site Staff